

A Detailed Conformational Analysis of 2-Bromo-1-phenylpropane by High Resolution Nuclear Magnetic Resonance spectroscopy and Molecular Orbital Calculations

by

84

Paul Hazendonk

A Thesis
Submitted to the Faculty of Graduate Studies
in Partial Fulfilment of the Requirements
for the Degree of

MASTER OF SCIENCE

Department of Chemistry
University of Manitoba
Winnipeg, Manitoba

© August, 1995



National Library
of Canada

Acquisitions and
Bibliographic Services Branch

395 Wellington Street
Ottawa, Ontario
K1A 0N4

Bibliothèque nationale
du Canada

Direction des acquisitions et
des services bibliographiques

395, rue Wellington
Ottawa (Ontario)
K1A 0N4

Your file *Votre référence*

Our file *Notre référence*

The author has granted an irrevocable non-exclusive licence allowing the National Library of Canada to reproduce, loan, distribute or sell copies of his/her thesis by any means and in any form or format, making this thesis available to interested persons.

L'auteur a accordé une licence irrévocable et non exclusive permettant à la Bibliothèque nationale du Canada de reproduire, prêter, distribuer ou vendre des copies de sa thèse de quelque manière et sous quelque forme que ce soit pour mettre des exemplaires de cette thèse à la disposition des personnes intéressées.

The author retains ownership of the copyright in his/her thesis. Neither the thesis nor substantial extracts from it may be printed or otherwise reproduced without his/her permission.

L'auteur conserve la propriété du droit d'auteur qui protège sa thèse. Ni la thèse ni des extraits substantiels de celle-ci ne doivent être imprimés ou autrement reproduits sans son autorisation.

ISBN 0-612-13179-3

Canada

**A DETAILED CONFORMATIONAL ANALYSIS OF 2-BROMO-1-PHENYLPROPANE
BY HIGH RESOLUTION NUCLEAR MAGNETIC RESONANCE
SPECTROSCOPY AND MOLECULAR ORBITAL CALCULATIONS**

BY

PAUL HAZENDONK

**A Thesis submitted to the Faculty of Graduate Studies of the University of Manitoba
in partial fulfillment of the requirements of the degree of**

MASTER OF SCIENCE

© 1995

**Permission has been granted to the LIBRARY OF THE UNIVERSITY OF MANITOBA
to lend or sell copies of this thesis, to the NATIONAL LIBRARY OF CANADA to
microfilm this thesis and to lend or sell copies of the film, and LIBRARY
MICROFILMS to publish an abstract of this thesis.**

**The author reserves other publication rights, and neither the thesis nor extensive
extracts from it may be printed or other-wise reproduced without the author's written
permission.**

Abstract

Ultra high resolution ^1H nuclear magnetic resonance spectroscopy was used to make an in depth study of the conformational properties of 2-bromo-1-phenylpropane. The relative rotamer stabilities were determined from the proton-proton vicinal coupling constants in the sidechain, using an extended Haasnoot form of the Karplus equation. These were compared with the results of semiempirical and ab initio molecular orbital calculations on this molecule.

To see whether the Karplus equation can be used to predict these vicinal couplings when allowing for varying degrees of torsional motion about the $\text{C}_\alpha\text{-C}_\beta$ bond, these couplings were classically averaged over the energy profile of rotation about this bond in three ways:

- i) The rotational isomeric state method; this method assumes three static rotamers.
- ii) 3-Cusp method; this approach averages over the bottom of the potential wells within $2.5RT$ of the minima.
- iii) Continuous method; this methods averages over the complete energy profile.

Using the continuous averaging approach and the Karplus equation, the effect of varying the barrier height to rotation about the $\text{C}_\alpha\text{-C}_\beta$ bond on the vicinal coupling constants was investigated. The behaviour of these coupling constants was discussed in terms of the symmetry of the potential

wells and angular dependence of the coupling constants about the minima of the wells.

From the six-bond coupling constants between the benzylic protons to the proton in the para ring position, $\langle \sin^2 \psi_H \rangle$ were determined, from which upper and lower limits of the average barriers to phenyl rotation were found. $\langle \sin^2 \psi_H \rangle$ values were also calculated from semiempirical and ab initio molecular orbital calculations in order to gain some insight into these barriers. ψ_H is the angle which the benzylic C-H bond makes with the plane of the ring. Experimental $\langle \sin^2 \psi_H \rangle$ values were used to predict ${}^4J_{\text{CH}_3, \text{H}_2}$ and $\langle \sin^2 \psi_H / 2 \rangle$ using modified expressions for ${}^4J_{\text{CH}_3, \text{H}_2}$ and ${}^5J_{\text{CH}_3, \text{H}_3}$ from toluene.

FPT MO INDO and CNDO/2 calculations were used to predict ${}^4J_{\text{H}_A, \text{H}_2}$, ${}^4J_{\text{H}_B, \text{H}_2}$, ${}^5J_{\text{H}_C, \text{H}_2}$, ${}^5J_{\text{H}_A, \text{H}_3}$, ${}^5J_{\text{H}_B, \text{H}_3}$, ${}^6J_{\text{H}_C, \text{H}_3}$, ${}^6J_{\text{H}_A, \text{H}_4}$, ${}^6J_{\text{H}_B, \text{H}_4}$ and ${}^7J_{\text{H}_C, \text{H}_4}$ which were classically averaged over the phenyl rotation. These results were compared with experiment. The methylene protons are designated A and B, the methine proton is C and the ortho, meta and para protons are in positions 2, 3 and 4, respectively.

Acknowledgements

I would like to thank everyone who has supported me with my studies. I would like to thank the Chemistry Department for giving me this opportunity for study at the University of Manitoba. I am grateful to NSERC for providing the funds and thus the freedom to give my undivided attention to my studies.

For helping me with the instrument and teaching me many tricks of the trade I would like to thank Kirk Marat. I owe a particular debt to Dr. McKinnon for synthesizing two of the molecules I studied.

To my fellow students I would like to extend my gratitude for providing a healthy environment conducive to study and research. In particular I would like to thank Guy Bernard, Scott Kroeker, Leo Spyroculous, Mark Soliven and Younes Bekkali for their assistance and dialogue.

I gratefully acknowledge my indebtedness to my mentor Dr Schaefer, who has supported and guided me in this research. I am thankful to him for giving me an excellent education and the opportunity to explore this field.

TABLE OF CONTENTS

<u>Chapter</u>		<u>Page</u>
	ABSTRACT	ii
	ACKNOWLEDGEMENTS	iv
	TABLE OF CONTENTS	v
	LIST OF FIGURES	viii
	LIST OF TABLES	xiv
1	INTRODUCTION	1
	1.1 The Karplus equation	2
	1.2 The rotational isometric state (RIS) method	5
	1.3 Introduction to the first problem	6
	1.4 Coupling constants between protons in the sidechain and those in the aromatic ring	9
	1.5 Internal rotational barriers and the J method	12
	1.6 Introduction to the second problem	16
	1.7 Significance of the experiment	18
2	MATERIALS AND METHODS	20
	2.1 Sources of compounds and NMR sample preparation	21
	2.2 Spectroscopic method and spectral processing and	

	analysis	22
2.3	Calculation of the θ profiles, $\langle \sin^2 \psi_i \rangle$, and ϕ profiles of 2-bromo-1-phenylpropane	23
2.4	FPT MO INDO and CNDO/2 calculations and the determination of the classical expectation values of the coupling constants between the nuclei of the sidechain and those of the aromatic ring	26
2.5	FPT MO INDO and CNDO/2 calculations and the determination of the classical expectation values of the coupling constants between the nuclei on the sidechain	28
3	RESULTS	32
3.1	^1H spectral results for 2-bromo-1-phenylpropane	33
3.2	The molecular orbital calculations for 2-bromo-1-phenylpropane	40
3.3	FPT MO INDO, CNDO/2 calculations, and classical averaging	56
4	DISCUSSION	78
4.1	Assignments of H_A and H_B	79
4.2	Prediction of the vicinal coupling constants of the	

	sidechain - a test of the rotational isomeric states	
	method	82
4.3	Determination of the conformation about the exocyclic $C_i(sp^2)-C_\alpha(sp^3)$ bond using ${}^6J_{HA,H4}$ and ${}^6J_{HB,H4}$. Discussion of the effect of the rotamer state on the barrier to rotation about the $C_i(sp^2)-C_\alpha(sp^3)$ bond and the computation of $\langle \sin^2 \psi_{HA} \rangle$ and $\langle \sin^2 \psi_{HB} \rangle$	101
4.4	Classical averaging over the θ profiles of coupling constants between the sidechain and ring protons predicted by FPT MO INDO AND CNDO/2	116
4.5	Summary of conformational information about 2-bromo-1-phenylpropane, compared with other molecules	121
5	OTHER INVESTIGATIONS	125
6	REFERENCES	126

LIST OF FIGURES

<u>Figure</u>		<u>Page</u>
1.5.1	A comparison between classical and quantum mechanical means of calculating $\langle \sin^2\theta \rangle$. For both methods $\langle \sin^2\theta \rangle$ is presented as a function of the twofold barrier height, V_2 , at 300 K	15
3.1.1	2-Bromo-1-phenylpropane	33
3.1.2	The aromatic region of the ^1H NMR spectrum of the 5 mol % 2-bromo-1-phenylpropane in CD_2Cl_2 .	35
3.1.3a	The methylene region of the ^1H NMR spectrum of the 5 mol % 2-bromo-1-phenylpropane in CD_2Cl_2 .	36
3.1.3b	The methylene region of the ^1H NMR spectrum of the 5 mol % 2-bromo-1-phenylpropane in CD_2Cl_2 .	37
3.1.4	The methine region of the ^1H NMR spectrum of the 5 mol % 2-bromo-1-phenylpropane in CD_2Cl_2 .	38
3.1.5	The methyl region of the ^1H NMR spectrum of the 5 mol % 2-bromo-1-phenylpropane in CD_2Cl_2 .	39
3.2.1	The Newman projections for 2-bromo-1-phenylpropane	41
3.2.2	3-Dimensional plot of relative heats of formation from AM1 as a function of phenyl rotation (θ) and	

	rotation about the C_{α} - C_{β} bond of the sidechain (ϕ)	43
3.2.3	3-Dimensional plot of relative energy from STO-3G as a function of phenyl rotation (θ) and rotation about the C_{α} - C_{β} bond of the sidechain (ϕ)	45
3.2.4	Relative energies of the three rotamers of 2-bromo-1-phenylpropane from AM1 as a function of phenyl rotation (θ) from the perpendicular form	49
3.2.5	Relative energies of the three rotamers of 2-bromo-1-phenylpropane from STO-3G as a function of phenyl rotation (θ) from the perpendicular form	50
3.2.6	Relative energies of the three rotamers of 2-bromo-1-phenylpropane from STO-3G* as a function of phenyl rotation (θ) from the perpendicular form	51
3.2.7	Relative energies from AM1, STO-3G and STO-3G* as a function of sidechain rotation (ϕ)	54
3.3.1	Graphical representation of the FPT MO INDO and CNDO/2 calculations of vicinal coupling constants between H_A , H_B , and H_C in the sidechain of 2-chloro-1-phenylpropane	59
3.3.2	Graphical representation of the INDO and CNDO/2 calculation of the four-bond coupling constants between:	

- A) H_A and the methyl hydrogens of 2-chloro-1-phenylpropane
- B) H_B and methyl hydrogens of 2-chloro-1-phenylpropane 60
- 3.3.3 FPT MO CNDO/2 calculations of couplings between H_A and the hydrogens of the aromatic ring, for the A rotamer of 2-chloro-1-phenylpropane, as a function of: 1. phenyl rotation (ϕ) 2. phenyl rotation offset such that H_A starts perpendicular to the ring ($\theta - 120^\circ$) 62
- 3.3.4 FPT MO CNDO/2 calculations of the couplings between H_A and the hydrogens of the aromatic ring for rotamer B (1) and C (2) of 2-chloro-1-phenylpropane as a function of θ . 63
- 3.3.5 FPT MO INDO calculations of couplings between H_A and the hydrogens of the aromatic ring for rotamer A of 2-chloro-1-phenylpropane, as a function of: 1) phenyl rotation (θ) 2) phenyl rotation offset such that H_A starts perpendicular to the ring ($\theta + 120^\circ$) 64
- 3.3.6 FPT MO INDO calculations of the couplings between H_A and the hydrogens of the aromatic ring for

- rotamer B (1) and C (2) of 2-chloro-1-phenylpropane
as a function of θ . 65
- 3.3.7 FPT MO CNDO/2 calculations of the couplings
between H_C and the hydrogens of the aromatic ring
for rotamer A (1) and B (2) of 2-chloro-1-
phenylpropane as a function of θ . 72
- 3.3.8 1. FPT MO CNDO/2 calculations of the couplings
between H_C and the hydrogens of the aromatic ring
for rotamer C of 2-chloro-1-phenylpropane as a
function of θ .
2. FPT MO INDO calculations of the couplings
between H_C and the hydrogens of the aromatic ring
for rotamer A of 2-chloro-1-phenylpropane as a
function of θ . 73
- 3.3.9 FPT MO INDO calculations of the couplings
between H_C and the hydrogens of the aromatic
ring for rotamer B (1) and C (2) of 2-chloro-1-
phenylpropane as a function of θ . 74
- 4.2.1 $^3J_{HA,HC}$ (Hz) of 2-bromo-1-phenylpropane as
predicted using an extended form of the Haasnoot
formulation of the Karplus equation 84
- 4.2.2 The energy profiles of ϕ rotation for 2-bromo-1-

	phenylpropane - curves 1 to 4 are in order of increasing barrier heights	84
4.2.3	Curve 1 - Barriers of 5 kJ/mol for B \leftrightarrow C and 1.5 kJ/mol for A \leftrightarrow B	86
4.2.4	Curve 2 - Barriers of 6 kJ/mol for B \leftrightarrow C and 2 kJ/mol for A \leftrightarrow B	87
4.2.5	Curve 3 - Barriers of 6 kJ/mol for B \leftrightarrow C and 5 kJ/mol for A \leftrightarrow B	88
4.2.6	Curve 4 - Barriers of 10 kJ/mol for B \leftrightarrow C and 10 kJ/mol for A \leftrightarrow B	89
4.2.7	STO-3G* energy as a function of ϕ	90
4.2.8	Prediction of the behaviour of the classical average of a function, which has a given shape and symmetry with respect to the centre of the population, with changes in barrier height.	92
4.2.9	$^3J_{\text{HB,HC}}$ (Hz) of 2-bromo-1-phenylpropane as predicted using an extended form of the Haasnoot formulation of the Karplus equation.	97
4.2.10	J distribution for $^3J_{\text{HB,HC}}$ in 2-bromo-1-phenylpropane	97
4.2.11	A comparison of the RIS method with the classical averaging procedure for symmetrical and	

	asymmetrical potential wells for an antisymmetric property.	100
4.5.1	Conformations of rotamer A, B, and C given by STO-3G*	123

LIST OF TABLES

<u>Table</u>		<u>Page</u>
2.5.1	Parameters, torsion angles and Mullay group electronegativities required for the extended Haasnoot formulation of the Karplus equation for the vicinal coupling constants in 2-bromo-1-phenylpropane	30
3.1.1	¹ H NMR spectral parameters of 2-bromo-1-phenylpropane in CS ₂ , CD ₂ Cl ₂ , and acetone-d ₆	34
3.2.1	Relative heat of formation from AM1 as a function of phenyl rotation (θ) and rotation about the C _{α} -C _{β} bond of the sidechain (ϕ).	42
3.2.2	Relative energy from STO-3G as a function of phenyl rotation (θ) and rotation about the C _{α} -C _{β} bond of the sidechain (ϕ).	44
3.2.3	Energies of the rotamers of 2-bromo-1-phenylpropane as a function of sidechain angular displacement with respect to the perpendicular form.	46
3.2.4	Energies of the rotamers of 2-bromo-1-phenylpropane as a function of the angle of the sidechain angular with respect to the perpendicular form, fit to a 17 term Fourier series.	47

- 3.2.5 Relative energies of the three rotamers of 2-bromo-1-phenylpropane from AM1, STO-3G, and STO-3G* as a function of sidechain angular displacement with respect to the perpendicular form. 48
- 3.2.6 Energy of 2-bromo-1-phenylpropane as a function of rotation about the sidechain $C_\alpha-C_\beta$ (ϕ). 52
- 3.2.7 Energy of the sidechain rotation in 2-bromo-1-phenylpropane as a function of ϕ , fit to a Fourier series truncated at 17 terms. 53
- 3.2.8 Fully optimized energies of the three rotamers of 2-bromo-1-phenylpropane. 55
- 3.3.1 Calculation of $\langle \sin^2(\theta + \pi/6) \rangle$ and $\langle \sin^2(\theta - \pi/6) \rangle$ to predict ${}^6J_{A,4}$ and ${}^6J_{B,4}$ for 2-bromo-1-phenylpropane 58
- 3.3.2 Calculation of ${}^6J_{90}$ for 2-chloro-1-phenylpropane using INDO results. 58
- 3.3.3 Prediction of the vicinal coupling constants and ${}^4J_{H,CH_3}$ of the sidechain, using Karplus, INDO and CNDO/2 methods. Averaged values were obtained using 3-point, 3-cusp and continuous methods. 61
- 3.3.4 Classical averaging of ${}^4J[H_A, H_2]$ of 2-chloro-1-

	phenylpropane over the energy profile for θ rotation.	66
3.3.5	Classical averaging of ${}^5J[H_A, H_3]$ of 2-chloro-1-phenylpropane over the energy profile for θ rotation.	67
3.3.6	Classical averaging of ${}^6J[H_A, H_4]$ of 2-chloro-1-phenylpropane over the energy profile for θ rotation.	68
3.3.7	Classical averaging of ${}^4J[H_B, H_2]$ of 2-chloro-1-phenylpropane over the energy profile for θ rotation.	69
3.3.8	Classical averaging of ${}^5J[H_B, H_2]$ of 2-chloro-1-phenylpropane over the energy profile for θ rotation.	70
3.3.9	Classical averaging of ${}^6J[H_B, H_2]$ of 2-chloro-1-phenylpropane over the energy profile for θ rotation.	71
3.3.10	Classical averaging of ${}^5J[H_C, H_2]$ of 2-chloro-1-phenylpropane over the energy profile for θ rotation.	75
3.3.11	Classical averaging of ${}^6J[H_C, H_3]$ of 2-chloro-1-phenylpropane over the energy profile for θ rotation.	76
3.3.12	Classical averaging of ${}^7J[H_C, H_2]$ of 2-chloro-1-phenylpropane over the energy profile for θ rotation.	77
4.1.1.	Populations of rotamers A, B and C in various solvents determined from ${}^3J_{H_A, H_C}$ and ${}^3J_{H_B, H_C}$	81
4.1.2	Populations of rotamers A, B and C in various solvents determined from ${}^3J_{H_A, H_C}$ and ${}^3J_{H_B, H_C}$ using ideal geometries	81

- 4.2.1 A comparison of the RIS method with the continuous method, when the rotational barriers $A \leftrightarrow B$ and $B \leftrightarrow C$ are varied 94
- 4.2.2 Barrier dependence of the contribution to ${}^3J_{HA,HC}$ from each rotamer, calculated from the Karplus equation and the energy curves 1 to 4 and including the STO-3G* profile 95
- 4.2.3 Barrier dependence of the contribution to ${}^3J_{HB,HC}$ from each rotamer, calculated from the Karplus equation and the energy curves 1 to 4 and including the STO-3G* profile 96
- 4.3.1 Comparing the rotationally averaged results with those from the static geometry: A test of whether the barrier heights in ϕ and θ are sufficiently large to use the results of the static rotamer geometries to describe the system 103
- 4.3.2 Calculation of ψ from $\langle\psi\rangle$ of each rotamer state and from the optimized geometries averaged over the rotamer populations 106
- 4.3.3 Calculation of $\langle\sin^2\psi\rangle$ by using the maximum of each θ profile as V_2 for the barrier, then averaging over the rotamer populations 107

4.3.4	A comparison of $\langle \sin^2(\theta + \gamma) \rangle$ evaluated using equation 4.3 and equation 2.2. An assessment of error introduced into the analysis by using 4.3 for the AM1 and STO-3G* energy profiles of rotamer B	110
4.3.5	Determination of $\langle \sin^2\psi_{HA} \rangle$ and $\langle \sin^2\psi_{HB} \rangle$ from ${}^6J_{HA,H4}$ and ${}^6J_{HB,H4}$	112
4.3.6	Estimation of the average barrier to rotation using the average value for $\langle \sin^2\psi_{HA} \rangle$ and $\langle \sin^2\psi_{HB} \rangle$	114
4.4.1	A comparison between experimental and predicted four-bond couplings between the benzylic protons and the ortho protons of the ring ${}^4J_{HA,H2}$ and ${}^4J_{HB,H2}$	117
4.4.2	A comparison between experimental and predicted $\langle \sin^2\psi/2 \rangle$ values	119

1 INTRODUCTION

1.1 The Karplus equation

Based on the valence bond description of ethane, Karplus found that the vicinal proton-proton coupling constant had a $\cos^2\phi$ dependence on the torsion angle between two C-H bonds (1-3). This behaviour of the vicinal coupling constant is largely a consequence of the direct interaction between the electrons in the two C-H bonds which is important in correlating the electron, and hence the proton, spins. The direct interaction, proportional to valence bond exchange integrals, is minimal when the two C-H bonds lie in mutually perpendicular planes ($\phi = 90^\circ$)(4). An acquaintance with trigonometry, together with the constraint that J be positive, suggests that the ϕ dependence between 0° and 180° be mainly on $\cos^2\phi$, perhaps slightly on $\cos\phi$. This is indeed true. The stereochemical significance is obvious. Later, with Barfield, Karplus reformulated the equation as follows (4)

$$J = A \cos^2\phi + B \cos\phi + C \qquad \mathbf{1.1}$$

Many attempts were made to modify the parameters A, B and C empirically (5-19), in order to achieve maximum predictive accuracy for several families of molecules including ethanes (5,6), peptides (8,9,11,15-18,20), amides (13,14), amines (12) and carboxylic acids (19).

The vicinal coupling constant is also strongly dependent on substituent electronegativity and several attempts were made to modify the equation to simulate this dependence (21-24). Initially, this was done by

Durette and Horton who suggested (24) that the original expression should be multiplied by a correction factor as in

$$J = (A \cos^2\phi + B \cos\phi + C) (1 - 0.1 \sum \Delta\chi_i) \quad 1.2$$

$\Delta\chi$ is the electronegativity difference between the substituent and hydrogen.

The orientation of a substituent with respect to the coupled protons is also an important consideration (21,25-31). Haasnoot et al. developed a six-term expression based on molecular orbital theory (22), with parameters which were functions of the electronegativity of both the first (α) and second (β) atoms of the substituents, as well as of the torsion angle and orientation (equation 1.3).

$$J = P_1 \cos^2\phi + P_2 \cos\phi + \sum \Delta\chi_i [P_3 + P_4 \cos^2(\zeta_i \phi + P_5 |\Delta\chi_i|)] \quad 1.3$$

ζ_i is ± 1 , dependent on the orientation of the substituent. A sixth parameter P_6 is employed for substituents with β atoms (22).

The Haasnoot form of the Karplus equation was reformulated by Imai and Osawa into a linear combination of 11 independent terms and 22 adjustable parameters (32-33). Included were the effects due to various structural features, such as the valence angle at both C-H bonds (ω), α and

β substituent electronegativity ($\Delta\chi_i^\alpha$ and $\Delta\chi_j^\beta$) and orientation (θ_i and ψ_j), carbon-carbon bond length (r_{C-C}), and proximity or through-space interactions as a function of r (the distance between a coupled proton and a nearby nonbonded atom). The expression (equation 1.4) was fit to a set of 198 coupling constants with a standard deviation of 0.33 Hz.

$$\begin{aligned}
 J = & A\cos\phi + B\cos2\phi + C\cos3\phi + D\cos^22\phi \\
 & + W(E\cos\phi \sum \Delta\chi_i^\alpha \cos\theta_i + F \sum \Delta\chi_i^\alpha \cos(2\theta_i) \\
 & + G \sum \Delta\chi_i^\alpha) + H\left[\frac{(\omega_1 + \omega_2)}{2} - 110\right] \\
 & + I(r_{C-C} - 1.5) + K \sum \Delta\chi_j^\beta \cos2\psi + Lr^{-4} + M
 \end{aligned}
 \tag{1.4}$$

A more popular shortened form with 14 adjustable parameters was developed by evaluating the relative importance of each term and eliminating those which were most insensitive to the variables (34,35). Coupling constants predicted with this equation (equation 1.5) fell within a standard deviation of 0.45 Hz for 195 data points.

$$\begin{aligned}
 J = & A\cos\phi + B\cos2\phi + W(E\cos\phi \sum \Delta\chi_i^\alpha \cos\theta_i) \\
 & + H\left[\frac{(\omega_1 + \omega_2)}{2} - 110\right] + M
 \end{aligned}
 \tag{1.5}$$

This form of the Karplus equation will be used in the following analysis.

1.2 The rotational isomeric state (RIS) method

Vicinal coupling constants are averages over all the conformations of the molecule (36). With the Karplus equation it is possible to predict the coupling constant in each of these conformations. Therefore it is possible in principle to determine the population of the conformations, provided there are enough measured coupling constants (21,36-38).

For substituted ethanes the Karplus equation in its various forms has been widely used in determining relative rotamer stabilities (36-40). In most applications it is assumed that the molecule can exist in three rigid rotamers (38). Using ideal geometries, where the torsion angles are 60° (gauche), 180° (trans) and 300° (gauche denoted as g') and with valence angles of 109.5° , coupling constants for each rotamer are calculated. The observed couplings can be expressed as the predicted couplings in each rotamer state averaged over the rotamer populations. Provided that there are enough equations, the rotamer populations can be determined. For instance, for a trisubstituted ethane with protons labelled A, B and C, the rotamer populations, P_1 , P_2 and P_3 , can be calculated from the following system of equations (21,36-39):

$$J_{A,B} = P_1 J_g^{A,B} + P_2 J_{g'}^{A,B} + P_3 J_t^{A,B}$$

$$J_{A,C} = P_1 J_{g'}^{A,C} + P_2 J_t^{A,C} + P_3 J_g^{A,C}$$

$$P_1 + P_2 + P_3 = 1$$

1.6

The above technique is known as the Rotational Isomeric States method (RIS) or sometimes as the n site method. It is based on the assumption that vicinal coupling constants in substituted ethanes can be adequately described as an average over three static conformations. What happens when torsional motion about the C-C bond is considered? Can the Karplus equation be used in an analysis that permits for some motion about the ethane C-C bond? What if the barrier to rotation about the C-C bond were small?

1.3 Introduction to the first problem

To see whether the Karplus equation can predict vicinal coupling constants over a range of torsional angles in each rotamer state, an investigation will be made into the vicinal couplings in 2-bromo-1-phenylpropane, a trisubstituted ethane. The rotamer populations will be determined with the RIS method using the extended version of the Haasnoot equation (equation 1.5). Both semiempirical and ab initio molecular orbital calculations will be performed on this molecule to find the optimum energy and geometry of each rotamer. The optimum geometries will be used with the RIS method to predict the rotamer populations. These populations will be compared with those predicted from the molecular orbital calculations and with those determined from ideal geometries.

Further, molecular orbital calculations will be done to determine the energy profile ($V(\phi)$) of rotation about the $C(sp^3)$ - $C(sp^3)$ (ϕ) bond. An expression for the two vicinal coupling constants as a function of ϕ ($J(\phi)$) will be developed from the extended Haasnoot form of the Karplus equation, using the optimum geometries along the energy profile. With $V(\phi)$ and $J(\phi)$ the average of the vicinal couplings will be evaluated in two ways. The first will be an average over all regions of $V(\phi)$ that fall within $2.5 RT$ of the minimum energies. Since this method samples the bottom of the energy well of each rotamer it is called the 3-cusp method. The second method involves calculating the average over the entire range of ϕ . This will be referred to as the continuous method. Both methods of averaging $J(\phi)$ involve weighting $J(\phi)$ at each value of ϕ according to the population of the conformation with ϕ prescribed by the Boltzmann distribution at $V(\phi)$. Thus the classical average of J over an interval a to b in ϕ is

$$\langle J \rangle = \frac{\int_a^b J(\phi) \exp\left(-\frac{V(\phi)}{RT}\right) d\phi}{\int_a^b \exp\left(-\frac{V(\phi)}{RT}\right) d\phi} \quad 1-7$$

This procedure assumes that the density of hindered rotamer states at ambient temperatures is sufficiently high that any quantum mechanical expectation value will be closely approximated by its classical average. This is the case with expectation values for phenyl rotation, as shown by studies

in this laboratory (41).

The vicinal coupling constants will also be calculated using FPT MO INDO and CNDO/2 computations on 2-chloro-1-phenylpropane with the optimum geometries from the ϕ profile. The INDO and CNDO/2 algorithms are not parameterized for bromine (42); when the geometries of the bromine compound are retained, substitution with chlorine in this manner should not grossly alter the results since the difference in electronegativity of bromine and chlorine is only 0.2 Pauling units (43). The CNDO/2 and INDO expressions for these couplings will be averaged using both the 3-cusp and continuous methods. The averaged CNDO/2 and INDO results will be compared with those from the Karplus equation.

The performance of the RIS method will be compared with the results of the continuous method applied to various barrier heights. The behaviour of these predicted coupling constants will be discussed in terms of the symmetry of $J(\phi)$ and $V(\phi)$ in the regions about the energy minima.

1.4 Coupling constants between protons in the sidechain and those in the aromatic ring.

Long range coupling constants between benzylic protons and the ring protons in toluene and its analogues can be described in terms of three mechanisms: the σ mechanism, the σ - π mechanism and the through-space mechanism (44). The σ mechanism transfers spin information through the σ -bonds of the molecule. The σ - π mechanism involves the transfer of the spin state information from the sidechain σ orbitals to the π orbitals of the ring through the hyperconjugative overlap between the benzylic C-H bond and the π system of the ring. This is followed by σ - π interaction between the π orbitals of the ring and σ orbitals of the ring C-H bond (45). The through-space mechanism entails the transfer of spin state information through two proximate orbitals in the bonds containing the nuclei (44). This phenomenon is also referred to as the non-bonded interaction (46).

Wasylishen and Schaefer propose that the angular dependence of the σ electron contribution to the 5-bond coupling ${}^5J_{CH_3, H_3}$ in toluene is given by (45)

$${}^5J_{CH_3, H_3} = {}^5J_{180}^{\sigma} \sin^2\left(\frac{\theta}{2}\right) \quad 1.8$$

where ${}^5J_{180}^{\sigma}$ pertains to the all-trans planar arrangement of the intervening bonds.

Analogous to the McConnell-Heller equation (47), the angular

dependence of contributions from the σ - π mechanism is given by

$$J^{\sigma-\pi} = J_{90}^{\sigma-\pi} \sin^2\theta \quad \mathbf{1-9}$$

A generalized equation for the angular dependence of these types of long range coupling constants takes the form (41)

$$J = J_{90}^{\sigma-\pi} \sin^2\theta + J_{180}^{\sigma} \sin^2\frac{\theta}{2} + J_{TS} \quad \mathbf{1-10}$$

J_{TS} is a term accounting for the through-space contribution to J .

The four-bond coupling constant ${}^4J_{CH_3,H_2}$ has been written as (48)

$${}^4J_{CH_3,H_2} = 6.90\pi \sin^2\theta - 0.32\cos^2\theta \quad \mathbf{1-11}$$

where π is the mutual atom-atom polarizability associated with the $2p_z$ orbitals in the C_1 - C_2 bond. In toluene π is -0.157, therefore equation 1-12 becomes

$${}^4J_{CH_3,H_2} = -1.08\langle \sin^2\theta \rangle - 0.320\langle \cos^2\theta \rangle \quad \mathbf{1-12}$$

The second term in the equation is attributed to the σ contribution to this

coupling constant.

The angular dependence of the five-bond coupling constants was investigated with a series of ortho-difluoro derivatives of toluene (49). These compounds were chosen to give a large range of $\langle \sin^2\theta \rangle$ and since they have symmetric evenfold barriers, $\langle \sin^2\theta/2 \rangle$ can be assumed to be 0.5 (50). The expression for ${}^5J_{\text{CH}_3, \text{H}_3}$ in toluene became

$${}^5J_{\text{CH}_3, \text{H}_3} = 0.336\langle \sin^2\theta \rangle + 0.322\langle \sin^2\frac{\theta}{2} \rangle \quad \mathbf{1-13}$$

From experiment and theoretical investigations it has been established that the six-bond coupling to the para proton in toluene is dependent only on $\sin^2\theta$ (51). Since $\langle \sin^2\theta \rangle$ is 0.5, and ${}^6J_{\text{CH}_3, \text{H}_4}$ is -0.602 Hz in toluene, the expression for the six bond coupling takes on the form (52)

$${}^6J_{\text{CH}_3, \text{H}_4} = -1.20\langle \sin^2\theta \rangle \quad \mathbf{1-14}$$

1.5 Internal rotational barriers and the J method

The generalized equation for the angular dependence of the six-bond coupling constant from a nucleus on the α carbon and a nucleus in the para ring position of a substituted toluene is given by (51)

$${}^6J = {}^6J_{0^\circ} + {}^6J_{90^\circ} \langle \sin^2\theta \rangle \quad 1-15$$

${}^6J_{90}$ and 6J_0 are this coupling constant when $\theta = 90^\circ$ and $\theta = 0^\circ$, respectively. In most cases 6J_0 is negligible for a saturated sidechain. However, this is not always the case, as in benzaldehyde and styrene, in which 6J_0 is + 10 mHz (53,54), and -120 mHz (55), respectively. Equation 1-15 implies that with an accurate value of ${}^6J_{90}$, $\langle \sin^2\theta \rangle$ can be calculated from an experimental 6J (51); $\langle \sin^2\theta \rangle$ is the ensemble average of $\sin^2\theta$ over all the hindered rotor states. Thus if the barrier to sidechain rotation is a simple function, it can readily be related to $\langle \sin^2\theta \rangle$ (51).

Take for instance an evenfold barrier, which is expressed as

$$\begin{aligned} V(\theta) &= V_{2N} \sin^2 N\theta \\ &= \frac{V_{2N}}{2} [1 - \cos^2 N\theta] \end{aligned} \quad 1-16$$

V_{2N} is the $2N$ -fold barrier height. The hamiltonian operator which describes a rotor hindered by this barrier is given by (56,57)

$$\hat{H} = -\frac{\hbar}{2I_r} \frac{d^2}{d\theta^2} + \frac{V_2}{2} [1 - \cos^2 2\theta] \quad 1-17$$

I_r is the reduced moment of inertia of the molecule. The Schrödinger equation is given by

$$\left\{ -\frac{\hbar}{2I_r} \frac{d^2}{d\theta^2} + \frac{V_{2N}}{2} [1 - \cos^2 2N\theta] \right\} \psi_m = E_m \psi_m \quad 1-18$$

which can be transformed into the form of the Mathieu equation (51,52). The solutions ψ_m are expressed as even Fourier series in θ (57,58). The expectation value of $\sin^2\theta$ is evaluated from

$$\langle \sin^2\theta \rangle = \frac{\sum_{m=0}^N \exp\left[-\frac{E_m}{RT}\right] \langle \psi_m | \sin^2\theta | \psi_m \rangle}{\sum_{m=0}^N \exp\left[-\frac{E_m}{RT}\right]} \quad 1-19$$

ψ_m are the hindered rotor states and E_m are the corresponding energies. The first 21 free rotor states provide an adequate basis set to obtain accurate $\langle \sin^2\theta \rangle$ values at ambient temperatures (51).

When the barrier to rotation is composed of many evenfold terms, the solutions to the Schrödinger equation can become complicated, and calculation of the expectation values over these states would become very

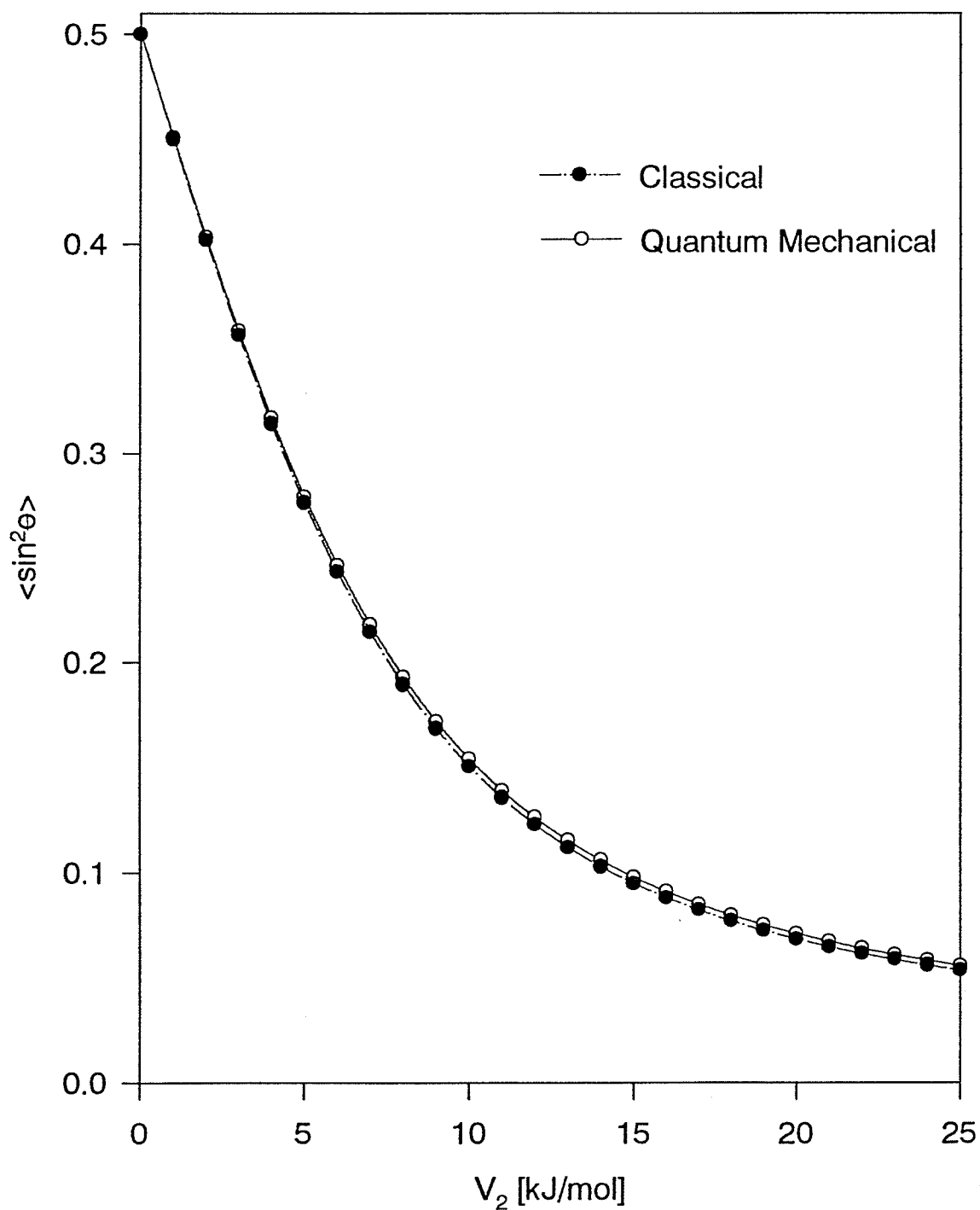
involved (41). The barriers to internal rotations of this type are small and therefore the rotational states are very closely spaced. Thus at ambient temperatures the ensemble average of the quantum mechanical expectation values will closely correspond to the classical average as in equation 1-20 ($V(\theta)$ is some series representation of the barrier in θ)(see figure 1.5.1). Thus it is often more convenient to calculate the classical expectation value for a given barrier than the quantum mechanical one via 1-20.

$$\langle \sin^2\theta \rangle \approx \frac{\int_0^{2\pi} \sin^2\theta \exp\left[-\frac{V(\theta)}{RT}\right] d\theta}{\int_0^{2\pi} \exp\left[-\frac{V(\theta)}{RT}\right] d\theta} \quad \mathbf{1-20}$$

A more complicated barrier leads to some interesting questions. How does one derive useful information from experimental $\langle \sin^2\theta \rangle$ values when the barrier is complex, containing several symmetric and asymmetric terms? Furthermore, how does one deal with a molecule which can exist in several states, each state having a different profile of phenyl rotation? Are molecular orbital calculations useful for providing answers to both questions?

Figure 1.5.1

A comparison between classical and quantum mechanical means of calculating $\langle \sin^2\theta \rangle$. For both methods $\langle \sin^2\theta \rangle$ is presented as a function of the twofold barrier height, V_2 , at 300 K.



1.6 Introduction to the second problem

2-Bromo-1-phenylpropane is an asymmetrically substituted ethylbenzene and, since the methine carbon of the $-\text{CHBrCH}_3$ group is chiral, the two benzylic protons have different chemical shifts and different couplings with the ring nuclei. A second objective of this investigation is to test the applicability of molecular orbital calculations for the prediction of $\langle \sin^2\theta \rangle$ for the benzylic protons. If so, are the calculations useful in interpreting the experimental $\langle \sin^2\theta \rangle$ in terms of some type of barrier to internal rotation?

2-Bromo-1-phenylpropane can exist in three rotamer states, where each will have a different energy profile for phenyl rotation. These energy profiles will be determined for each rotamer using both semiempirical and ab initio molecular orbital computations. The classical expectation values of $\sin^2\theta$ will be calculated using equation 1-20 and averaged according to the rotamer populations. Another approach assumes that the phenyl barrier in each rotamer is twofold and that each rotamer has a different stable conformation of the C-C bond with respect to the phenyl ring. For each rotamer the maximum of the θ profile is taken to be the apparent twofold barrier height, V_2 , from which $\langle \sin^2\theta \rangle$ values are determined. These are then averaged over the rotamer distributions. The computed $\langle \sin^2\theta \rangle$ values from both methods will be compared with the corresponding experimental value as calculated from equation 1-15 using ${}^6J_{90}$ based on the group electronegativity of $-\text{CHBrCH}_3$.

Upper and lower limits of the barrier in each solution will be determined using the average $\langle \sin^2\theta \rangle$ of the two benzylic protons. These barriers will be compared with the averaged computed barrier from the molecular orbital calculations.

The $\langle \sin^2\theta \rangle$ values of the two benzylic protons determined from ${}^6J_{\text{HX,H4}}$ measurements will be used to predict ${}^4J_{\text{HX,H4}}$ with a modified equation 1-12; $\langle \sin^2\theta/2 \rangle$ for each benzylic proton will be calculated from corresponding experimental $\langle \sin^2\theta \rangle$ values with a modified equation 1-13. These values for $\langle \sin^2\theta/2 \rangle$ will be compared with those calculated from molecular orbital results. Both equations 1-12 and 1-13 will have the term representing the π contribution adjusted to the $-\text{CHBrCH}_3$ group electronegativity.

INDO has been known to give semiquantitative accuracy for couplings from benzylic protons into the ring protons (45). An FPT MO INDO and CNDO/2 investigation will be made into these couplings, along with the very long range coupling from the methine proton into the ring. These will be calculated at various values of θ for each rotamer, and their classical averages over the θ profiles will be computed. The predicted values of all these coupling constants will be compared with experiment.

1-7 Significance of the experiment

2-Bromo-1-phenylpropane poses a significant challenge to nmr spectral analysis. Very high resolution is required to resolve the peaks in the aromatic region because extremely small couplings from the protons in the methyl and methine groups are present. The protons of 2-bromo-1-phenylpropane make up a $ABB'CC'MNOX_3$ spin system, giving rise to a total of 6592 possible transitions, which have relatively few degeneracies, a consequence of the asymmetry of this molecule.

A detailed investigation into an asymmetrically substituted ethylbenzene like 2-bromo-1-phenylpropane has not been done with ultra high resolution nuclear magnetic resonance spectroscopy, looking into both the conformation of the sidechain and of the phenyl ring. A separate analysis of two nonequivalent benzylic protons, determining their individual couplings into the ring, has not been done before. This laboratory has worked with molecules of this size previously (59-62). For example, studies have been made of molecules like 2-methyl-1-(3,5-dibromophenyl)ethane (63), isobutylbenzene (61), isopropyl benzene (60) and 3-phenylpentane (62), where sidechain and phenyl conformation were investigated and apparent two and fourfold barriers were found. With 1-bromo-2-(3,5-bromophenyl)ethane, 1-amino-2-(3,5-dibromophenyl)ethane and 1-methyl-2-(3,5-bromophenyl)ethane, a similar analysis was performed. However, in these cases an attempt was also made to determine the barrier of the gauche rotamers (63).

Much work has been done on the conformation within the sidechain of related molecules (36-38,40,64-66). These investigations are mainly limited to determining the relative stabilities of the rotamer states from the vicinal coupling constants. In one case, the effect of the phenyl group on the barrier to rotation of the central butane bond of 2,2-dimethyl-3-phenylbutane was investigated (67). In this study, however, there was no method employed to find the actual orientation of the phenyl group with respect to the sidechain. Only vicinal couplings were employed.

2 MATERIALS AND METHODS

2.1 Sources of compounds, and NMR sample preparation

All solvents were obtained from the Aldrich Chemical Company, except for CS_2 , which came from BDH Chemicals. (\pm)-2-Bromo-1-phenylpropane was bought from the Aldrich Chemical Company.

Samples for NMR analysis were prepared of (\pm)- 2-bromo-1-phenylpropane as 5 mol % solutions in the following solvent systems:

- i) 99.5 mol % acetone- d_6 (99.5 atom %), 0.25 mol % C_6F_6 and 0.25 mol % TMS.
- ii) 89.5 mol % CS_2 , 10 mol % cyclohexane- d_{12} , 0.25 mol % C_6F_6 and 0.25 mol % TMS.
- iii) 99.5 mol % dichloromethane- d_2 (99.6 mol %), 0.25 mol % C_6F_6 and 0.25% TMS.

The solutions were filtered through a piece of cotton wool into a 5 mm od nmr sample tube. The solutions were degassed by the freeze-pump-thaw method, using at least 5 cycles, after which the tubes were flame sealed.

2.2 Spectroscopic method and spectral processing and analysis

All NMR spectroscopy was performed on a Bruker AM 300 spectrometer at a probe temperature of 300 K. Survey ^1H NMR spectra were obtained for which spectral widths of 6000 Hz were necessary. From these spectra, offsets and spectral widths were determined for regions of interest.

Ultra high resolution spectra were obtained of these predetermined regions. In order to achieve this resolution, extensive shimming was performed on the region containing the TMS peak. A proper shim was indicated by a lorentzian line with a width at half height of less than 0.1 Hz before resolution enhancement. The spectral widths of these regions varied from 60 to 200 Hz. Acquisition times were typically 40 s. In most cases 64 scans were acquired. The digital resolution ranged from 0.002 to 0.006 Hz per point.

The free induction decays (FIDs) were zero filled twice. The amount of gaussian broadening was based on how far the FID extended over the acquisition time. Typically values of 0.5 to 0.6 were used. Lorentzian broadening ranged from -0.10 to -0.20, the magnitude depending on the signal to noise ratio.

All spectral analyses were done with the ASSIGN program, using NUMARIT (68) as a front-end. The ^1H spectrum of 2-bromo-1-phenylpropane was analyzed as if it arose from an $\text{ABB}'\text{CC}'\text{MNOX}_3$ spin system.

2.3 Calculation of the θ profiles, $\langle \sin^2 \psi_i \rangle$, and ϕ profiles of 2-bromo-1-phenylpropane.

Semiempirical and ab initio molecular orbital calculations were performed, at AM1 and STO-3G levels, for 2-bromo-1-phenylpropane as a function of rotation about the C_1-C_7 ($\theta = 90 - C_8C_7C_1C_2$) and C_7-C_8 ($\phi = C_9C_8C_7C_1$) bonds (see figure 3.1.1), at 15° intervals, allowing the geometries to optimize. From a plot of relative energy as a function of θ and ϕ , three minima were picked out. At each of these minima, θ and ϕ were allowed to relax, giving rise to the optimized geometries of the three rotamer states. Further calculations were performed to allow the hydrogens on the ring to move out of plane; these are referred to as the relaxed geometries.

In the energy surface mentioned above, corresponding to the minima in the ϕ dimension, there is a trough in the potential surface along the θ dimension (see figures 3.2.1 to 3.2.4). The geometries with ϕ values closest to those at the bottom of the trough were noted for each interval in θ . These geometries were used in further calculations permitting the angle ϕ to relax, but keeping θ fixed. By tracing the bottom of the trough in this manner, the energy profile of phenyl rotation was determined for a given rotamer state. This procedure was used for all three rotamer states, and these calculations were taken to the STO-3G* level. A similar but reversed approach, where ϕ is fixed and θ is relaxed, was taken to calculate the energy profile of sidechain rotation.

The energy profiles in both θ and ϕ were fit to a Fourier series

truncated to 17 terms, using a curve fit routine in the Sigma Plot program.

This Fourier series was of the form

$$V(\gamma) = C_0 + \sum_{n=1}^8 [S_n \sin(n\gamma) + C_n \cos(n\gamma)] \quad 2.1$$

where γ is either θ or ϕ . Using the Fourier coefficients, the classical expectation values of $\sin^2\psi_i$ were calculated for each rotamer, j , as in equation 2.2. The angle ψ_i represents the angle between the C₇-H bond and the plane of the ring. For 2-bromo-1-phenylpropane, ψ_{HA} is $\theta + \pi/6$ and ψ_{HB} is $\theta - \pi/6$.

$$\langle \sin^2\psi_i \rangle_j = \frac{\int_0^{2\pi} \sin^2\psi_i(\theta) \exp\left(-\frac{V_j(\theta)}{RT}\right) d\theta}{\int_0^{2\pi} \exp\left(-\frac{V_j(\theta)}{RT}\right) d\theta} \quad 2.2$$

In the expression for $\langle \sin^2\psi_i \rangle_j$, $V_j(\theta)$ represents the energy profile of rotamer j , R is the ideal gas constant, and T is the temperature. The $\langle \sin^2\psi_i \rangle_j$ values were further averaged over all three rotamer states using an average weighted according to the integral

$$P_j = \int_0^{2\pi} \exp\left(-\frac{V_j(\theta)}{RT}\right) d\theta \quad 2.3$$

Therefore the value for $\langle \sin^2 \psi_i \rangle$ is given by the expression

$$\langle \sin^2 \psi_i \rangle = \frac{\sum_{j=1}^3 P_j \langle \sin^2 \psi_i \rangle_j}{\sum_{j=1}^3 P_j} \quad 2.4$$

Thus the population of each rotamer, Pop_j , was calculated as

$$Pop_j = \frac{100 P_j}{\sum_{j=1}^3 P_j} \quad [\%] \quad 2.5$$

2.4 FPT MO INDO and CNDO/2 calculations and the determination of the classical expectation values of the coupling constants between the nuclei of the sidechain and those of the aromatic ring

FPT MO INDO and CNDO/2 calculations, using STO-3G* geometries of the θ energy profiles of 2-bromo-1-phenylpropane, were done to estimate ${}^xJ(H_s, H_r)$ (where s and r stand for side chain and ring, $x=4,5,6$) as a function of θ .

The FPT MO INDO and CNDO/2 curves for each rotamer were fit to a Fourier series truncated at 17 terms

$$J(\theta)_j = C_0 + \sum_{n=1}^8 [S_n \sin(n\theta) + C_n \cos(n\theta)] \quad 2.6$$

The resulting expressions for the θ dependence of J , $J(\theta)_j$, along with the θ energy profiles, $V(\theta)_j$, for each rotamer were used to calculate the classical expectation value of each coupling constant for each rotamer. The classical expectation value of $J(\theta)_j$, with energy profile $V(\theta)_j$, is given by

$$\langle J(\theta) \rangle_j = \frac{\int_0^{2\pi} J(\theta)_j \exp\left[-\frac{V(\theta)_j}{RT}\right] d\theta}{\int_0^{2\pi} \exp\left[-\frac{V(\theta)_j}{RT}\right] d\theta} \quad 2.7$$

These averaged values were further averaged over the three rotamer states,

weighted according to the integral P_j from equation 2.3

$$\langle J \rangle = \frac{\sum_{j=1}^3 P_j \langle J \rangle_j}{\sum_{j=1}^3 P_j} \quad 2.8$$

Average values were also obtained in the absence of a barrier, which is given as

$$\langle J(\theta) \rangle_j^{free} = \frac{\int_0^{2\pi} J(\theta)_j d\theta}{2\pi} \quad 2.9$$

2.5 FPT MO INDO and CNDO/2 calculations and the determination of the classical expectation values of the coupling constants between the nuclei on the sidechain.

INDO and CNDO/2 MO FPT calculations, using ST0-3G* geometries of the ϕ energy profiles of 2-bromo-1-phenylpropane, were done to estimate $^xJ(H_s, H_s)$ (where s stands for side chain, x= 3,4) as a function of ϕ . The resulting curves in ϕ were fit to a Fourier series truncated to 17 terms.

The ϕ dependence of the vicinal coupling constants for both molecules was also predicted using an extended version of the Haasnoot formulation (22) of the Karplus equation, namely

$$J(\psi) = A \cos\psi + B \cos 2\psi + WE \cos\psi \sum \Delta\chi_i \cos\xi_i + H \left\{ \frac{(\omega_1 + \omega_2)}{2} - 110 \right\} + M \quad 2.10$$

In this expression ψ is the dihedral angle between the C-H bonds of the coupled protons in the ethane fragment. Also, $\Delta\chi_i = \chi_i - \chi_H$ is the Mullay group electronegativity (43,69,70) with respect to that of hydrogen of a substituent which makes a dihedral angle ξ_i with the proton of the coupling pair opposite to it across the C₇-C₈ bond. The angles ω_1 and ω_2 are the valence angles of the bond containing the coupled protons. A, B, W, E, H and M are optimal parameters for a trisubstituted ethane based on a set of 198 experimental vicinal coupling constants (34,35).

For both molecules, the difference between the valence angles, $(\omega_1 - \omega_2)$, of the two coupled protons was calculated for each increment in ϕ , using STO-3G* geometries. These values were fit to a 17 term fourier series giving rise to an expression for $(\omega_1 - \omega_2)$ in ϕ , $\Delta\omega(\phi)$. Using the parameters from table 2.1 and $\Delta\omega(\phi)$, an expression for each of the vicinal coupling constants was derived in terms of ϕ . Note that in table 2.1 there is a different phase relationship between ψ and ϕ for each vicinal coupling constant.

Three approaches were used to calculate an average of the vicinal coupling constants over the ϕ profiles. The continuous method, which is essentially the same method used for the averages over θ above, gives the average of the expression of the vicinal coupling constant as a function of ϕ . The continuous average can therefore be expressed as

$$\langle J \rangle = \frac{\int_0^{2\pi} J(\phi) \exp\left[-\frac{V(\phi)}{RT}\right] d\phi}{\int_0^{2\pi} \exp\left[-\frac{V(\phi)}{RT}\right] d\phi} \quad 2.11$$

A second approach, which I call the 3-cusp method, averages only over the portions of the profile that fall within $2.5 RT$ of the minima in the ϕ profile. Near each minimum the limits of integration are determined from the ϕ profile, a_j and b_j . Thus the expression for the average is

$$\langle J \rangle = \frac{\sum_{j=0}^3 \int_{a_j}^{b_j} J(\phi) \exp\left[-\frac{V(\phi)}{RT}\right]}{\sum_{j=0}^3 \int_{a_j}^{b_j} \exp\left[-\frac{V(\phi)}{RT}\right]} \quad 2.12$$

Table 2.5.1 Parameters, torsion angles and Mullay group electronegativities required for the extended Haasnoot formulation of the Karplus equation for the vicinal coupling constants in 2-bromo-1-phenylpropane.

2-Bromo-1-phenylpropane		
3J	${}^3J_{A,C}$	${}^3J_{B,C}$
ψ^a	$\phi + 4\pi/3$	ϕ
A^b	-1.3556	
B	4.9649	
E	1.0374	
H	-0.2061	
M	6.4068	
W	1.41	
$\xi_{CH_3}^a$	$\phi + 2\pi/3$	$\phi + 4\pi/3$
ξ_{Br}	ϕ	$\phi + 2\pi/3$
ξ_ϕ	$\phi + 2\pi/3$	$\phi + 2\pi/3$
$\Delta\chi_{CH_3}^c$	0.24	
$\Delta\chi_{Br}$	0.73	
$\Delta\chi_\phi$	0.32	

^aAll angle ψ and ξ were read from the computed STO-3G structure. ^bAll parameters A, B, E, H, M, and W are taken from reference 35. ^cAll Mullay electronegativities were taken from references 43,69 and 70.

The last method, known as the three-site, or rotational isomeric states method, as normally used in the literature, evaluates the coupling constants at the optimized rotamer geometries and computes a weighted average according to the rotamer populations. Let ΔE_j and J_j be the relative energy and coupling constant of rotamer j , respectively, then the three site average is

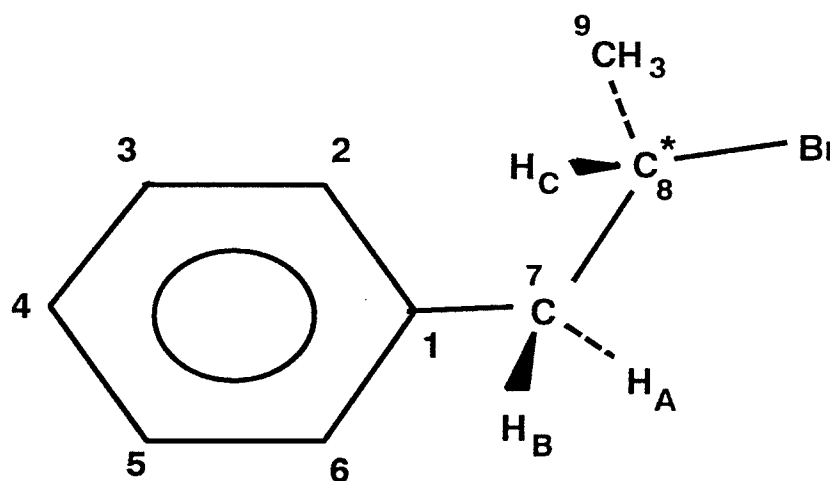
$$\langle J \rangle = \frac{\sum_{j=0}^3 J_j \exp\left[-\frac{\Delta E_j}{RT}\right]}{\sum_{j=0}^3 \exp\left[-\frac{\Delta E_j}{RT}\right]} \quad 2.13$$

3 RESULTS

3.1 ^1H spectral results for 2-bromo-1-phenylpropane

The ^1H spectral parameters for 5 mol % solutions of 2-bromo-1-phenylpropane in acetone- d_6 , CS_2 , and CD_2Cl_2 are summarized in table 3.1.1. The labelling scheme in table 3.1.1 is based on figure 3.1.1 below. There are no significant correlations between the parameters.

Figure 3.1.1 2-Bromo-1-phenylpropane



The following spectra and corresponding simulations, figures 3.1.2 to 3.1.5, are for the solution in CD_2Cl_2 . All figures have the simulation on top, with the spectrum on the bottom. The scale refers to TMS as zero.

Table 3.1.1¹H NMR spectral parameters of 2-bromo-1-phenylpropane in CS₂, CD₂Cl₂, and acetone-d₆.

	CS ₂	CD ₂ Cl ₂	Acetone-d ₆		CS ₂	CD ₂ Cl ₂	Acetone-d ₆
ν ₂ =ν ₆	2123.876 ^{a,b}	2159.174	2180.098	⁵ J _{2,5}	0.590	0.592	0.608
ν ₃ =ν ₅	2156.976	2189.260	2191.422	⁴ J _{A,2}	-0.506	-0.533	-0.534
ν ₄	2139.900	2171.460	2171.862	⁴ J _{B,2}	-0.570	-0.553	-0.551
ν _A	887.464	950.692	943.756	⁵ J _{A,3}	0.281	0.277	0.278
ν _B	949.891	921.461	934.933	⁵ J _{B,3}	0.255	0.276	0.263
ν _C	1242.187	1292.624	1321.868	⁶ J _{A,4}	-0.309	-0.347	-0.358
ν _{CHB}	483.147	503.633	498.340	⁶ J _{B,4}	-0.387	-0.367	-0.375
² J _{A,B}	-13.826	-14.053	-14.012	⁵ J _{C,2}	±0.023	±0.030	±0.024
³ J _{A,C}	7.620	7.425	7.506	⁶ J _{C,3}	±0.011	±0.033	±0.012
³ J _{B,C}	6.622	6.776	6.626	⁷ J _{C,4}	±0.014	±0.031	±0.011
³ J _{C,CHB}	6.620	6.627	6.605	⁶ J _{CH3,2}	±0.024	±0.032	±0.028
⁴ J _{A,CHB}	± 0.121	±0.030	± 0.009	⁷ J _{CH3,3}	±0.020	±0.033	±0.017
⁴ J _{B,CHB}	± 0.125	±0.057	± 0.051	⁸ J _{CH3,4}	±0.024	±0.032	±0.015
³ J _{2,3}	7.661	7.671	7.691	Calculated trans	6592	6660	6592
³ J _{3,4}	7.461	7.464	7.463	Assigned trans	5453	4717	5849
⁴ J _{2,4}	1.249	1.261	1.259	Total Peaks	1067	1378	803
⁴ J _{2,6}	1.937	1.942	1.928	Largest Diff	0.017	0.015	0.018
⁴ J _{2,5}	1.444	1.463	1.450	RMS Deviation	0.007	0.007	0.007

^a Standard deviations for the spectral parameters in all three solvents are ≤ 0.0006 Hz. ^b All values are in Hertz

Figure 3.1.2

The aromatic region of the ^1H NMR spectrum of the 5 mol % 2-bromo-1-phenylpropane in CD_2Cl_2 . Simulation required lorentzian lineshapes 0.05 Hz wide. Spectral processing was performed with GB = 0.40 and LB = -0.10.

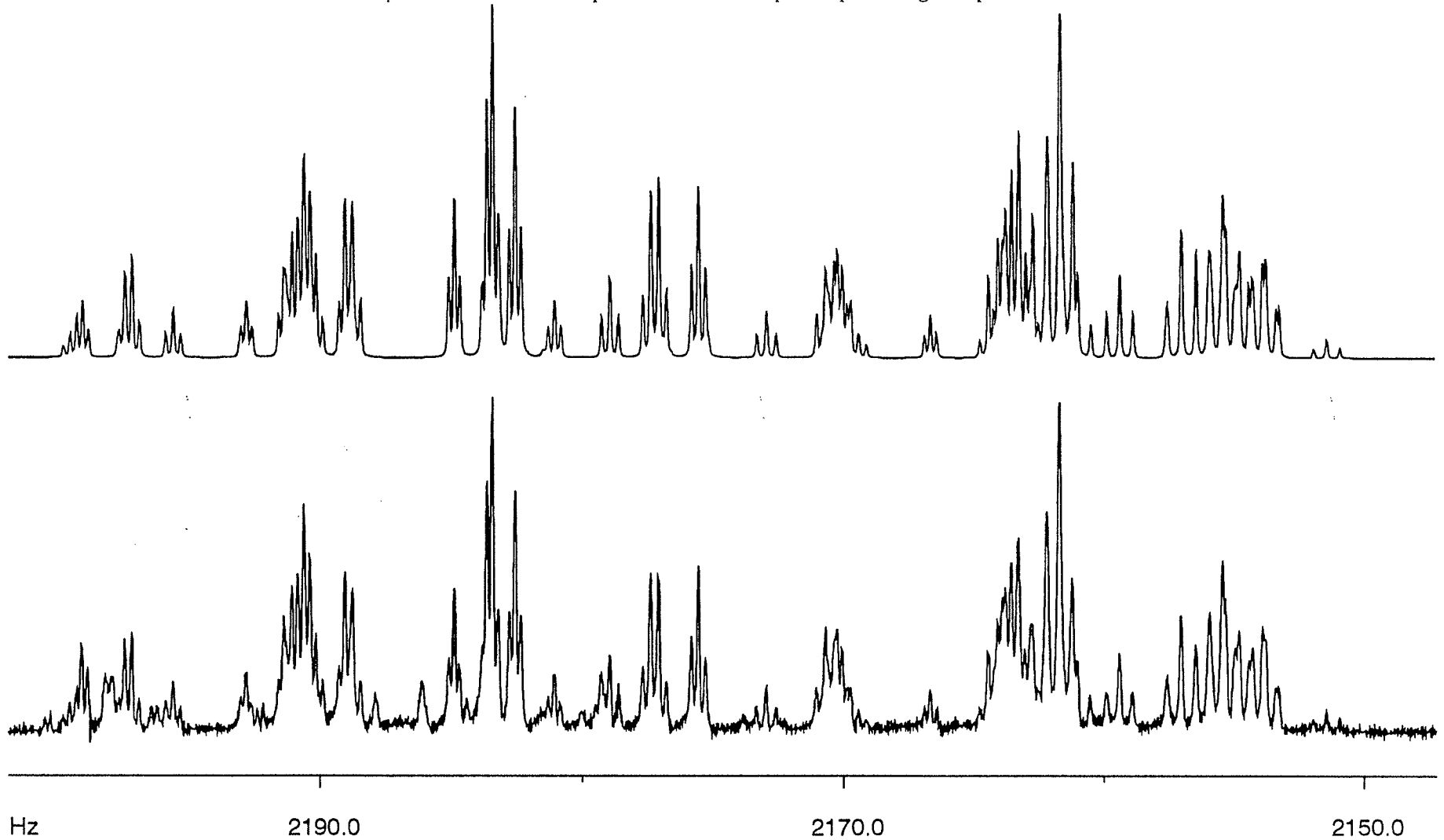


Figure 3.1.3a

The methylene region of the ^1H NMR spectrum of the 5 mol % 2-bromo-1-phenylpropane in CD_2Cl_2 . Simulation required lorentzian lineshapes 0.10 Hz wide. Spectral processing was performed with GB = 0.60 and LB = -0.10.

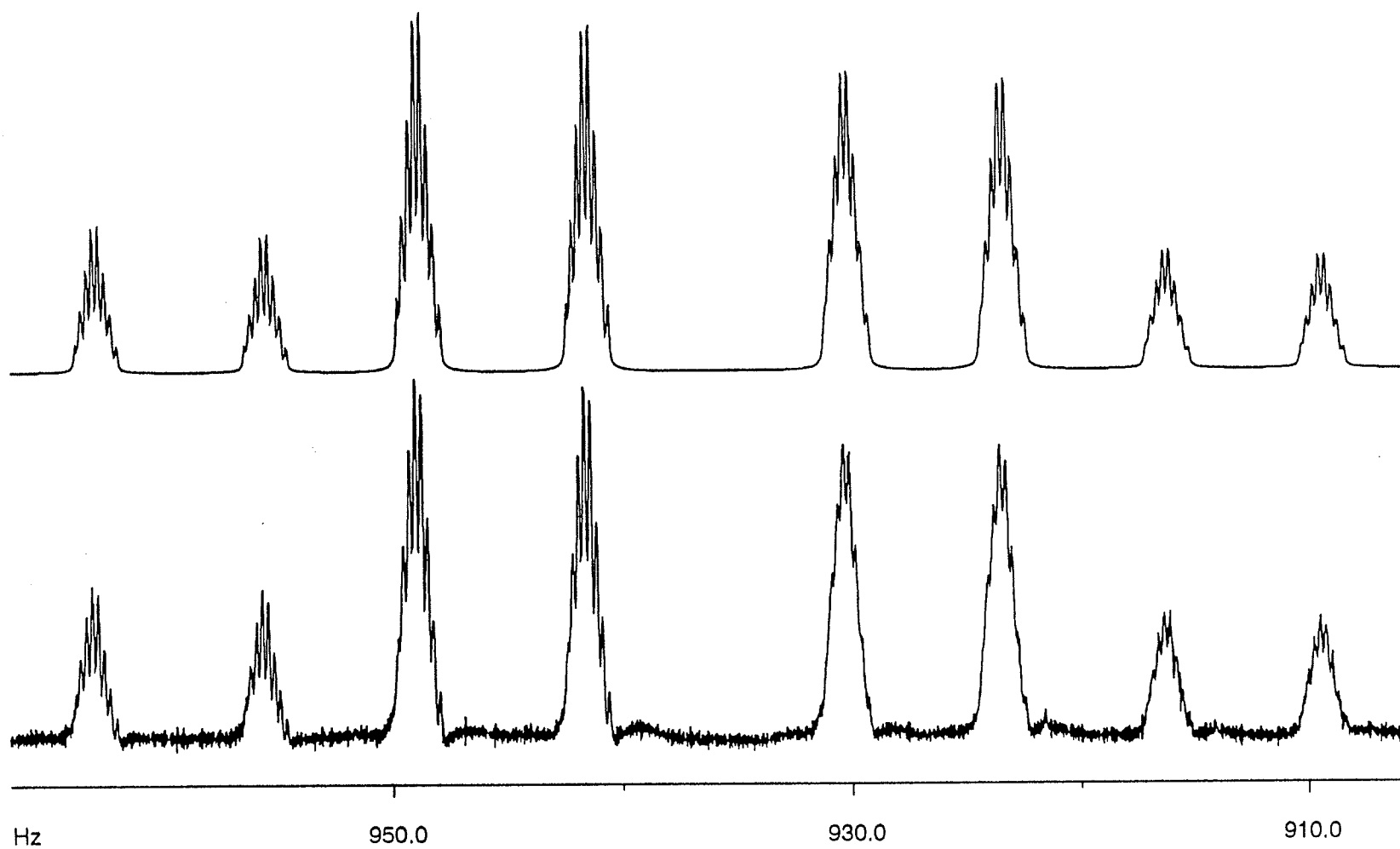


Figure 3.1.3b

The methylene region of the ^1H NMR spectrum of the 5 mol % 2-bromo-1-phenylpropane in CD_2Cl_2 . Simulation required gaussian lineshapes 0.04 Hz wide. Spectral processing was performed with GB = 0.40 and LB = -0.23.

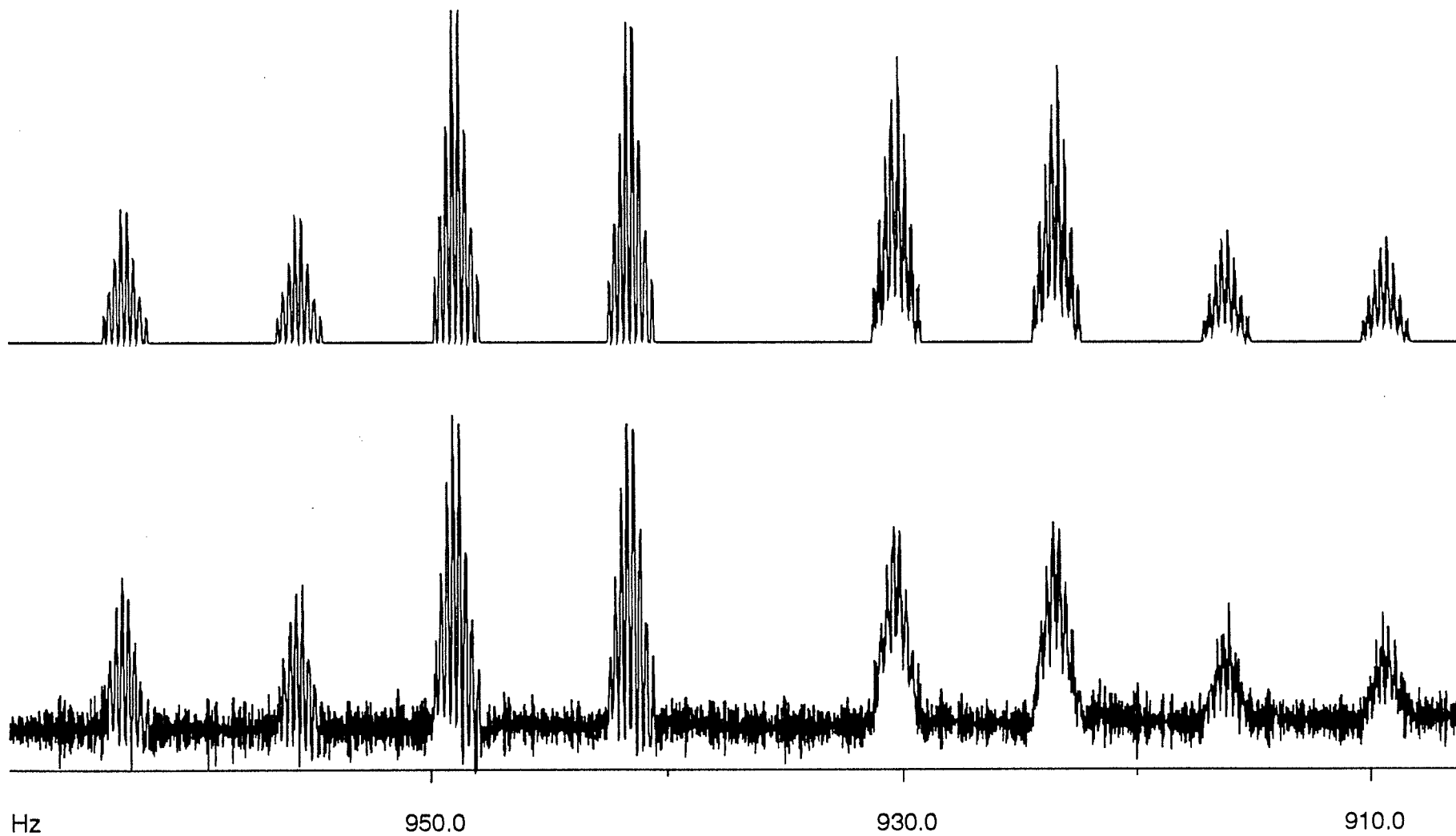


Figure 3.1.4 The methine region of the ^1H NMR spectrum of the 5 mol % 2-bromo-1-phenylpropane in CD_2Cl_2 . Simulation required lorentzian lineshapes 0.09 Hz wide. Spectral processing was performed with GB = 0.05 and LB = -0.15.

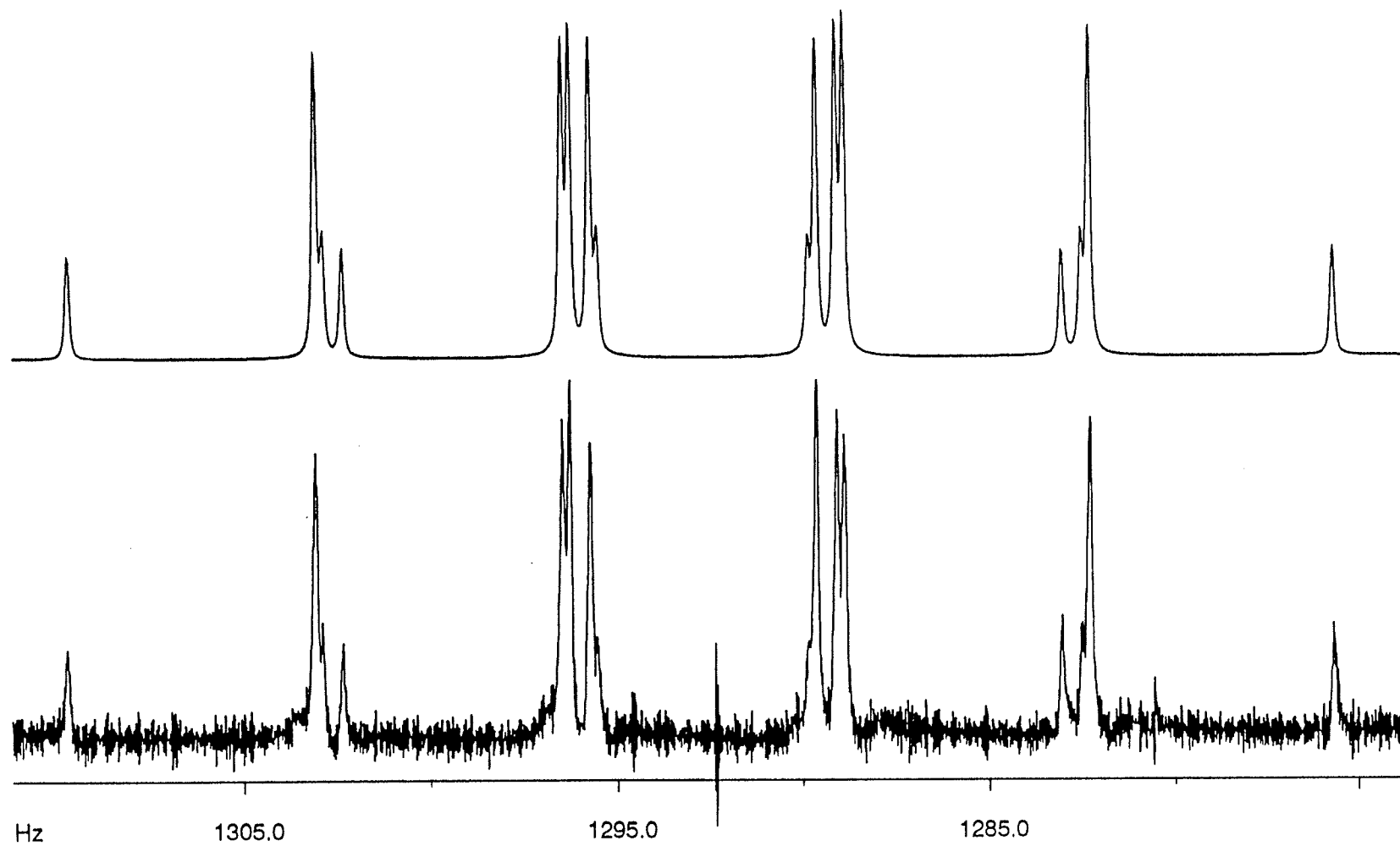
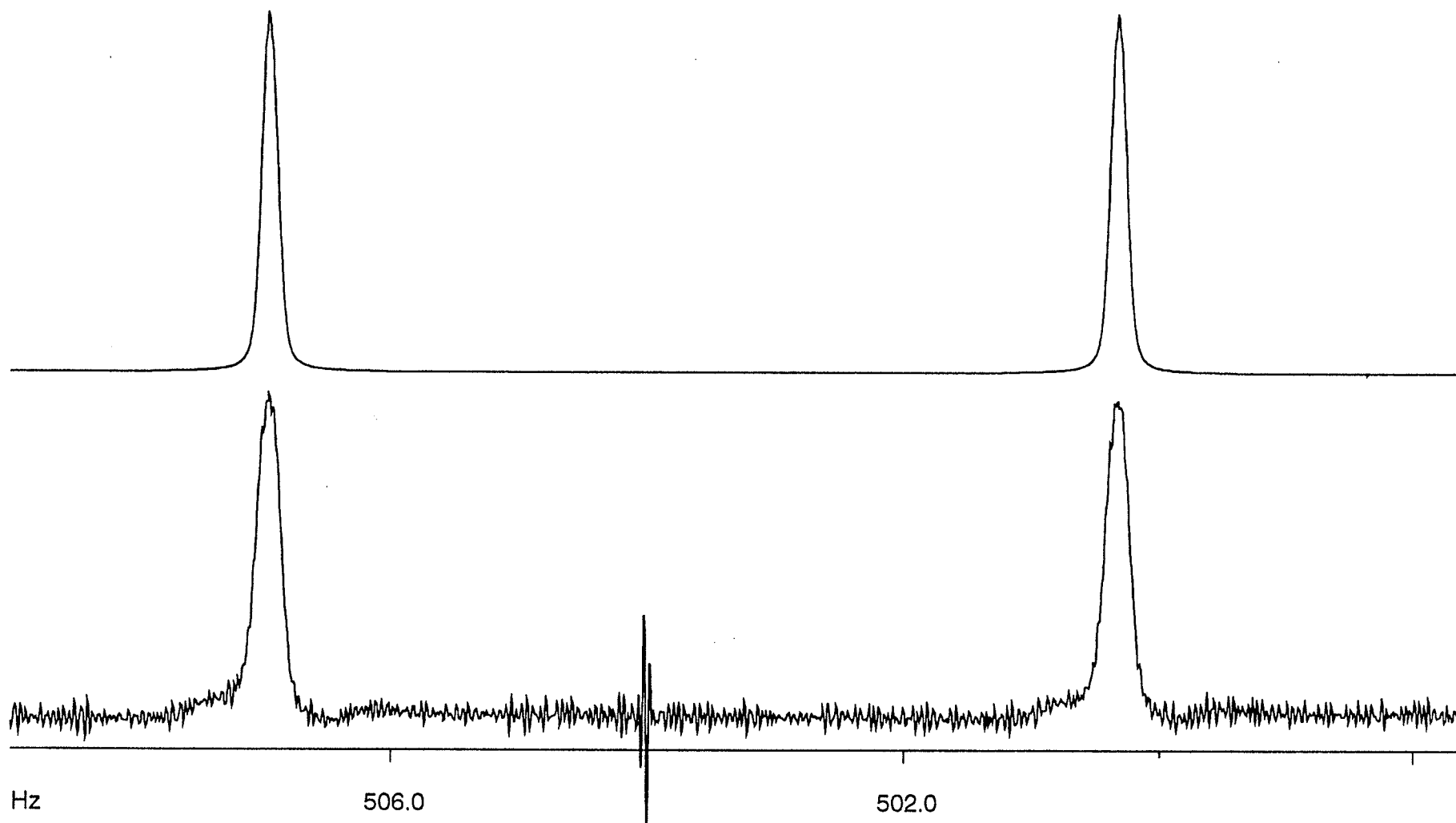


Figure 3.1.5

The methyl region of the ^1H NMR spectrum of the 5 mol % 2-bromo-1-phenylpropane in CD_2Cl_2 . Simulation required lorentzian lineshapes 0.045 Hz wide. Spectral processing was performed with GB = 0.60 and LB = -0.13.



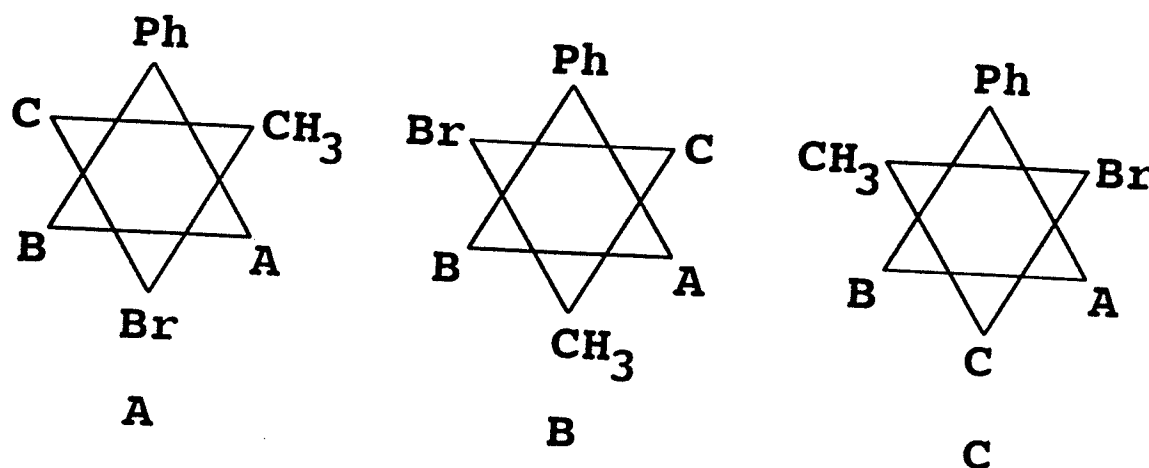
3.2 The molecular orbital calculations for 2-bromo-1-phenylpropane

Tables 3.2.1 and 3.2.2 show the relative heats of formation (AM1) and relative energies (STO-3G) as a function of θ and ϕ . θ and ϕ in this case and throughout the study are normally defined as the torsion angles [$90^\circ - C_8C_7C_1C_2$], and $C_9C_8C_7C_1$ (refer to figure 3.1.1). Note that only part of the surface is reported. The perpendicular form refers to the structure where $\theta = 0^\circ$. The angle ϕ is the torsion angle about the C_7-C_8 bond, which is zero when the phenyl group and the methyl group are coplanar. The outlined values roughly trace out the troughs along the θ dimension, used to calculate the energy profile about θ for rotamers A and B (see section 2.2.1).

Figures 3.2.2 and 3.2.3 are 3-dimensional plots of the aforementioned data. In this case angle θ is defined as the torsion angle $C_8C_7C_1C_2$. These plots also used negative angles for ϕ , where values past 180° increase from -180° (at 180°) to 0° (at 360°).

Tables 3.2.3 and 3.2.4 correspond to the energy profiles of rotation about θ for each rotamer state and their respective fits to the 17 term Fourier series. The results from calculation using the AM1, STO-3G, and STO-3G* basis sets are summarised. Rotamers A, B, and C refer to values of ϕ near 300° (-60°), 180° (-180°) and 60° , respectively (see figure 3.2.1 below). In this case the energies for each curve are calculated relative to their respective minima. Figure 3.2.4 to 3.2.7 are the corresponding plots.

Figure 3.2.1 The Newman projections for 2-bromo-1-phenylpropane



Tables 3.2.6 and 3.2.7 correspond to the energy profile of rotation about ϕ for the AM1, STO-3G and STO-3G* basis sets, and their fits to the Fourier series. Figure 3.2.7 is the graphical representation.

Table 3.2.8 summarizes the results of the calculations which allowed θ and ϕ to optimize. Further calculations are also shown in which the ring hydrogen atoms were allowed to deviate from the aromatic plane.

Table 3.2.1

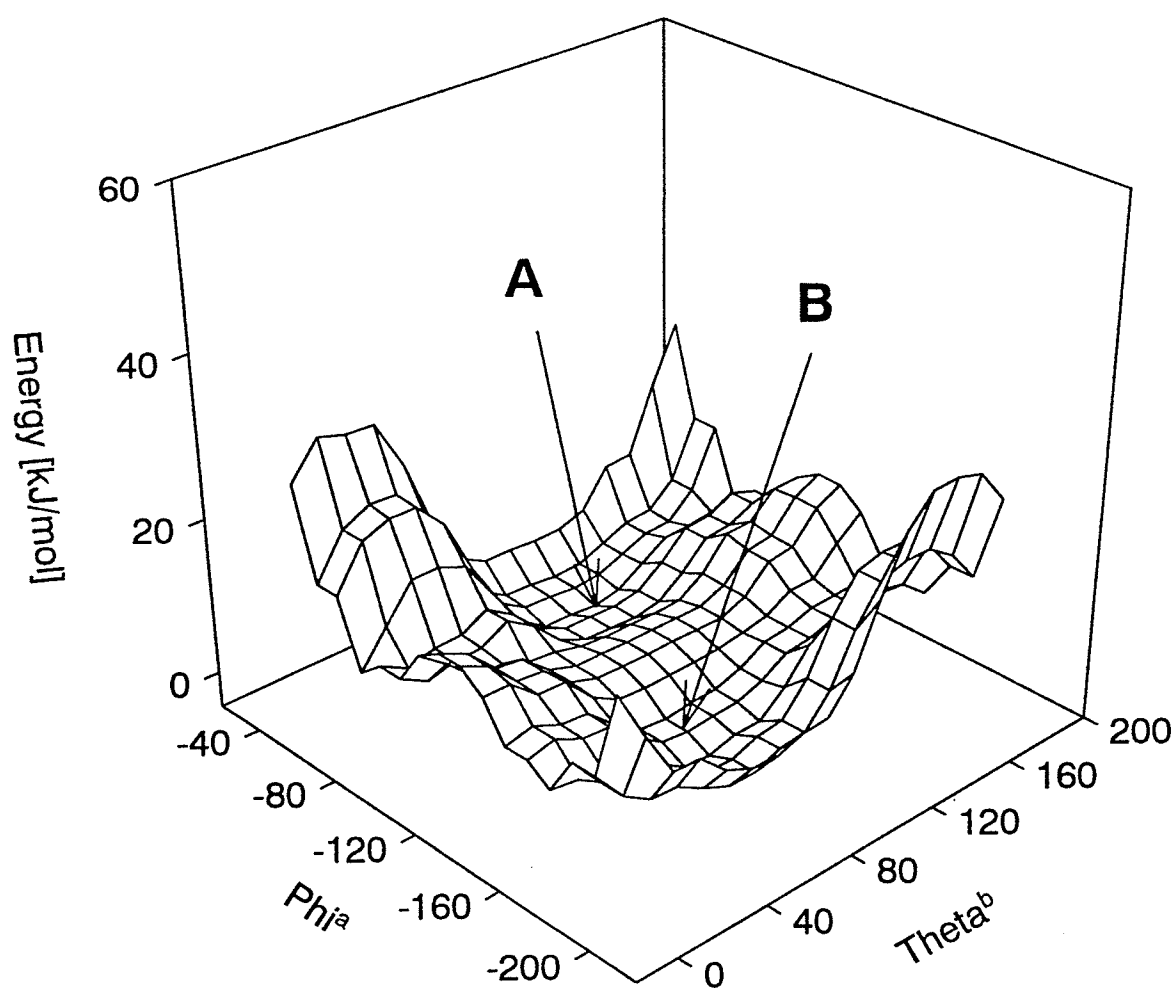
Relative heat of formation from AM1 as a function of phenyl rotation (θ) and rotation about the $C_\alpha-C_\beta$ bond of the sidechain (ϕ).

θ	Φ	315	300	285	270	255	240	225	210	195	180	165	Φ	θ
				A					B					
0		5.27 ^a	1.87	0.87	2.15	4.17	5.01	3.82	1.74	0.90	2.46	6.18		0
15		7.18	4.10	3.34	3.80	4.55	5.05	3.77	1.39	0.00	1.16	5.00		15
30		13.4	10.2	8.46	7.25	5.37	5.16	4.03	1.78	0.32	1.28	5.20		30
45		22.3	17.6	13.6	9.51	5.78	6.31	5.97	4.08	2.35	2.80	6.76		45
60		28.8	21.5	15.0	7.54	7.13	9.58	9.68	7.40	4.78	4.78	10.0		60
75		29.9	19.9	10.5	6.68	10.4	13.3	12.6	9.11	5.82	7.25	16.1		75
90		25.6	14.5	6.18	8.62	13.1	14.9	12.7	8.30	6.35	11.4	22.7		90
105		18.8	7.43	5.84	9.79	13.1	13.4	10.1	6.66	8.09	15.7	27.3		105
120		10.8	4.47	5.42	8.24	10.2	9.56	6.92	6.10	9.89	18.0	28.3		120
135		6.29	3.11	3.22	4.91	6.32	6.15	5.12	5.95	9.93	17.0	24.8		135
150		5.10	1.82	1.12	2.50	4.25	4.91	4.46	4.82	7.53	12.5	17.8		150
165		4.99	1.52	0.51	1.98	4.08	4.93	4.00	2.91	3.64	6.46	10.2		165
180		5.27	1.87	0.87	2.15	4.17	5.01	3.82	1.74	0.90	2.46	6.18		180
0														0
	Φ	315	300	285	270	255	240	225	210	195	180	165	Φ	

^aAll values reported are in kJ/mol relative to the absolute minimum value of 0.014308 A.U. at $\theta = 15^\circ$ and $\phi = 195^\circ$

Figure 3.2.2

3-Dimensional plot of relative heats of formation from AM1 as a function of phenyl rotation (θ) and rotation about the C_α - C_β bond of the sidechain (ϕ).



^a $\phi = \langle C_9C_8C_7C_1 \rangle$ using negative angles.
^b $\theta = \langle C_8C_7C_1C_2 \rangle$

Table 3.2.2

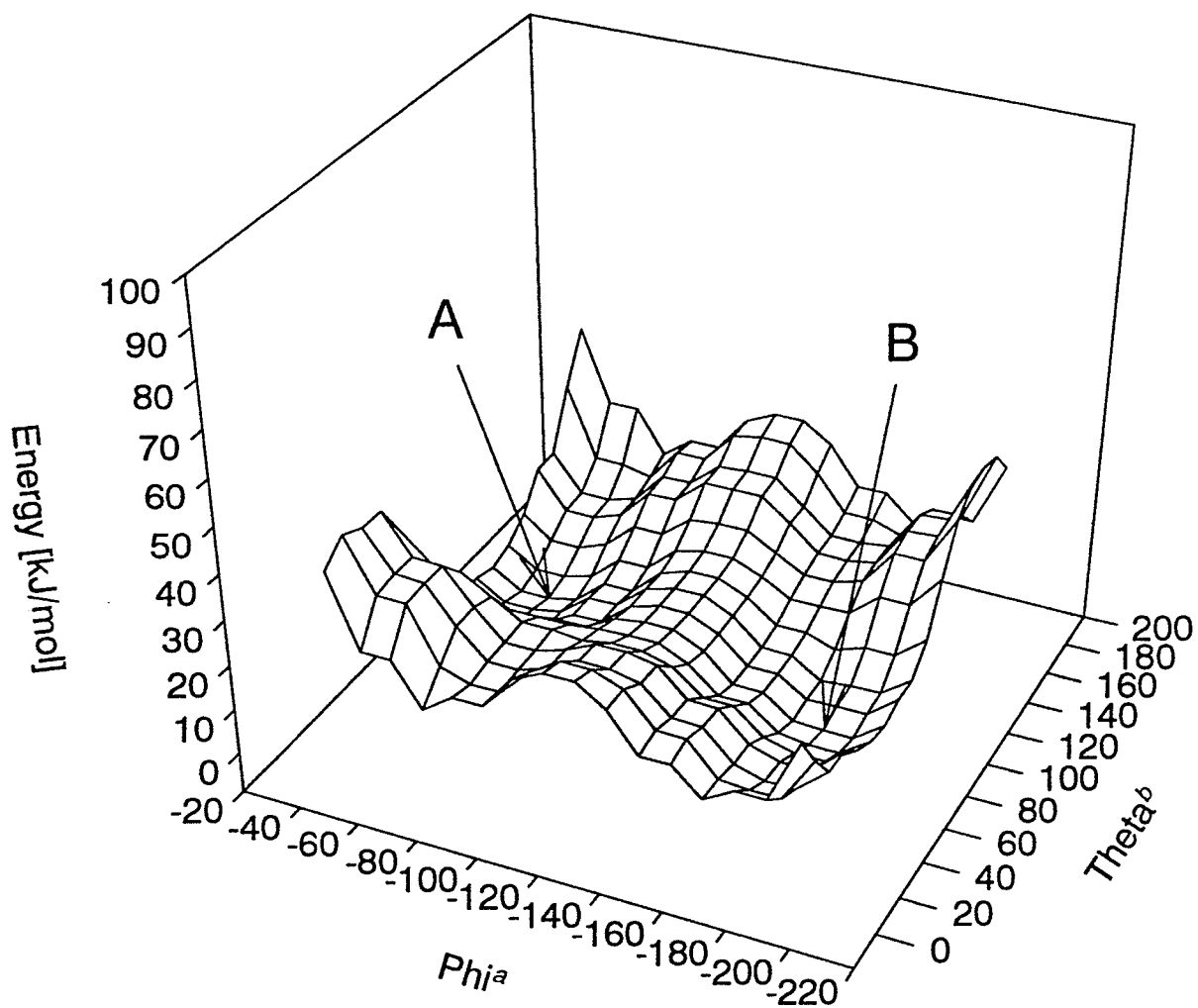
Relative energy from STO-3G as a function of phenyl rotation (θ) and rotation about the C_α - C_β bond of the sidechain (ϕ).

θ	Φ	315	300	285	270	255	240	225	210	195	180	165	Φ	θ	
			A						B						
0		5.42 ^a	1.48	2.59	7.61	13.0	15.0	12.0	6.19	1.98	2.34	7.40		0	
15		10.6	6.83	7.47	10.8	14.3	15.5	12.2	6.26	1.41	1.04	5.93		15	
30		20.3	16.3	15.3	15.5	16.2	16.5	13.5	7.96	3.06	2.17	6.69		30	
45		31.8	26.2	22.3	18.4	17.7	18.9	16.9	11.8	6.45	4.73	9.12		45	
60		40.2	31.9	24.1	17.8	19.8	23.1	21.7	15.9	9.49	7.31	13.3		60	
75		42.6	31.2	19.1	16.9	23.3	27.4	25.0	17.7	10.5	10.0	20.4		75	
90		38.8	23.0	13.6	18.2	26.1	29.0	24.9	16.5	10.6	14.5	28.8		90	
105		28.6	13.0	11.6	19.0	25.9	27.2	21.8	14.0	11.8	19.7	35.0		105	
120		16.2	7.82	10.1	16.9	22.4	22.6	17.6	12.2	13.3	22.5	36.4		120	
135		8.99	4.32	6.62	12.5	17.4	18.1	14.5	11.1	12.9	21.0	31.8		135	
150		5.33	1.26	2.94	8.44	13.9	15.6	13.0	9.43	9.78	15.0	22.9		150	
165		3.99	0.00	1.34	6.85	12.7	14.9	12.2	7.40	5.15	7.31	12.7		165	
180		5.42	1.48	2.59	7.61	13.0	15.0	12.0	6.19	1.98	2.34	7.40		180	
θ	Φ	315	300	285	270	255	240	225	210	195	180	165	Φ	θ	

^aAll values reported are in kJ/mol relative to the absolute minimum value of -2887.724483 A.U. at $\theta = 165^\circ$ and $\phi = 300^\circ$

Figure 3.2.3

3-Dimensional plot of relative energy from STO-3G as a function of phenyl rotation (θ) and rotation about the $C_\alpha-C_\beta$ bond of the sidechain (ϕ).



$${}^a\phi = \langle C_9 C_8 C_7 C_1 \text{ using negative angles.} \\ {}^b\theta = \langle C_8 C_7 C_1 C_2$$

Table 3.2.3

Energies of the rotamers of 2-bromo-1-phenylpropane as a function of sidechain angular displacement with respect to the perpendicular form.

Angle θ	ROTAMER A			ROTAMER B			ROTAMER C		
	AM1	STO-3G	STO-3G*	AM1	STO-3G	STO-3G*	AM1	STO-3G	STO-3G*
0	0.409 ^a	1.350	1.323	0.845	0.975	0.934	0.000	0.000	0.000
15	2.886	6.551	6.429	0.000	0.000	0.000	2.161	1.621	1.691
30	----- ^b	15.366	15.126	0.303	1.354	1.421	4.184	4.963	5.060
45	5.250	17.563	17.557	2.192	4.092	4.189	5.655	8.007	8.048
60	5.910	17.658	17.645	4.263	6.574	6.635	7.308	10.914	10.936
75	6.055	16.245	16.223	5.561	8.446	8.423	8.907	13.716	13.780
90	5.547	13.576	13.554	6.287	9.857	9.737	10.113	16.004	16.142
105	4.641	10.398	10.377	6.455	10.905	10.684	10.731	17.488	17.684
120	3.612	7.261	7.244	5.871	11.068	10.829	10.364	17.496	17.703
135	2.084	4.079	4.066	5.005	10.300	10.154	8.814	15.537	15.744
150	0.451	1.230	1.225	4.348	8.271	8.261	4.217	9.623	9.721
165	0.000 ^c	0.000	0.000	2.769	4.487	4.491	0.358	2.917	2.926
180	0.409	1.350	1.323	0.845	0.975	0.934	0.00	0.000	0.000

^aAll values are in kJ/mol. ^bNo optimal energy value found at $\theta = 30^\circ$ for rotamer A. ^cAll values in each column relative to the minimum value in that column.

Table 3.2.4

Energies of the three rotamers of 2-bromo-1-phenylpropane as a function of the angle of the sidechain with respect to the perpendicular form, fit to a 17 term Fourier series

F.S ^a	ROTAMER A			ROTAMER B			ROTAMER C		
	AM1	STO-3G	STO-3G*	AM1	STO-3G	STO-3G*	AM1	STO-3G	STO-3G*
C ₀	3.47 ^b	9.28	9.24	3.66	6.36	6.31	6.067	9.86	9.95
S ₁	0.00	0.00	0.00	0.00	0.00	0.00	0.00	0.00	0.00
C ₁	0.00	0.01	0.01	0.00	0.00	0.00	0.00	0.00	0.00
S ₂	1.84	6.82	6.78	-1.59	-3.26	-3.15	-0.97	-3.30	-3.36
C ₂	-2.34	-5.62	-5.65	-2.70	-4.29	-4.23	-4.93	-7.67	-7.72
S ₃	0.00	0.00	0.00	0.00	0.00	0.00	0.00	0.00	0.00
C ₃	0.00	0.01	0.01	0.00	0.00	0.00	0.00	0.00	0.00
S ₄	0.51	0.64	0.59	-0.62	-0.64	-0.70	0.96	0.64	0.69
C ₄	-0.33	-1.80	-1.79	-0.01	-0.88	-0.91	-1.05	-1.83	-1.89
S ₅	0.00	0.00	0.00	0.00	0.00	0.00	0.00	0.00	0.00
C ₅	-0.00	0.01	0.01	0.00	0.00	0.00	0.00	0.00	0.00
S ₆	0.19	-0.18	-0.20	-0.14	-0.12	-0.13	0.52	0.41	0.43
C ₆	-0.15	-0.64	-0.60	0.01	-0.15	-0.17	-0.14	-0.36	-0.38
S ₇	0.00	0.00	0.00	0.00	0.00	0.00	0.00	0.00	0.00
C ₇	-0.01	0.01	0.01	0.00	0.00	0.00	0.00	0.00	0.00
S ₈	-0.08	-0.44	-0.42	0.08	0.06	0.06	0.08	0.08	0.08
C ₈	-0.15	-0.12	-0.09	-0.08	-0.06	-0.06	0.08	0.03	0.03
Δ ^c	0.05	0.10	0.10	0.02	0.01	0.01	0.04	0.02	0.03

^aCoefficients of the Fourier series. ^bAll values are in kJ/mol. ^cStandard deviation.

Table 3.2.5

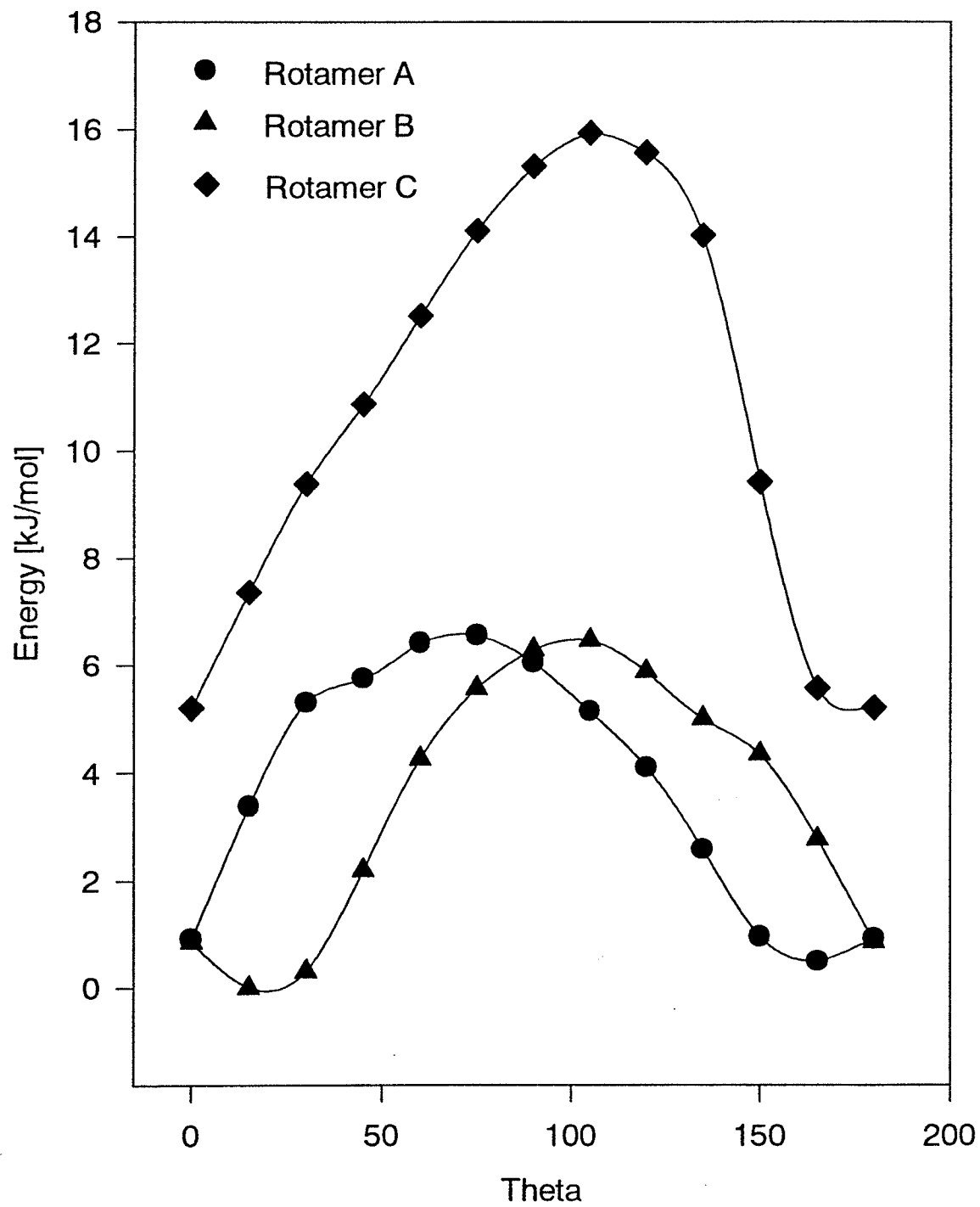
Relative energies of the three rotamers of 2-bromo-1-phenylpropane from AM1, STO-3G and STO-3G* as a function of sidechain angular displacement with respect to the perpendicular form.

Angle θ	AM1			STO-3G			STO3G*		
	Energy A	Energy B	Energy C	Energy A	Energy B	Energy C	Energy A	Energy B	Energy C
0	0.906 ^{a,b}	0.845	5.202	1.350 ^c	1.673	4.270	1.323 ^c	1.590	4.168
15	3.382	0.000	7.363	6.551	0.698	5.891	6.429	0.656	5.859
30	----- ^d	0.303	9.386	15.366	2.052	9.234	15.126	2.077	9.228
45	5.746	2.192	10.857	17.563	4.790	12.277	17.556	4.846	12.215
60	6.406	4.263	12.509	17.658	7.273	15.184	17.645	7.291	15.104
75	6.551	5.561	14.109	16.245	9.144	17.986	16.223	9.0796	17.948
90	6.043	6.287	15.315	13.576	10.556	20.275	13.554	10.393	20.309
105	5.137	6.455	15.933	10.398	11.603	21.758	10.377	11.340	21.852
120	4.108	5.871	15.566	7.261	11.766	21.766	7.244	11.486	21.871
135	2.580	5.005	14.016	4.079	10.998	19.807	4.066	10.810	19.911
150	0.948	4.348	9.419	1.230	8.969	13.893	1.225	8.917	13.889
165	0.496	2.769	5.560	0.000	5.185	7.186	0.000	5.147	7.094
180	0.906	0.844	5.202	1.350	1.673	4.270	1.323	1.590	4.168

^aAll values in kJ/mol. ^bAll AM1 values are relative to the AM1 value of rotamer B at $\theta = 15^\circ$. ^cAll STO-3G and STO-3G* values are relative to the STO-3G and STO-3G* value of rotamer A at $\theta = 165^\circ$. ^dNo optimal energy value at $\theta = 30^\circ$ for rotamer A.

Figure 3.2.4

Relative^a energies of the three rotamers of 2-bromo-1-phenylpropane from AM1, as a function of phenyl rotation (θ) from the perpendicular form^b.

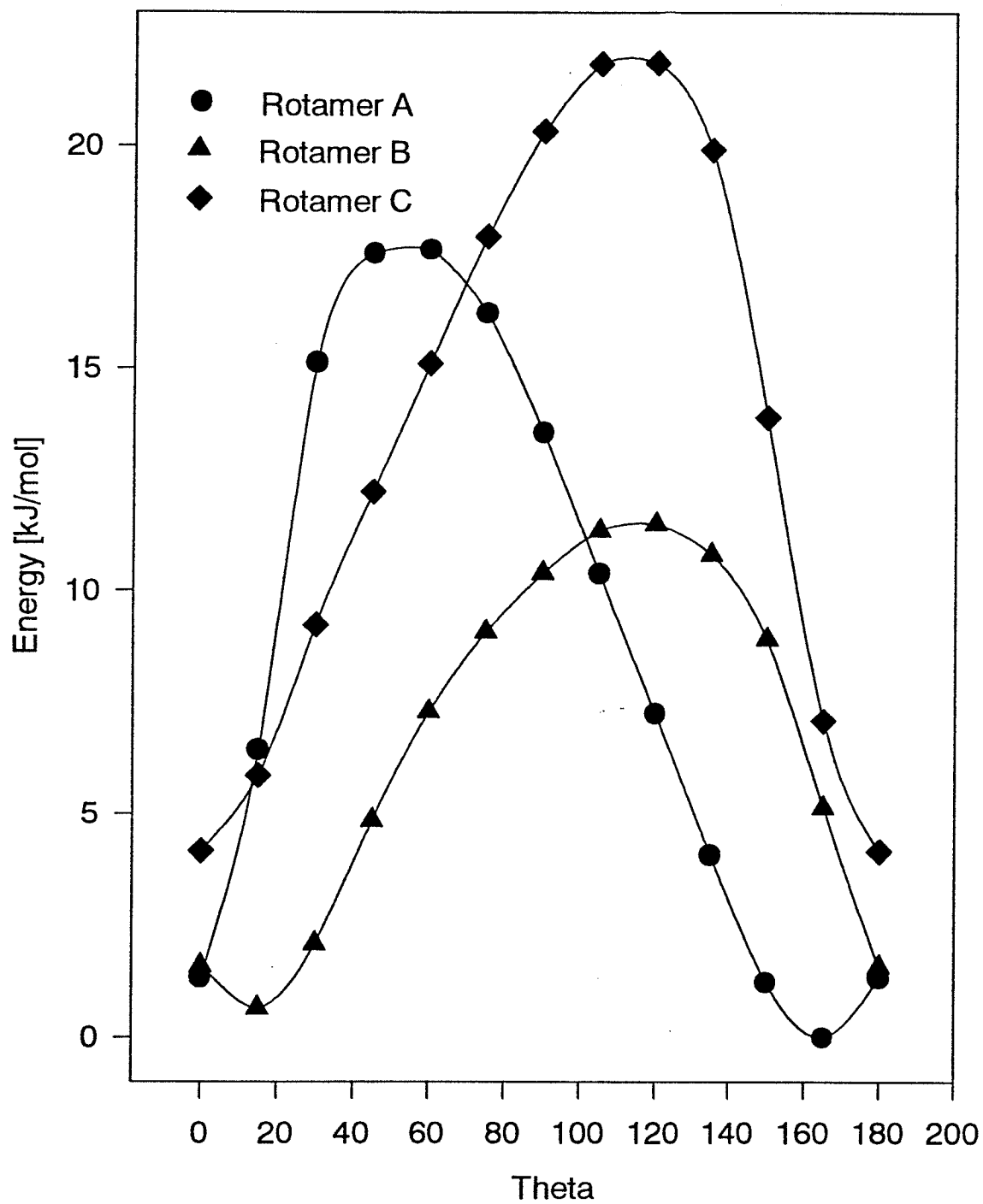


^aAll values are reported relative to the minimum energy of rotamer A.

^bIn the perpendicular form $\theta = 0^\circ$.

Figure 3.2.5

Relative^a energies of the three rotamers of 2-bromo-1-phenylpropane from STO-3G, as a function of phenyl rotation (θ) from the perpendicular form^b.

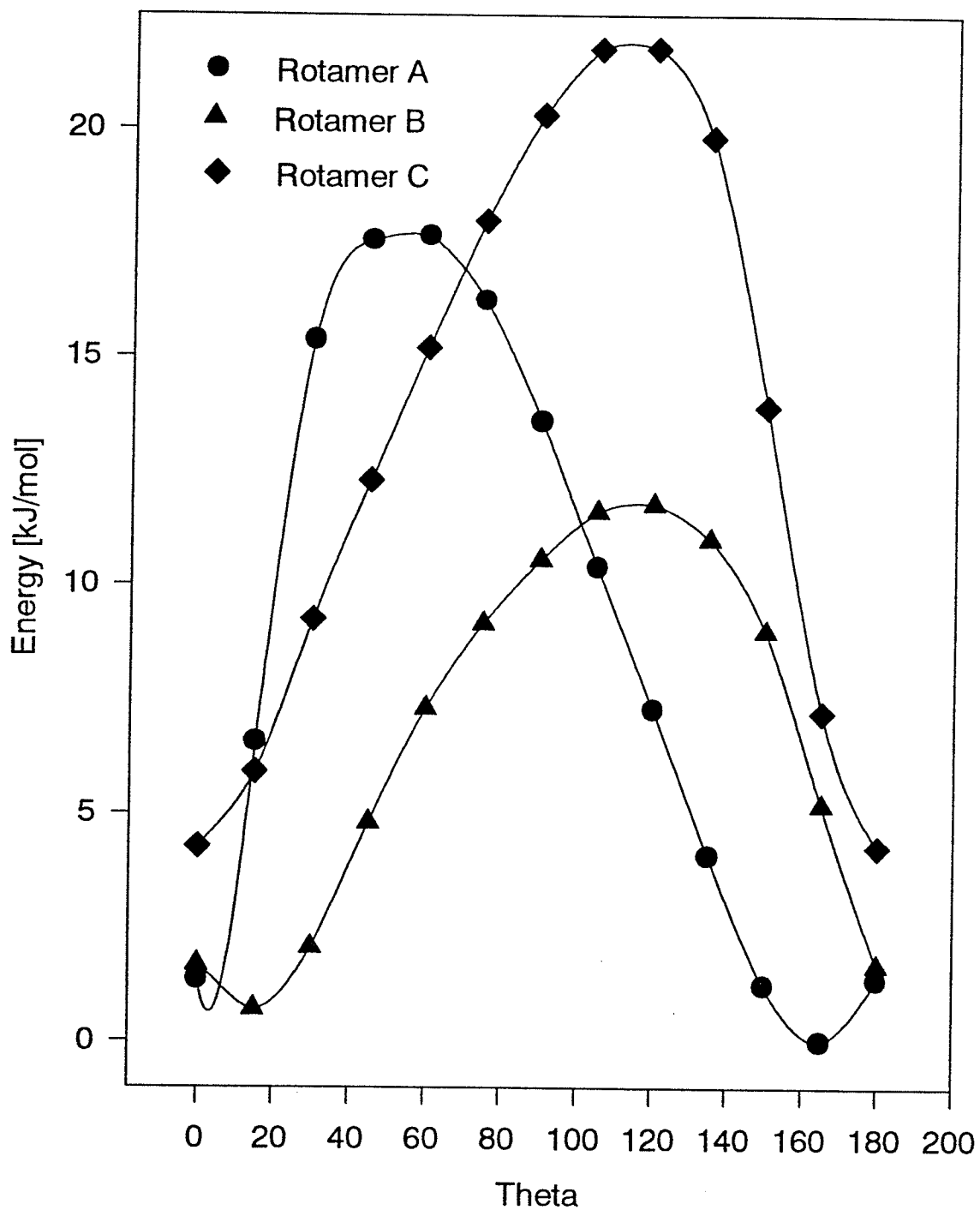


^aAll values are reported relative to the minimum energy of rotamer A.

^bIn the perpendicular form $\theta = 0^\circ$.

Figure 3.2.6

Relative^a energies of the three rotamers of 2-bromo-1-phenylpropane from STO-3G*, as a function of phenyl rotation (θ) from the perpendicular form^b.



^aAll values are reported relative to the minimum energy of rotamer A.

^bIn the perpendicular form $\theta = 0^\circ$.

Table 3.2.6

Energy of 2-bromo-1-phenylpropane as a function of rotation about the sidechain C_α-C_β (ϕ).

Angle ϕ	AM1	AM1 ^a	STO-3G	STO-3G*	STO-3G* ^a
0	14.174 ^b	14.179	22.592	22.282	22.286
15	12.648	12.653	19.712	19.255	19.260
30	9.469	9.476	12.576	12.168	12.174
45	6.542	6.545	6.349	6.127	6.127
60	5.008	5.011	4.079	3.965	3.951
75	6.428	6.430	6.816	6.734	6.712
90	9.870	9.870	13.288	13.154	13.144
105	13.664	13.661	20.054	19.787	19.791
120	15.968	15.967	23.531	23.073	23.081
135	14.681	14.682	21.175	20.590	20.599
150	10.333	10.333	13.979	13.417	13.426
165	4.980	4.978	5.919	5.528	5.536
180	1.096	1.095	1.043	0.882	0.887
195	0.000	0.000	1.332	1.373	1.376
210	1.429	1.431	6.059	6.178	6.181
225	3.829	3.856	11.961	12.002	12.021
240	4.924	4.930	14.887	14.785	14.789
255	4.102	4.107	12.688	12.530	12.532
270	2.032	2.036	6.826	6.679	6.678
285	0.557	0.564	1.333	1.254	1.252
300	1.569	1.576	0.000	0.000	0.000
315	5.022	5.027	3.991	4.036	4.039
330	9.431	9.435	11.656	11.668	11.670
345	12.935	12.940	19.231	19.112	19.115
360	14.174	14.179	22.592	22.282	22.286

^a Relaxed geometries ^bAll values are in kJ/mol.

Table 3.2.7

Energy of sidechain rotation in 2-bromo-1-phenylpropane as a function of ϕ , fit to a Fourier series truncated at 17 terms.

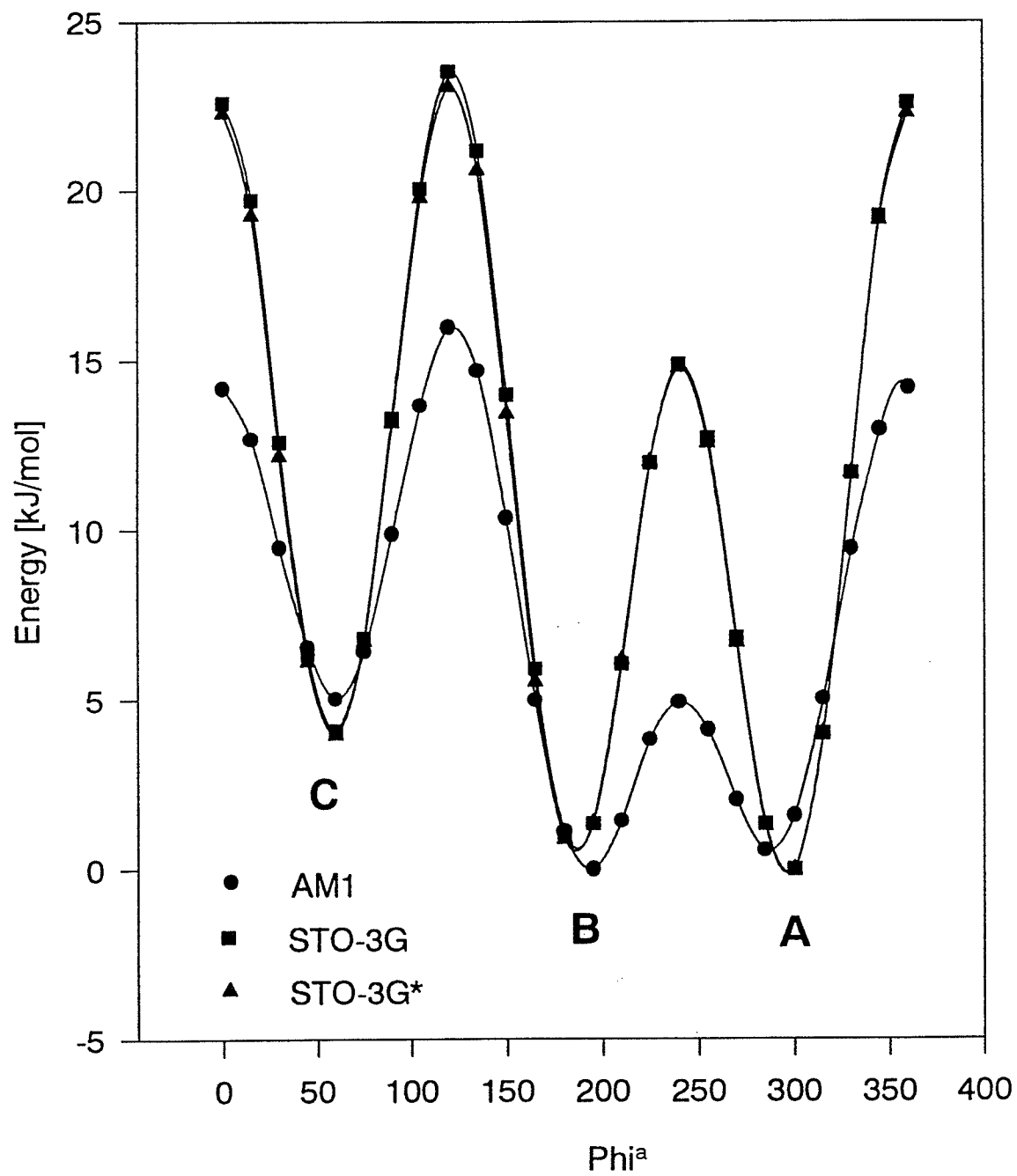
F.S ^a	AM1	STO-3G	STO-3G*
C ₀	7.11 ^b	10.88	10.69
S ₁	4.14	3.65	3.49
C ₁	2.03	1.34	1.36
S ₂	-2.34	-1.66	-1.58
C ₂	0.83	0.75	0.70
S ₃	0.19	0.42	0.24
C ₃	4.54	9.32	9.22
S ₄	-0.20	-0.34	-0.34
C ₄	-0.36	0.03	0.03
S ₅	-0.04	-0.01	-0.03
C ₅	-0.04	0.11	0.11
S ₆	0.03	0.07	0.06
C ₆	0.01	0.14	0.14
S ₇	0.00	0.01	0.01
C ₇	-0.01	0.01	0.02
S ₈	-0.02	0.02	0.01
C ₈	0.04	0.02	0.03
Δ^c	0.02	0.01	0.01

^a Fourier series coefficients

^b All values are in kJ/mol.

^c Standard deviation.

Figure 3.2.7
Relative energies from AM1, STO-3G and STO-3G* as a function of sidechain rotation (ϕ).



^aRotation about $\phi = C_9C_8C_7C_1$.

Table 3.2.8

Fully optimized energies of the three rotamers of 2-bromo-1-phenylpropane

AM1		Rotamer A		Rotamer B		Rotamer C	
Absolute Energy ^a		0.014485		0.014277		0.016191	
ΔE^b	μ^c	0.546	0.718	0.000	0.641	5.026	0.624

STO-3G							
Absolute Energy		-2887.724549		-2887.724289		-2887.722930	
ΔE	μ	0.000	1.826	0.683	1.797	4.249	1.760

STO-3G (relaxed)							
Absolute Energy		-2887.724553		-2887.724291		-2887.722939	
ΔE	μ	0.000	1.826	0.687	1.799	4.237	1.764

STO-3G*							
Absolute Energy		-2888.414279		-2888.414037		-2888.412697	
ΔE	μ	0.000	1.879	0.636	1.805	4.152	1.764

STO-3G* (relaxed)							
Absolute Energy		-2888.414283		-2888.414040		-2888.412707	
ΔE	μ	0.000	1.878	0.640	1.807	4.139	1.767

^aAll absolute energy values are in atomic units. ^bAll relative energies are in kJ/mol. ^cAll dipole moments are in Debyes.

3.3 FPT MO INDO, CNDO/2 calculations, and classical averaging

Since INDO and CNDO/2 methods are not parameterized for the use of bromine, the chlorine analogue, 2-chloro-1-phenylpropane, is used instead. The geometries of 2-bromo-1-phenylpropane were retained, except that the C-Cl bond length was allowed to optimize at the STO-3G* level. The results of ${}^X J_{Y,Z}$, ${}^{X+1} J_{C,Z}$, ${}^3 J_{Y,C}$, and ${}^4 J_{Y,CH_3}$ (where X=4,5 and 6; Y= H_A, H_B and H_C and Z= H_2, H_3 and H_4) were fit to the 17 term Fourier series.

Figures 3.3.1 to 3.3.9 are some examples where these coupling constants are plotted as a function of ϕ or θ . Figure 3.3.1 shows the vicinal couplings of H_A and H_B with H_C as functions of ϕ . Figure 3.3.2 illustrates the ϕ dependence of the four-bond coupling between the methyl protons and H_A and H_B . In the remaining figures the θ dependence of the coupling between H_A and the protons on the aromatic ring is depicted.

With the energy profiles about θ , $\langle \sin^2(\theta + \pi/6) \rangle$ and $\langle \sin^2(\theta - \pi/6) \rangle$ were calculated for each rotamer at AM1, STO-3G, and STO-3G* levels. The ensemble averages over the three rotamers were also determined. The results of these calculations are tabulated in table 3.3.1. The INDO values for ${}^6 J_{90}(H_A, H_4)$ and ${}^6 J_{90}(H_B, H_4)$ were found for all three rotamers and their ensemble averages were determined according to the AM1, STO-3G and STO-3G* calculations. These numbers are given in table 3.3.2.

Using the energy profiles about ϕ and the INDO and CNDO/2 results for ${}^3 J_{H,H_C}$ and ${}^4 J_{H,CH_3}$, averaged values of these coupling constants were

calculated. Three types of classical averages were found, using the continuous, the 3-cusp and the 3-site methods. These values are arranged in table 3.3.3 according to the basis set employed.

Tables 3.3.4 to 3.3.12 summarize the classical averages for the couplings of H_A , H_B and H_C into the ring. With the θ energy profiles for each basis set, the classical averages were calculated for each rotamer. Three different types of averages were determined. The first was the classical average ($\langle J \rangle_i$). Secondly, for H_A and H_B the classical average was found with θ offset by 120° and -120° . This was done to see whether there is a substituent effect on these couplings which is independent of the shape of the barrier. When the initial angle is offset in this manner, both H_A and H_B experience the same $\langle \sin^2 \theta \rangle$. This calculation was not necessary for H_C . Finally the average was determined without a barrier to rotation ($\langle J \rangle_i^{\text{free}}$). The ensemble averages were calculated for all three types of calculations according to the three bases. Tables 3.3.4, 3.3.5 and 3.3.6 summarize the results for ${}^4J_{A,2}$, ${}^5J_{A,3}$ and ${}^6J_{A,4}$. Tables 3.3.7, 3.3.8 and 3.3.9 show the values for ${}^4J_{B,2}$, ${}^5J_{B,3}$ and ${}^6J_{B,4}$. Tables 3.3.10, 3.3.11 and 3.3.12 report the results for ${}^5J_{C,2}$, ${}^6J_{C,3}$ and ${}^7J_{C,4}$.

Table 3.3.1

Calculation of $\langle \sin^2(\theta + \pi/6) \rangle$ and $\langle \sin^2(\theta - \pi/6) \rangle$ to predict ${}^6J_{A,A}$ and ${}^6J_{B,A}$ for 2-bromo-1-phenylpropane.

Basis	AM1			STO-3G			STO-3G*		
	A	B	C	A	B	C	A	B	C
Rotamer	A	B	C	A	B	C	A	B	C
Population [%]	44.10	51.44	4.46	50.24	42.40	7.36	49.97	42.53	7.50
$\langle \sin^2(\theta + \pi/6) \rangle_i$	0.247 ^a	0.516	0.294	0.116	0.505	0.336	0.117	0.501	0.333
$\langle \sin^2(\theta - \pi/6) \rangle_i$	0.525	0.243	0.327	0.535	0.159	0.230	0.534	0.161	0.231
$\langle \sin^2(\theta + \pi/6) \rangle$	0.387			0.297			0.297		
$\langle \sin^2(\theta - \pi/6) \rangle$	0.371			0.353			0.352		

Table 3.3.2

Calculation of ${}^6J_{90}$ for 2-chloro-1-phenylpropane using INDO results.

Rotamer	A	B	C
${}^6J_{90}[H_A, H_4]_i$	-1.081 ^{a,b}	-1.106	-1.109
${}^6J_{90}[H_B, H_4]_i$	-1.125	-1.082	-1.116
Basis	AM1	STO-3G	STO-3G*
${}^6J_{90}[H_A, H_4]$	-1.097 ^c	-1.094	-1.094
${}^6J_{90}[H_B, H_4]$	-1.103	-1.106	-1.106

^aAll values are in Hertz. ^b INDO values based on 2-chloro-1-phenylpropane. ^cAveraged with populations based on calculations performed with the indicated basis.

Figure 3.3.1

Graphical representation of the FPT MO INDO and CNDO/2 calculations of vicinal coupling constants between H_A , H_B and H_C in the sidechain of 2-chloro-1-phenylpropane.

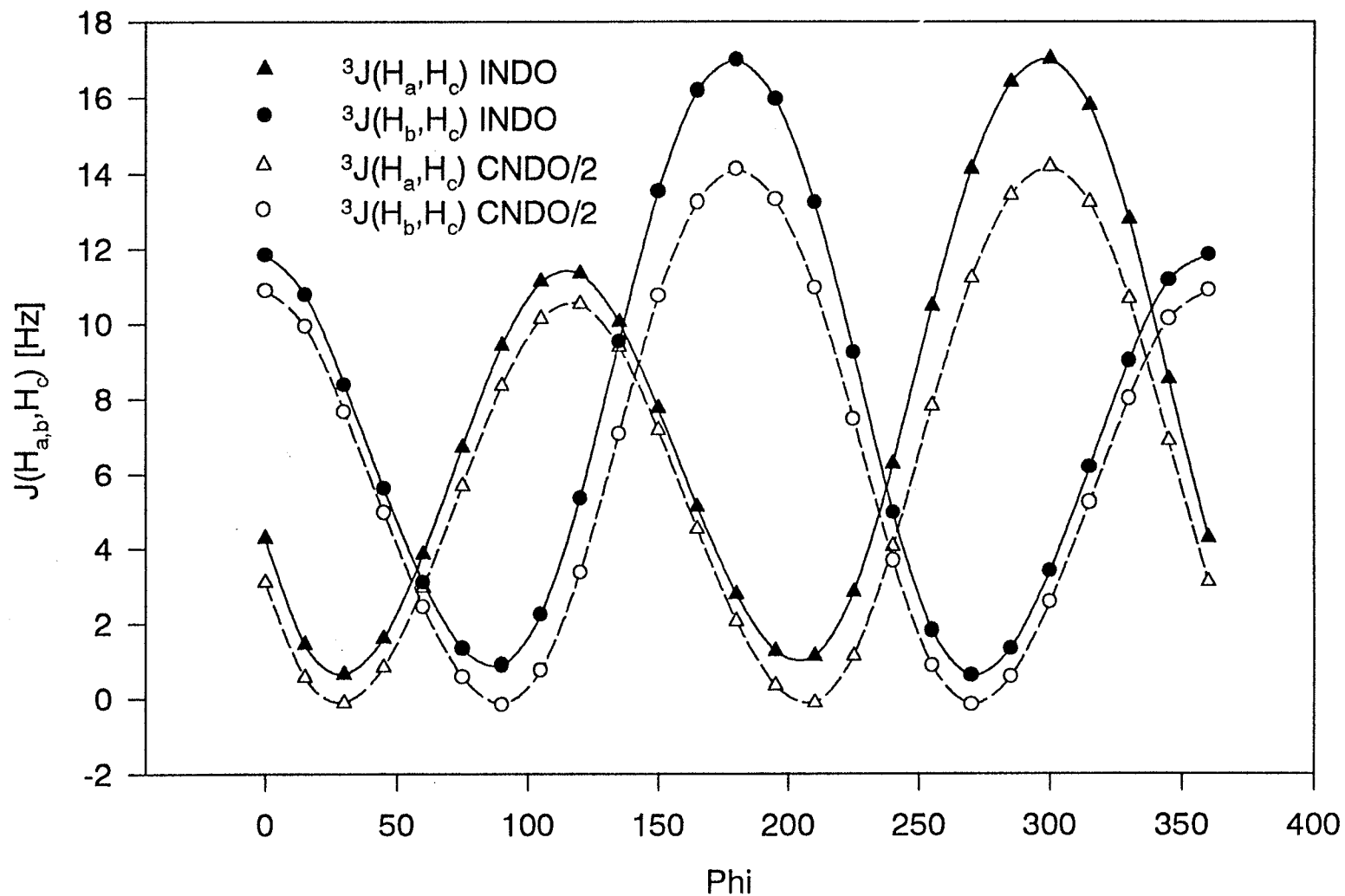


Figure 3.3.2

Graphical representation of the INDO and CNDO/2 calculation of the four-bond coupling constants between:

- A.) H_A and the methyl hydrogens of 2-chloro-1-phenylpropane.
B.) H_B and methyl hydrogens of 2-chloro-1-phenylpropane.

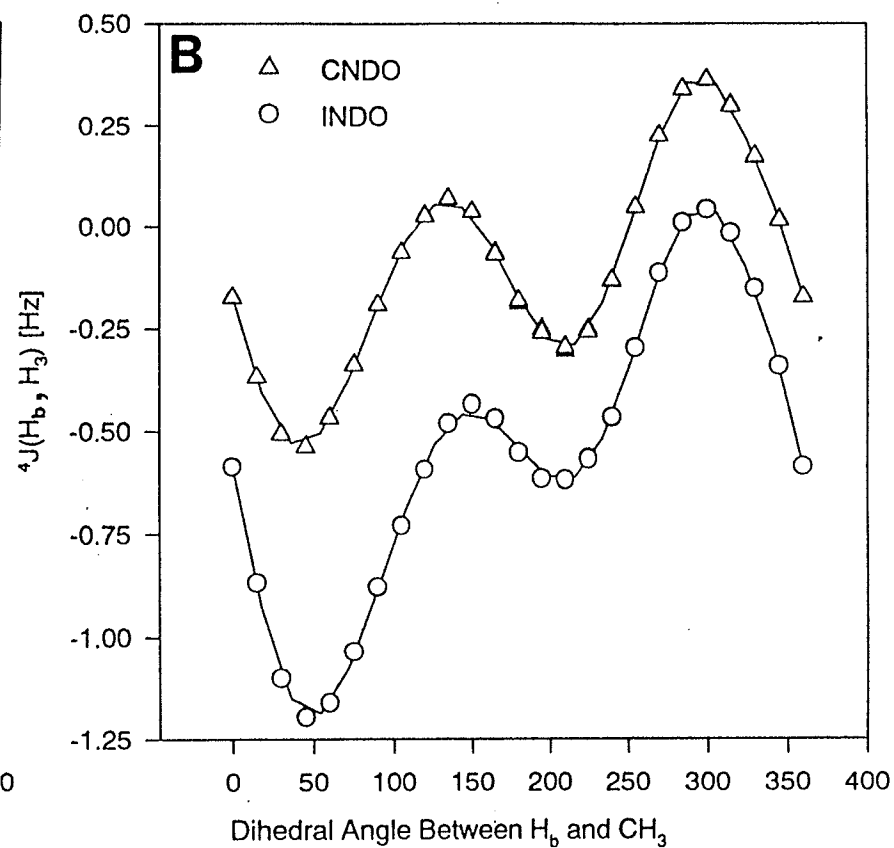
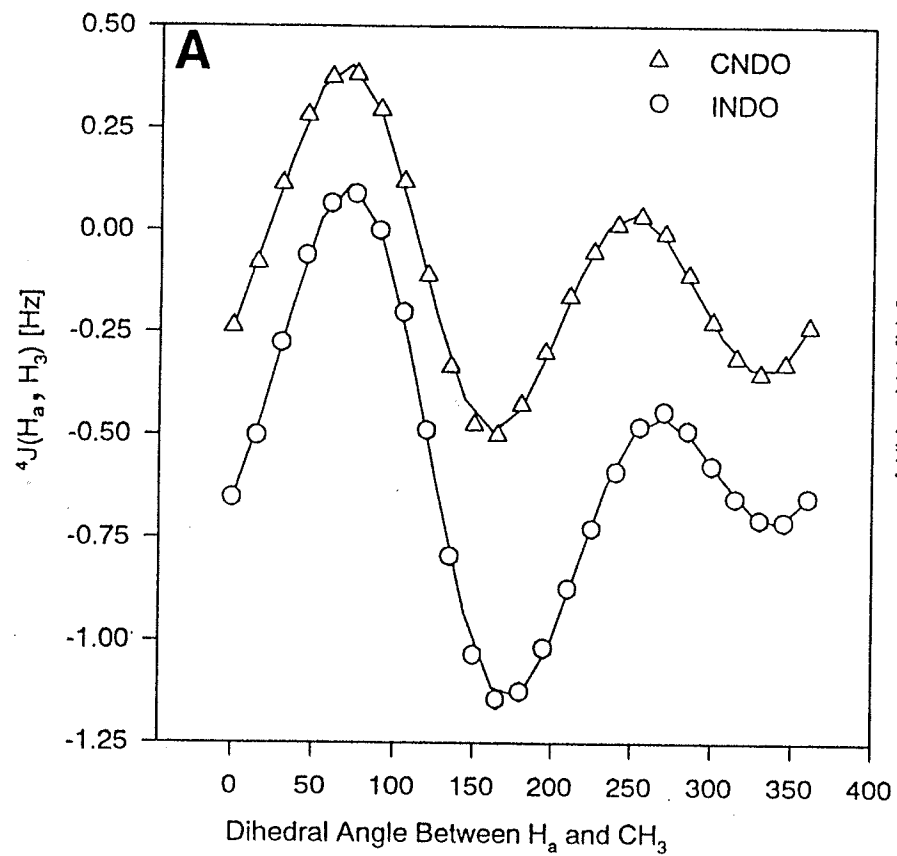


Table 3.3.3

Prediction of the vicinal coupling constants and $^4J_{H,CH_3}$ of the sidechain, using Karplus, INDO and CNDO/2 methods. Averaged values were obtained using 3-point, 3-cusp, and continuous methods.

BASIS	Karplus			INDO			CNDO/2		
	AM1 ^a	STO-3G ^a	STO-3G* ^a	AM1 ^a	STO-3G ^a	STO-3G* ^a	AM1 ^a	STO-3G ^a	STO-3G* ^a
$J_{A,C}$ Continuous	6.21 ^b	7.52	7.47	7.77	9.71	9.63	5.99	7.84	7.79
$J_{A,C}$ 3-Cusp	6.21	7.55	7.50	7.78	9.73	9.68	5.99	7.87	7.83
$J_{A,C}$ 3-Point	6.27	7.63	7.59	7.87	9.88	9.82	6.12	8.01	7.96
$J_{B,C}$ Continuous	6.73	6.57	6.60	8.74	8.21	8.26	7.05	6.65	6.69
$J_{B,C}$ 3-Cusp	6.70	6.59	6.61	8.70	8.24	8.26	7.02	6.67	6.70
$J_{B,C}$ 3-Point	7.01	6.62	6.64	9.20	8.29	8.33	7.46	6.72	6.75
J_{A,CH_3} Continuous				-0.72	-0.70	-0.70	-0.18	-0.21	-0.21
J_{A,CH_3} 3-Cusp				-0.72	-0.70	-0.70	-0.17	-0.21	-0.21
J_{A,CH_3} 3-Point				-0.74	-0.70	-0.70	-0.19	-0.21	-0.21
J_{B,CH_3} Continuous				-0.39	-0.33	-0.33	-0.03	0.05	0.04
J_{B,CH_3} 3-Cusp				-0.39	-0.32	-0.33	-0.03	0.05	0.05
J_{B,CH_3} 3-Point				-0.39	-0.32	-0.32	-0.02	0.06	0.05

^aAveraging carried out with energies based on M.O. calculations with the indicated basis set. ^bAll values are in Hertz

Figure 3.3.3

FPT MO CNDO/2 calculations of couplings between H_A and the hydrogens of the aromatic ring, for the A rotamer of 2-chloro-1-phenylpropane, as a function of:

1. phenyl rotation (θ). 2. phenyl rotation offset such that H_A starts perpendicular to the ring ($\theta - 120^\circ$).

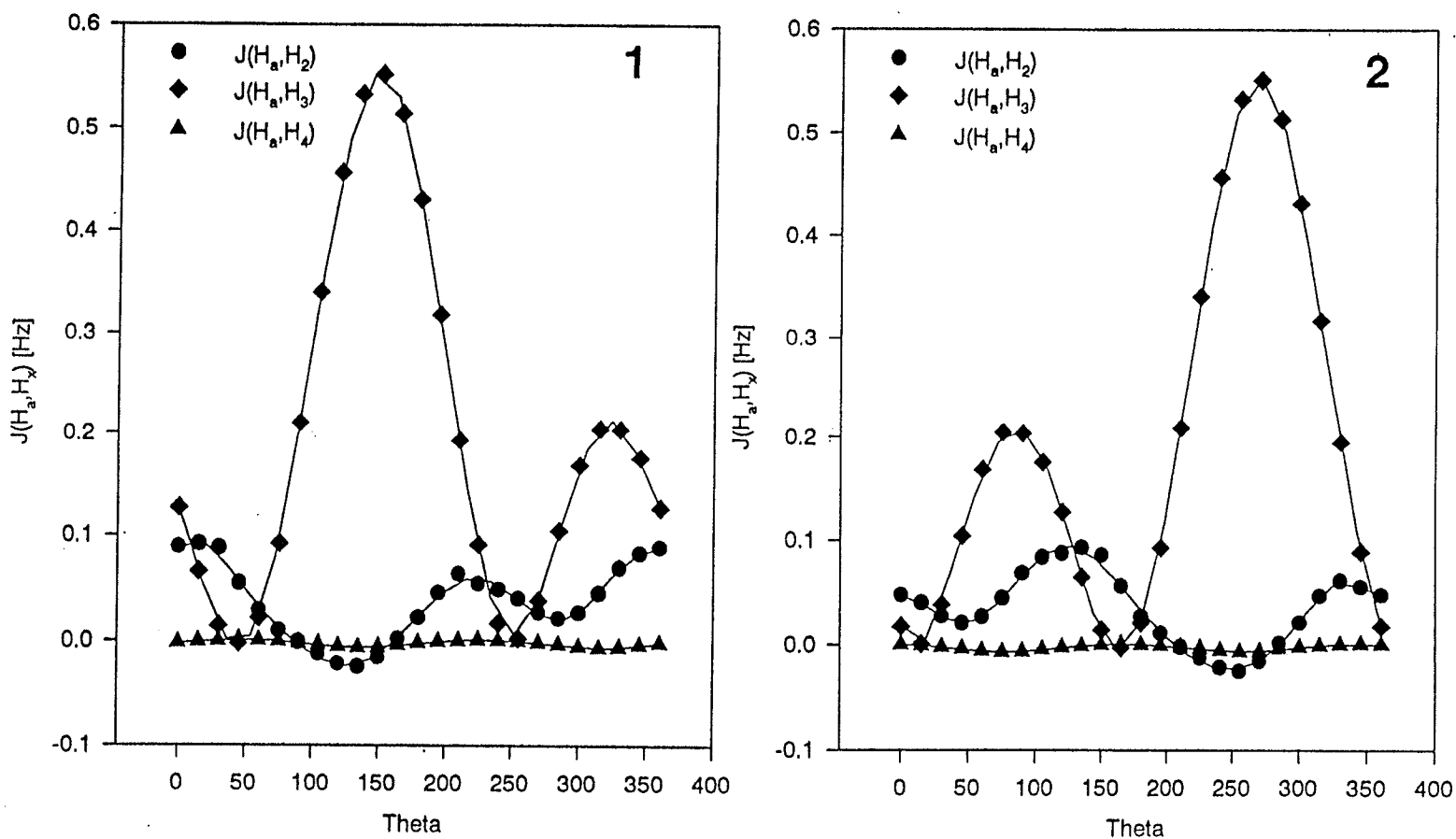


Figure 3.3.4

FPT MO CNDO/2 calculations of the couplings between H_A and the hydrogens of the aromatic ring, for rotamer B (1) and C (2) of 2-chloro-1-phenylpropane, as a function of θ .

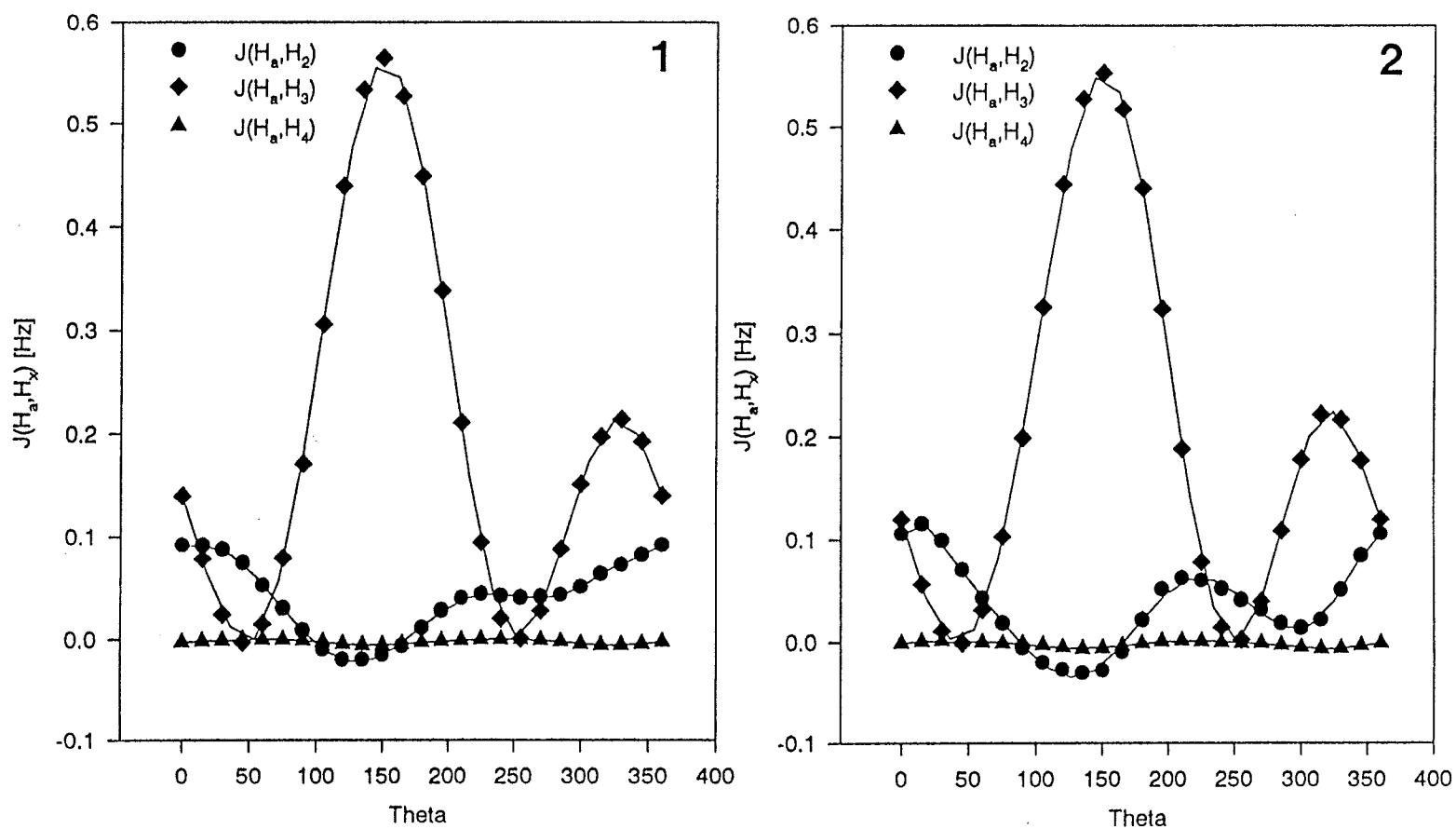


Figure 3.3.5

FPT MO INDO calculations of couplings between H_A and the hydrogens of the aromatic ring, for the A rotamer of 2-chloro-1-phenylpropane, as a function of :

1. phenyl rotation (θ). 2. phenyl rotation offset such that H_A starts perpendicular to the ring ($\theta+120^\circ$).

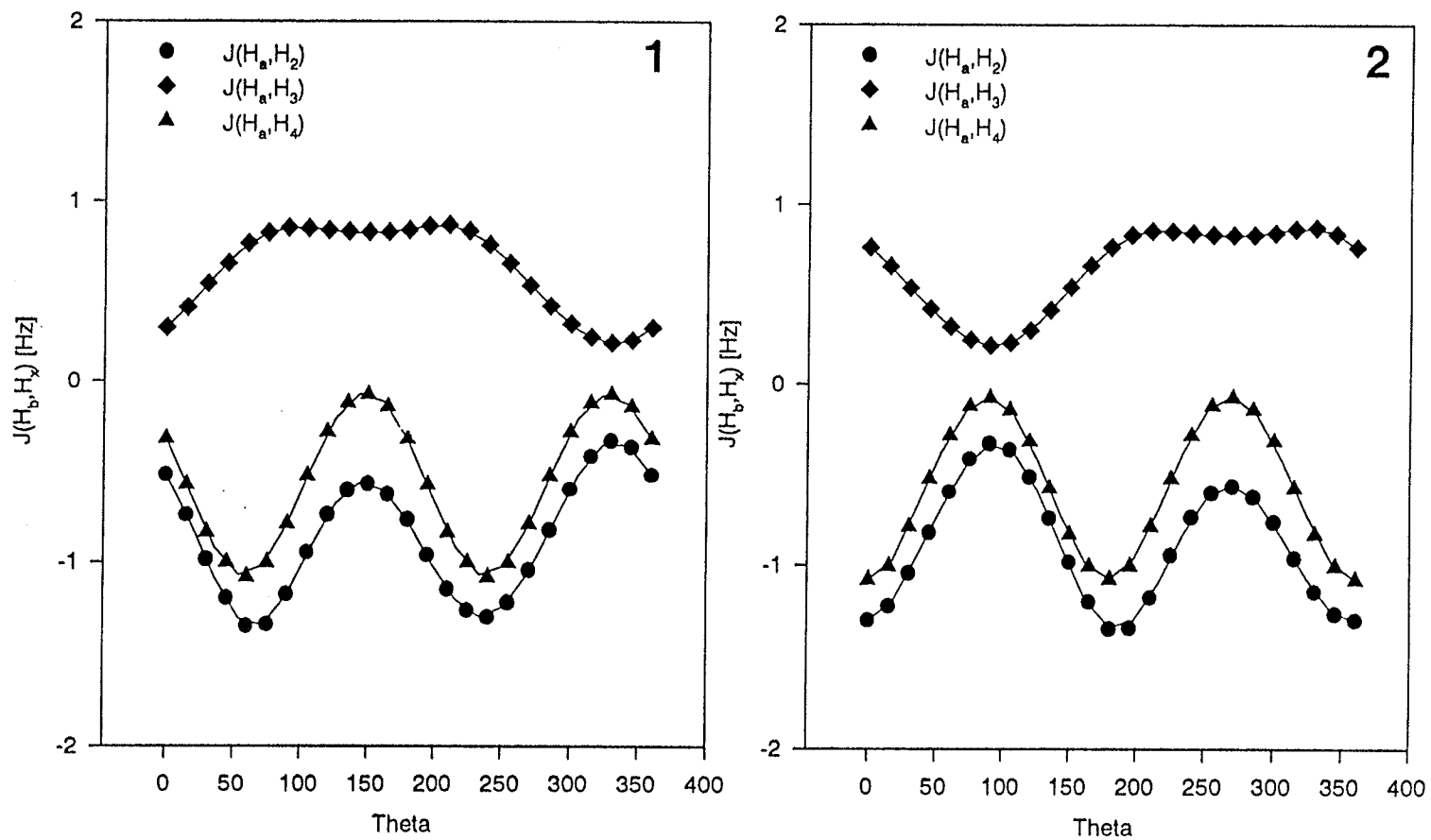


Figure 3.3.6

FPT MO INDO calculations of the couplings between H_A and the hydrogens of the aromatic ring, for rotamer B (1) and C (2) of 2-chloro-1-phenylpropane, as a function of θ .

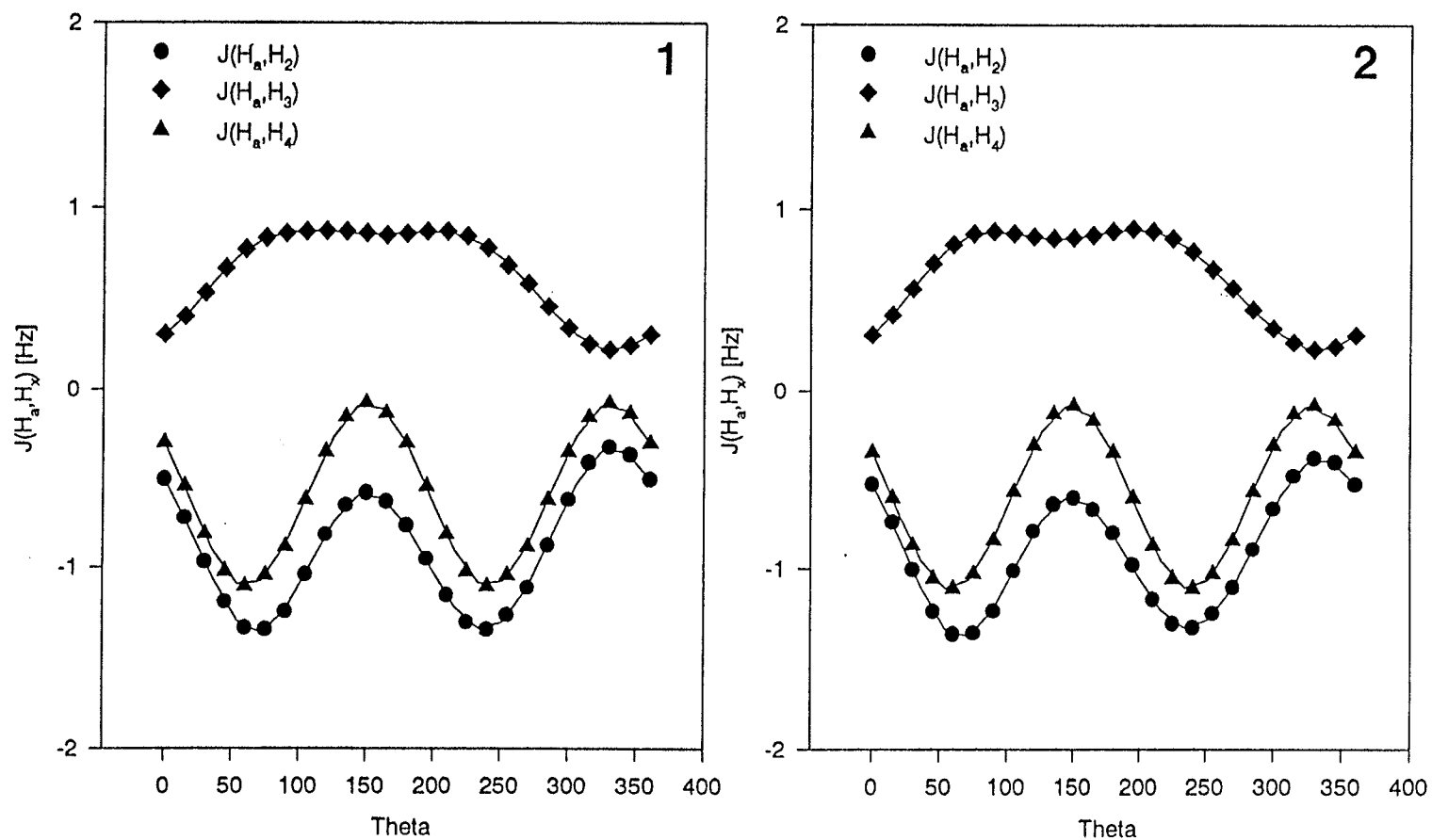


Table 3.3.4Classical averaging of ${}^4J[\text{H}_A, \text{H}_2]$ of 2-chloro-1-phenylpropane over the energy profile^a for θ rotation.

Basis	AM1			STO-3G			STO-3G*		
	A	B	C	A	B	C	A	B	C
Rotamer									
Φ	300°	180°	60°	300°	180°	60°	300°	180°	60°
^b Population [%]	44.10	51.44	4.46	50.24	42.40	7.36	49.97	42.53	7.50
^c $\langle J \rangle$, CNDO/2	0.037 ^d	0.051	0.054	0.038	0.055	0.065	0.038	0.055	0.065
^e $\langle J \rangle$, CNDO/2 OS	0.048	0.036	0.047	0.055	0.036	0.042	0.055	0.036	0.042
^f $\langle J \rangle$, ^{free} CNDO/2	0.034	0.038	0.035	0.034	0.038	0.035	0.034	0.038	0.035
^g $\langle J \rangle$, CNDO/2	0.045			0.047			0.047		
^g $\langle J \rangle$, CNDO/2 OS	0.042			0.046			0.046		
^g $\langle J \rangle$, ^{free} CNDO/2	0.036			0.036			0.036		
^c $\langle J \rangle$, INDO	-0.656	-0.879	-0.713	-0.545	-0.858	-0.738	-0.545	-0.855	-0.736
^e $\langle J \rangle$, INDO OS	-1.066	-1.130	-1.238	-1.165	-1.219	-1.292	-1.165	-1.220	-1.292
^f $\langle J \rangle$, ^{free} INDO	-0.878	-0.898	-0.914	-0.878	-0.898	-0.914	-0.878	-0.898	-0.914
^g $\langle J \rangle$, INDO	-0.773			-0.692			-0.691		
^g $\langle J \rangle$, INDO OS	-1.107			-1.197			-1.197		
^g $\langle J \rangle$, ^{free} INDO	-0.890			-0.889			-0.889		
Solvent	CS ₂			Acetone-d ₆			CD ₂ Cl ₂		
$J_{\text{experimental}}$	-0.506			-0.534			-0.533		

^{a,b}Calculation based on the energies from the MO calculations of 2-bromo-1-phenylpropane. ^c Averaged over the energy profile of each individual rotamer. ^dAll calculated and experimental couplings are in Hertz. ^eAverage for each rotamer using θ offset by 120°.

^fAveraged without a barrier to rotation. ^g Averaged over all three rotamer states.

Table 3.3.5Classical averaging of ${}^5J[\text{H}_A, \text{H}_3]$ of 2-chloro-1-phenylpropane over the energy profile^a for θ rotation.

Basis	AM1			STO-3G			STO-3G*		
	A	B	C	A	B	C	A	B	C
Rotamer									
Φ	300°	180°	60°	300°	180°	60°	300°	180°	60°
^b Population [%]	44.10	51.44	4.46	50.24	42.40	7.36	49.97	42.53	7.50
^c $\langle J \rangle_i$ CNDO/2	0.288 ^d	0.199	0.267	0.333	0.204	0.250	0.332	0.205	0.250
^e $\langle J \rangle_i$ CNDO/2 OS	0.117	0.111	0.065	0.072	0.075	0.047	0.072	0.075	0.047
^f $\langle J \rangle_i^{\text{free}}$ CNDO/2	0.203	0.203	0.203	0.203	0.203	0.203	0.203	0.203	0.203
^g $\langle J \rangle$ CNDO/2	0.241			0.272			0.272		
^g $\langle J \rangle$ CNDO/2 OS	0.111			0.071			0.071		
^g $\langle J \rangle^{\text{free}}$ CNDO/2	0.203			0.203			0.203		
^c $\langle J \rangle_i$ INDO	0.577	0.653	0.609	0.548	0.646	0.619	0.548	0.646	0.618
^e $\langle J \rangle_i$ INDO OS	0.697	0.718	0.759	0.728	0.742	0.773	0.728	0.742	0.773
^f $\langle J \rangle_i^{\text{free}}$ INDO	0.640	0.658	0.662	0.640	0.658	0.662	0.640	0.658	0.662
^g $\langle J \rangle$ INDO	0.618			0.595			0.595		
^g $\langle J \rangle$ INDO OS	0.711			0.737			0.737		
^g $\langle J \rangle^{\text{free}}$ INDO	0.650			0.649			0.649		
Solvent	CS ₂			Acetone-d ₆			CD ₂ Cl ₂		
J _{experimental}	0.281			0.278			0.277		

^{a, b, c, d, e, f, g} Same as in table 3.3.4.

Table 3.3.6Classical averaging of ${}^6J[H_A, H_4]$ of 2-chloro-1-phenylpropane over the energy profile^a for θ rotation.

Basis	AM1			STO-3G			STO-3G*		
	A	B	C	A	B	C	A	B	C
Rotamer									
Φ	300°	180°	60°	300°	180°	60°	300°	180°	60°
^b Population [%]	44.10	51.44	4.46	50.24	42.40	7.36	49.97	42.53	7.50
^c $\langle J \rangle_i$ CNDO/2	-0.004 ^d	-0.001	-0.002	-0.004	-0.001	-0.001	-0.004	-0.001	-0.001
^e $\langle J \rangle_i$ CNDO/2 OS	-0.001	-0.001	0.000	0.000	-0.001	0.000	0.000	-0.001	0.000
^f $\langle J \rangle_i^{\text{free}}$ CNDO/2	-0.002	-0.002	-0.002	-0.002	-0.002	-0.002	-0.002	-0.002	-0.002
^g $\langle J \rangle$ CNDO/2	-0.002			-0.003			-0.003		
^g $\langle J \rangle$ CNDO/2 OS	-0.001			0.000			0.000		
^g $\langle J \rangle^{\text{free}}$ CNDO/2	-0.002			-0.002			-0.002		
^c $\langle J \rangle_i$ INDO	-0.317	-0.585	-0.395	-0.190	-0.566	-0.439	-0.190	-0.562	-0.436
^e $\langle J \rangle_i$ INDO OS	-0.802	-0.849	-0.987	-0.927	-0.949	-1.040	-0.927	-0.950	-1.041
^f $\langle J \rangle_i^{\text{free}}$ INDO	-0.565	-0.590	-0.593	-0.565	-0.590	-0.593	-0.565	-0.590	-0.593
^g $\langle J \rangle$ INDO	-0.458			-0.367			-0.367		
^g $\langle J \rangle$ INDO OS	-0.834			-0.945			-0.945		
^g $\langle J \rangle^{\text{free}}$ INDO	-0.579			-0.577			-0.578		
Solvent	CS ₂			Acetone-d ₆			CD ₂ Cl ₂		
$J_{\text{experimental}}$	-0.309			-0.358			-0.347		

^{a,b,c,d,e,f,g}Same as in table 3.3.4.

Table 3.3.7Classical averaging of ${}^4J[\text{H}_B, \text{H}_2]$ of 2-chloro-1-phenylpropane over the energy profile^a for θ rotation.

Basis	AM1			STO-3G			STO-3G*		
Rotamer	A	B	C	A	B	C	A	B	C
Φ	300°	180°	60°	300°	180°	60°	300°	180°	60°
^b Population [%]	44.10	51.44	4.46	50.24	42.40	7.36	49.97	42.53	7.50
^c $\langle J \rangle$, CNDO/2	0.040 ^d	0.050	0.049	0.050	0.055	0.047	0.050	0.055	0.047
^e $\langle J \rangle$, CNDO/2 OS	0.023	0.051	0.034	0.023	0.052	0.039	0.032	0.052	0.038
^f $\langle J \rangle$ ^{free} , CNDO/2	0.023	0.042	0.031	0.023	0.042	0.031	0.023	0.042	0.031
^g $\langle J \rangle$, CNDO/2	0.046			0.052			0.052		
^g $\langle J \rangle$, CNDO/2 OS	0.038			0.037			0.037		
^g $\langle J \rangle$ ^{free} , CNDO/2	0.033			0.031			0.031		
^c $\langle J \rangle$, INDO	-0.930	-0.641	-0.719	-0.921	-0.565	-0.632	-0.921	-0.567	-0.634
^e $\langle J \rangle$, INDO OS	-1.153	-1.080	-1.253	-1.269	-1.165	-1.297	-1.269	-1.168	-1.298
^f $\langle J \rangle$ ^{free} , INDO	-0.938	-0.872	-0.911	-0.938	-0.872	-0.911	-0.938	-0.872	-0.911
^g $\langle J \rangle$, INDO	-0.772			-0.749			-0.749		
^g $\langle J \rangle$, INDO OS	-1.120			-1.227			-1.228		
^g $\langle J \rangle$ ^{free} , INDO	-0.904			-0.908			-0.908		
Solvent	CS ₂			Acetone-d ₆			CD ₂ Cl ₂		
$J_{\text{experimental}}$	-0.570			-0.551			-0.553		

^{a, b, c, d, e, f, g} Same as in table 3.3.4.

Table 3.3.8Classical averaging of ${}^5J[\text{H}_B, \text{H}_3]$ of 2-chloro-1-phenylpropane over the energy profile^a for θ rotation.

Basis	AM1			STO-3G			STO-3G*		
	A	B	C	A	B	C	A	B	C
Rotamer									
Φ	300°	180°	60°	300°	180°	60°	300°	180°	60°
^b Population [%]	44.10	51.44	4.46	50.24	42.40	7.36	49.97	42.53	7.50
^c $\langle J \rangle_i$ CNDO/2	0.183 ^d	0.291	0.265	0.177	0.319	0.300	0.177	0.318	0.299
^c $\langle J \rangle_i$ CNDO/2 OS	0.110	0.111	0.060	0.065	0.075	0.039	0.065	0.075	0.038
^f $\langle J \rangle_i^{\text{free}}$ CNDO/2	0.194	0.204	0.201	0.194	0.204	0.201	0.194	0.203	0.201
^g $\langle J \rangle$ CNDO/2	0.242			0.246			0.246		
^g $\langle J \rangle$ CNDO/2 OS	0.108			0.067			0.067		
^g $\langle J \rangle^{\text{free}}$ CNDO/2	0.199			0.199			0.199		
^c $\langle J \rangle_i$ INDO	0.649	0.588	0.605	0.646	0.568	0.581	0.646	0.569	0.582
^c $\langle J \rangle_i$ INDO OS	0.709	0.702	0.743	0.741	0.724	0.757	0.741	0.724	0.757
^f $\langle J \rangle_i^{\text{free}}$ INDO	0.648	0.648	0.652	0.648	0.648	0.652	0.648	0.648	0.652
^g $\langle J \rangle$ INDO	0.616			0.608			0.608		
^g $\langle J \rangle$ INDO OS	0.707			0.735			0.735		
^g $\langle J \rangle^{\text{free}}$ INDO	0.648			0.648			0.648		
Solvent	CS ₂			Acetone-d ₆			CD ₂ Cl ₂		
$J_{\text{experimental}}$	0.255			0.263			0.276		

^{a, b, c, d, e, f, g} Same as in table 3.3.4.

Table 3.3.9Classical averaging of ${}^6J[\text{H}_\text{B}, \text{H}_4]$ of 2-chloro-1-phenylpropane over the energy profile^a for θ rotation.

Basis	AM1			STO-3G			STO-3G*		
Rotamer	A	B	C	A	B	C	A	B	C
Φ	300°	180°	60°	300°	180°	60°	300°	180°	60°
^b Population [%]	44.10	51.44	4.46	50.24	42.40	7.36	49.97	42.53	7.50
^c $\langle J \rangle$, CNDO/2	-0.001 ^d	-0.003	-0.002	-0.001	-0.003	-0.003	-0.001	-0.003	-0.003
^e $\langle J \rangle$, CNDO/2 OS	-0.001	0.000	0.000	0.000	0.001	0.000	0.000	0.001	0.000
^f $\langle J \rangle$, ^{free} CNDO/2	-0.002	-0.002	-0.002	-0.002	-0.002	-0.002	-0.002	-0.002	-0.002
^g $\langle J \rangle$, CNDO/2	-0.002			-0.002			-0.002		
^g $\langle J \rangle$, CNDO/2 OS	0.000			0.000			0.000		
^g $\langle J \rangle$, ^{free} CNDO/2	-0.002			-0.002			-0.002		
^e $\langle J \rangle$, INDO	-0.621	-0.321	-0.394	-0.627	-0.239	-0.295	-0.626	-0.241	-0.297
^e $\langle J \rangle$, INDO OS	-0.843	-0.820	-0.983	-0.974	-0.920	-1.042	-0.974	-0.921	-1.043
^f $\langle J \rangle$, ^{free} INDO	-0.600	-0.571	-0.589	-0.600	-0.571	-0.589	-0.600	-0.571	-0.589
^g $\langle J \rangle$, INDO	-0.456			-0.438			-0.438		
^g $\langle J \rangle$, INDO OS	-0.838			-0.956			-0.956		
^g $\langle J \rangle$, ^{free} INDO	-0.584			-0.587			-0.587		
Solvent	CS ₂			Acetone-d ₆			CD ₂ Cl ₂		
$J_{\text{experimental}}$	-0.387			-0.375			-0.367		

^{a,b,c,d,e,f,g} Same as in table 3.3.4.

Figure 3.3.7

FPT MO CNDO/2 calculations of the coupling between H_C and the hydrogens of the aromatic ring, for rotamer A (1) and B (2) of 2-chloro-1-phenylpropane, as a function of θ .

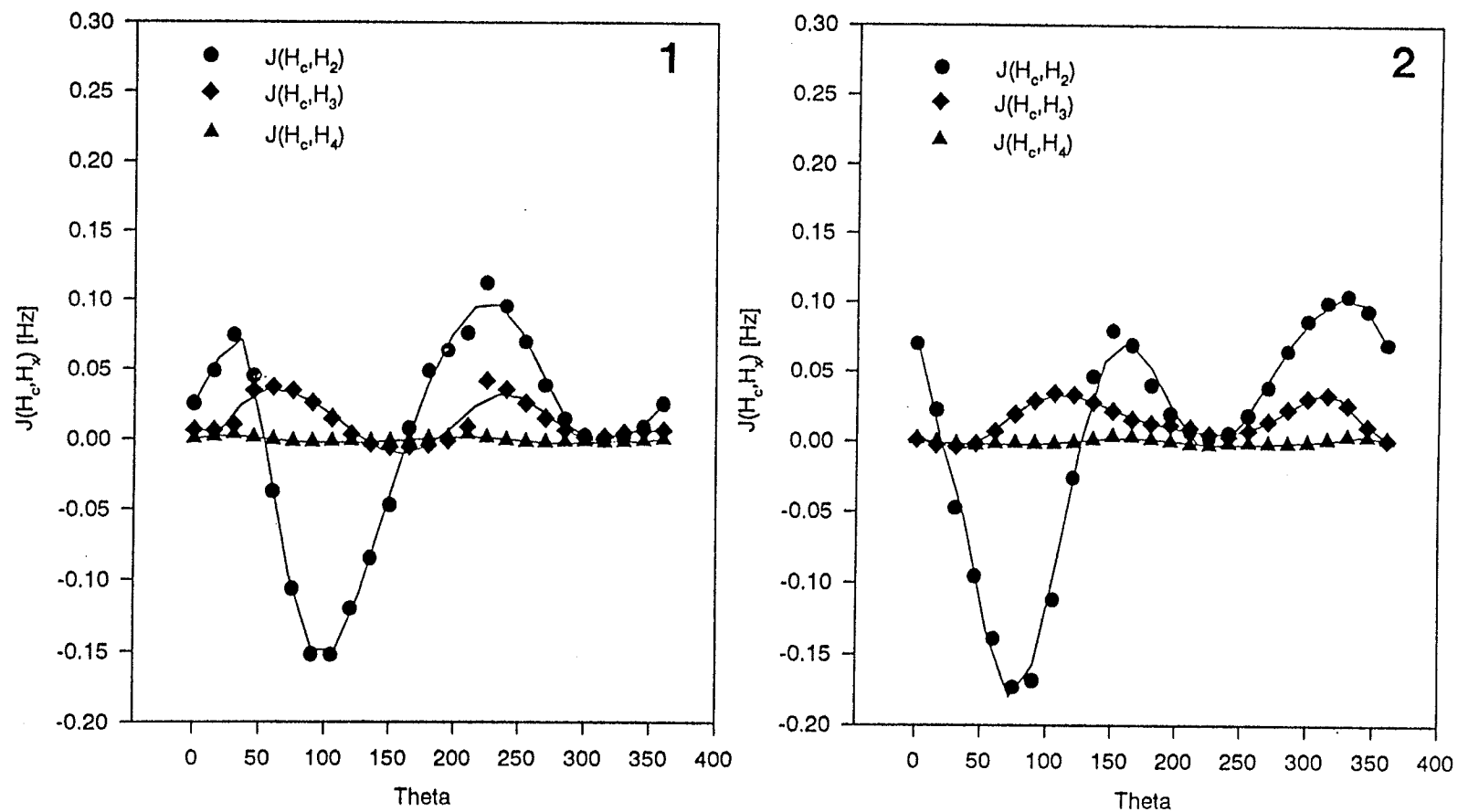


Figure 3.3.8

- 1.) FPT MO CNDO/2 calculations of the coupling between H_C and the hydrogens of the aromatic ring, for rotamer C of 2-chloro-1-phenylpropane, as a function of θ .
- 2.) FPT MO INDO calculations of the coupling between H_C and the hydrogens of the aromatic ring, for rotamer A of 2-chloro-1-phenylpropane, as a function of θ .

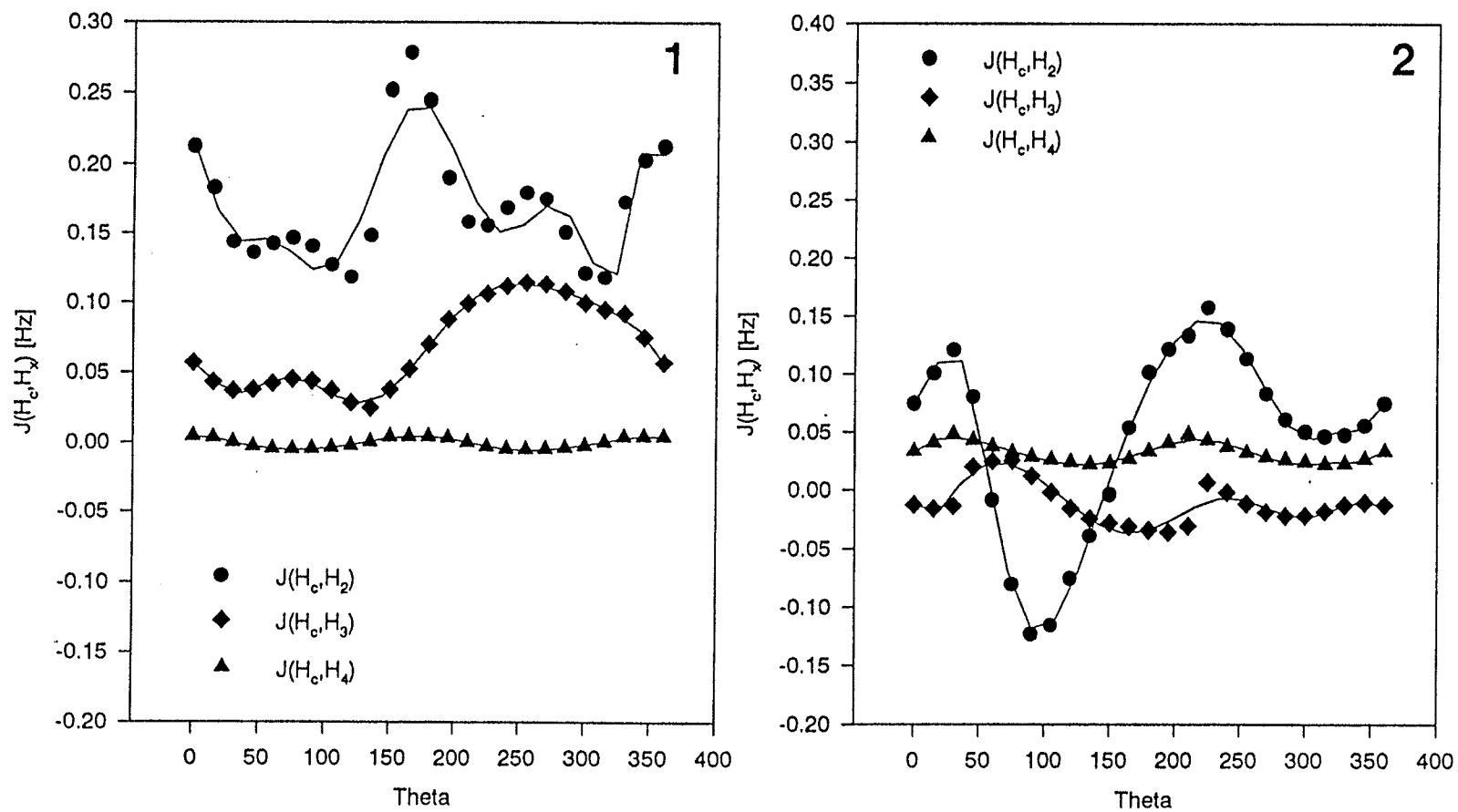


Figure 3.3.9

FPT MO INDO calculations of the coupling between H_C and the hydrogens of the aromatic ring, for rotamer B (1) and C (2) of 2-chloro-1-phenylpropane, as a function of θ .

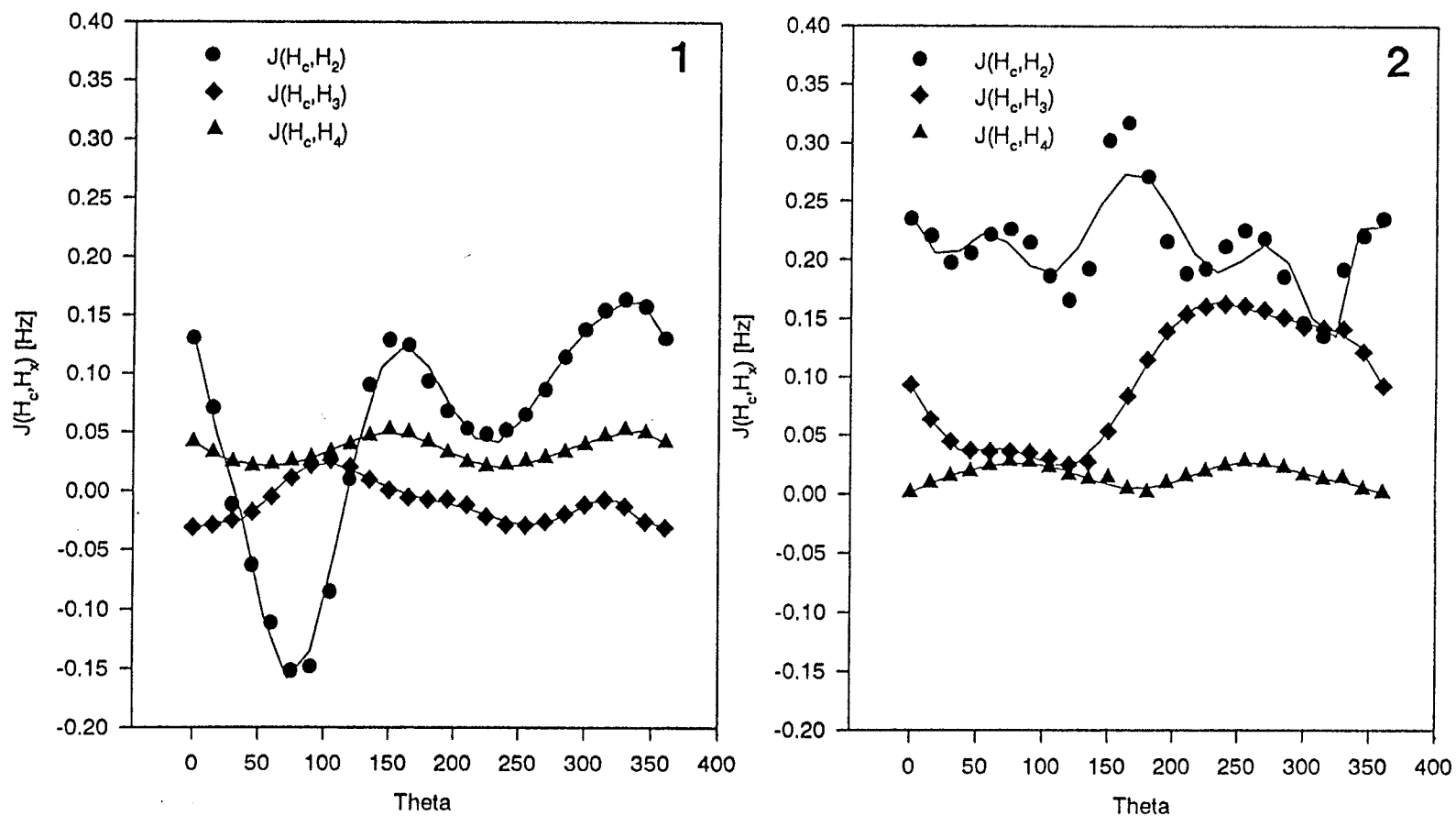


Table 3.3.10Classical averaging of $^5J[\text{H}_\text{C}, \text{H}_2]$ of 2-chloro-1-phenylpropane over the energy profile^a for θ rotation.

Basis	AM1			STO-3G			STO-3G*		
Rotamer	A	B	C	A	B	C	A	B	C
Φ	300°	180°	60°	300°	180°	60°	300°	180°	60°
^b Population [%]	44.10	51.44	4.46	50.24	42.40	7.36	49.97	42.53	7.50
^c $\langle J \rangle_i$ CNDO/2	0.002 ^d	0.012	0.213	0.003	0.016	0.212	0.003	0.017	0.212
^e $\langle J \rangle_i^{\text{free}}$ CNDO/2	0.001	0.004	0.169	0.001	0.004	0.169	0.001	0.004	0.169
^f $\langle J \rangle$ CNDO/2	0.017			0.024			0.025		
^f $\langle J \rangle^{\text{free}}$ CNDO/2	0.010			0.015			0.015		
^c $\langle J \rangle_i$ INDO	0.049	0.059	0.244	0.051	0.065	0.241	0.051	0.065	0.241
^e $\langle J \rangle_i^{\text{free}}$ INDO	0.045	0.049	0.212	0.045	0.049	0.212	0.045	0.049	0.212
^f $\langle J \rangle$ INDO	0.063			0.071			0.071		
^f $\langle J \rangle^{\text{free}}$ INDO	0.055			0.059			0.059		
SOLVENT	CS ₂			Acetone-d ₆			CD ₂ Cl ₂		
J _{exp}	±0.023			±0.024			±0.030		

^{a,b}Calculation based on the energies from the MO calculations of 2-bromo-1-phenylpropane. ^c Averaged over the energy profile of each individual rotamer. ^dAll calculated and experimental couplings are in Hertz. ^eAveraged without a barrier to rotation. ^f Averaged over all three rotamer states.

Table 3.3.11Classical averaging of ${}^6J[\text{H}_C, \text{H}_3]$ of 2-chloro-1-phenylpropane over the energy profile^a for θ rotation.

Basis	AM1			STO-3G			STO-3G*		
	A	B	C	A	B	C	A	B	C
Φ	300°	180°	60°	300°	180°	60°	300°	180°	60°
^b Population [%]	44.10	51.44	4.46	50.24	42.40	7.36	49.97	42.53	7.50
^c $\langle J \rangle_i$ CNDO/2	0.000 ^d	0.008	0.065	0.006	0.006	0.065	0.001	0.006	0.065
^e $\langle J \rangle_i^{\text{free}}$ CNDO/2	0.013	0.015	0.069	0.013	0.015	0.069	0.013	0.015	0.069
^f $\langle J \rangle$ CNDO/2	0.007			0.010			0.008		
^f $\langle J \rangle^{\text{free}}$ CNDO/2	0.017			0.018			0.018		
^c $\langle J \rangle_i$ INDO	-0.019	-0.016	0.102	-0.021	-0.018	0.103	-0.021	-0.018	0.103
^e $\langle J \rangle_i^{\text{free}}$ INDO	-0.011	-0.010	0.096	-0.011	-0.010	0.096	-0.011	-0.010	0.096
^f $\langle J \rangle$ INDO	-0.012			-0.011			-0.010		
^f $\langle J \rangle^{\text{free}}$ INDO	-0.006			-0.003			-0.003		
SOLVENT	CS ₂			Acetone-d ₆			CD ₂ Cl ₂		
J _{exp}	±0.011			±0.012			±0.033		

^{a,b,c,d,e,f}Same as in table 3.3.10.

Table 3.3.12Classical averaging of ${}^7J[\text{H}_C, \text{H}_4]$ of 2-chloro-1-phenylpropane over the energy profile^a for θ rotation.

Basis	AM1			STO-3G			STO-3G*		
Rotamer	A	B	C	A	B	C	A	B	C
Φ	300°	180°	60°	300°	180°	60°	300°	180°	60°
^b Population [%]	44.10	51.44	4.46	50.24	42.40	7.36	49.97	42.53	7.50
^c $\langle J \rangle_i$ CNDO/2	-0.001 ^d	0.000	0.003	-0.001	0.000	0.003	-0.001	0.000	0.003
^e $\langle J \rangle_i^{\text{free}}$ CNDO/2	0.000	0.000	-0.001	0.000	0.000	-0.001	0.000	0.000	-0.001
^f $\langle J \rangle$ CNDO/2	0.000			0.000			0.000		
^f $\langle J \rangle^{\text{free}}$ CNDO/2	0.000			0.000			0.000		
^c $\langle J \rangle_i$ INDO	0.029	0.033	0.007	0.027	0.033	0.006	0.027	0.033	0.006
^e $\langle J \rangle_i^{\text{free}}$ INDO	0.032	0.035	0.016	0.032	0.035	0.016	0.032	0.035	0.016
^f $\langle J \rangle$ INDO	0.030			0.028			0.028		
^f $\langle J \rangle^{\text{free}}$ INDO	0.033			0.032			0.032		
SOLVENT	CS ₂			Acetone-d ₆			CD ₂ Cl ₂		
J _{exp}	±0.014			±0.011			±0.031		

^{a, b, c, d, e, f} Same as in table 3.3.10.

4 DISCUSSION

4.1 Assignments of H_A and H_B

The assignment of the chemical shifts of H_A and H_B is based on arguments derived from trends in the substituent effect on the proton chemical shifts due to bromine and methyl groups vicinal to the protons in question.

The chemical shift data for substituted ethyl benzenes such as 1-methyl-2-(3,5-dibromophenyl)ethane and 1-bromo-2-(3,5-dibromophenyl)ethane (63) can be used to determine the effect of methyl or bromine substitution on the chemical shift of a vicinal trans or gauche proton. The chemical shifts of the alpha protons of 2.5 mol % ethylbenzene (57), 11 mol % 1-methyl-2-(3,5-dibromophenyl)ethane (63), and 11 mol % 1-bromo-2-(3,5-dibromophenyl)ethane (63) in CS_2 are 775.31, 750.26 and 910.06 Hz to high frequency from internal TMS at 300 MHz. For 1-methyl-2-(3,5-dibromophenyl)ethane (63) and 1-bromo-2-(3,5-dibromophenyl)ethane the anti forms are favoured by 0.43 and 0.37 kcal./mol (63). The bromine atoms on the aromatic ring have a negligible effect on the chemical shift of the alpha protons, as is seen with isopropylbenzene and its brominated derivative (60). The frequencies of H_A and H_B in 2-bromo-1-phenylpropane are 887.5 Hz and 949.9 Hz. The effect of a methyl group in a trans orientation to a vicinal proton is to deshield it by 0.20 ppm (71,72). Then it follows that a gauche methyl group will shield it by 52.0 Hz (0.173 ppm.), whereas gauche and trans bromines will deshield the proton by 145.7 and 103.7 Hz, respectively (0.485 and 0.346 ppm.). This is consistent with

observations made by T. J. Curphey. He found that bromines in a beta position to methylene protons tend to deshield them by ~ 0.60 ppm (73). Bromine thus deshields a proton in the gauche position to a larger degree than in a trans orientation. This is consistent with a heavy atom effect of bromine in the proximate gauche orientation, not expected to be present in the trans arrangement.

The same analysis with a reversed assignment for H_A and H_B finds that gauche and trans bromine substituents deshield a vicinal proton by 53.3 and 368.0 Hz (0.18 and 1.23 ppm), respectively. These values imply that H_9 is shielded with respect to H_8 by 60.1 Hz (0.20 ppm) in 1,2-dibromo-1-phenylethane. The original assignment implies that H_9 is deshielded relative to H_8 by 7.7 Hz; the observed value is 17.7 Hz as measured in this laboratory (74).

With the first assignment the relative proportions of the rotamers were calculated in the three solvents, using ${}^3J_{HA,HC}$ and ${}^3J_{HB,HC}$ and the extended Haasnoot form of the Karplus equation. This was done with either STO-3G geometries, as in table 4.1.1, or ideal geometries, as in table 4.1.2. The rotamer populations are largely unaffected by a change in solvent, which is consistent with the dipole moment calculations, where no significant change in dipole moments between rotamers is seen.

When the results of the STO-3G* calculations are combined with the Karplus relationship and are averaged over the ϕ energy profile, the predicted vicinal coupling constants correspond exactly with experiment. To

reverse the assignment for the CS₂ solution would require both the Karplus equation and/or the STO-3G calculations to be wrong.

Table 4.1.1

Populations of rotamers A, B and C in various solvents determined from $^3J_{\text{HA,HC}}$ and $^3J_{\text{HB,HC}}$.

	$^3J_{\text{HA,HC}}$ [Hz]	$^3J_{\text{HB,HC}}$ [Hz]	Pop'n of rotamer A [%]	Pop'n of rotamer B [%]	Pop'n of rotamer C [%]
STO-3G*	-----	-----	50.0	42.5	7.5
CS ₂	7.620	6.620	51.2 ^a	39.1	9.7
CD ₂ Cl ₂	7.425	6.776	49.1	40.9	9.9
Acetone	7.506	6.626	49.9	39.2	10.9

^aDetermined using the extended Haasnoot Karplus equation, with STO-3G* geometries.

Table 4.1.2

Populations of rotamers A, B and C in various solvents determined from $^3J_{\text{HA,HC}}$ and $^3J_{\text{HB,HC}}$ using ideal geometries.

	$^3J_{\text{HA,HC}}$ [Hz]	$^3J_{\text{HB,HC}}$ [Hz]	Pop'n of rotamer A [%]	Pop'n of rotamer B [%]	Pop'n of rotamer C [%]
STO-3G*	-----	-----	50.0	42.5	7.5
CS ₂	7.620	6.620	51.7 ^a	37.9	10.5
CD ₂ Cl ₂	7.425	6.776	49.5	39.8	10.7
Acetone	7.506	6.626	50.3	38.1	11.6

^aDetermined using the extended Haasnoot Karplus equation, with ideal dihedral angles (60°, 180°, 300°) and tetrahedral valence angles (109.5°).

4.2 Prediction of the vicinal coupling constants of the sidechain - a test of the rotational isomeric states method.

As seen in table 3.3.3, for each basis set and type of J calculation, the three approaches to averaging the coupling constant in question give similar results. In all cases the continuous method yields values that are slightly smaller than the rotational isomeric states (RIS) approach. The 3-cusp method gives results closer to the continuous method than to the RIS calculations.

For all three procedures, averaging over the AM1 profiles give numbers which are markedly different from those generated with the STO-3G and STO-3G* curves. The AM1 result with the Karplus method suggests that ${}^3J_{HA,HC}$ is smaller than ${}^3J_{HB,HC}$ by about 0.5 Hz, which is opposite to experiment in which ${}^3J_{HA,HC}$ is greater than ${}^3J_{HB,HC}$ by 1.0 Hz. This discrepancy can be ascribed to AM1 favouring rotamer B by 0.6 kJ/mol over A, rather than to a gross error in the Karplus equation. The semiempirical FPT MO methods predict the same trend; however, the difference between ${}^3J_{HA,HC}$ and ${}^3J_{HB,HC}$ is 1 Hz.

Recall that the INDO and CNDO/2 calculations were performed on 2-chloro-1-phenylpropane, because they were not parameterized for bromine. The couplings predicted using the chlorine analogue should be smaller, because chlorine is more electronegative than bromine. However, the electronegativity difference is small (ca. 0.2 Pauling units (43)) and

therefore the difference between the predicted couplings should not be large (ca. 0.1 Hz, the difference between bromoethane and chloroethane (75)).

The prediction of the vicinal couplings in the side chain using STO-3G and STO-3G* energies leads to remarkably accurate results when predicting the coupling with the Karplus equation. All three averaging techniques achieve agreement with experiment to within ± 0.13 Hz. For ${}^3J_{\text{HA,HC}}$, the RIS value is the closest, while ${}^3J_{\text{HB,HC}}$ is best predicted by the continuous method. For all three methods INDO overestimates both ${}^3J_{\text{HA,HC}}$ and ${}^3J_{\text{HB,HC}}$ by 1.6 to 2.2 Hz, whereas the difference between them is calculated as 0.41 to 0.63 Hz. CNDO/2 gives results closer to those from experiment for all three approaches; it overestimates the couplings by 0.05 to 0.40 Hz. The difference between the couplings is 0.8 to 0.9 Hz. Thus FPT MO CNDO/2 yields better results than INDO, but not nearly as accurate as those from the modified Karplus equation.

The RIS approach agrees closely with the continuous method since each of the barriers to interconversion of the rotamer states is high. According to the STO-3G* calculations the energy barriers between rotamer states are 14.8 kJ/mol for $A \leftrightarrow B$, 23.1 kJ/mol for $B \leftrightarrow C$, and 22.3 kJ/mol for $A \leftrightarrow C$ (see figure 4.2.2). Figures 4.2.3 to 4.2.7 show what happens to the population distribution of the rotamers, and the way in which the Karplus curve for ${}^3J_{\text{HA,HC}}$ (figure 4.2.1) is sampled, when barriers are varied

Figure 4.2.1

$^3J_{\text{H}_A\text{H}_C}$ (Hz) of 2-bromo-1-phenylpropane as predicted using an extended form of the Haasnoot formulation of the Karplus equation

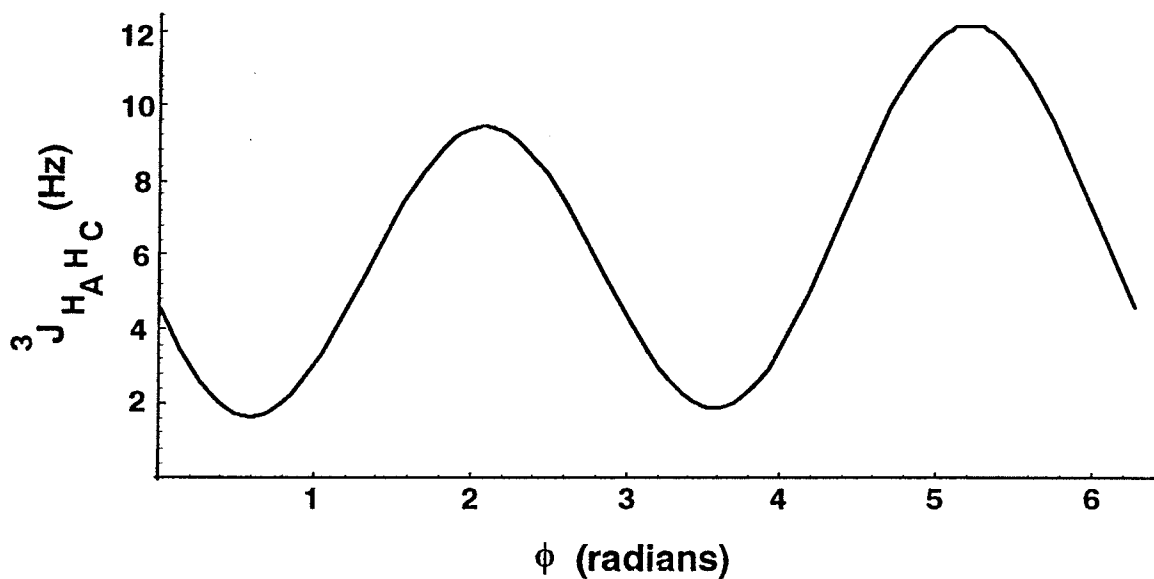
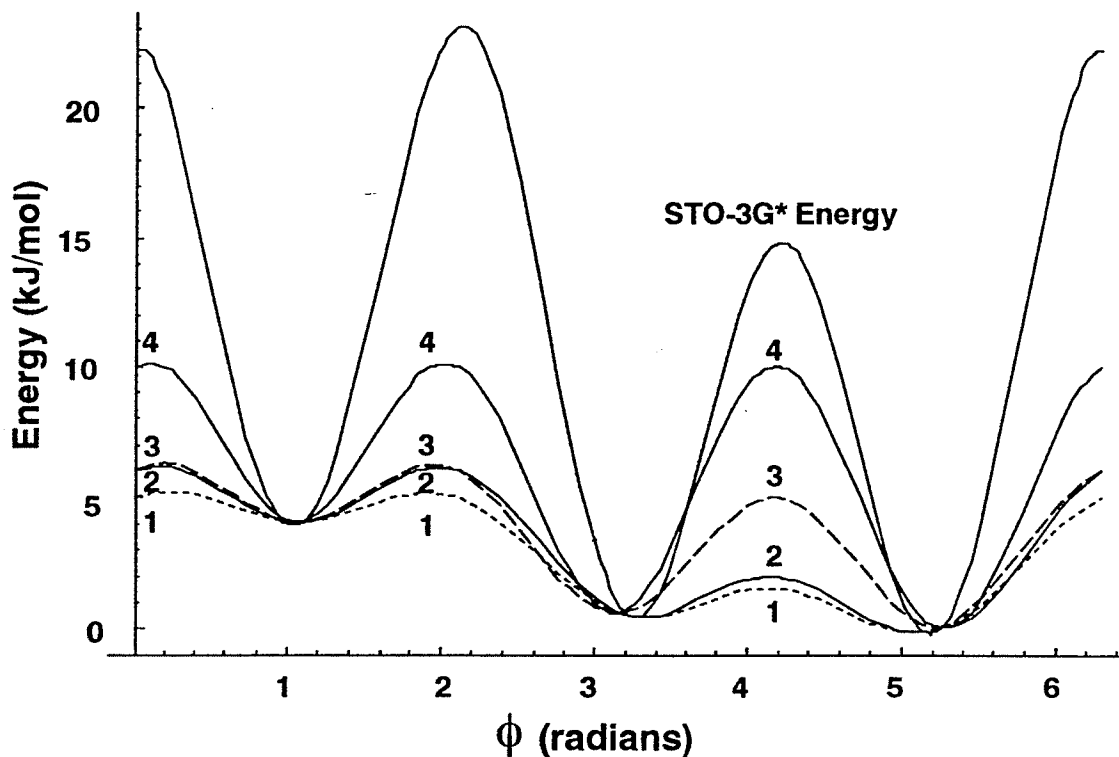


Figure 4.2.2

The energy profiles of ϕ rotation for 2-bromo-1-phenylpropane - curves 1 to 4 are in order of increasing barrier heights.



from 1.5 kJ/mol to 10 kJ/mol for $A \leftrightarrow B$, and 5 to 10 kJ/mol for both $B \leftrightarrow C$ and $C \leftrightarrow A$. In all four generated curves the barriers $B \leftrightarrow C$ and $C \leftrightarrow A$ were kept the same and optimal rotamer energies from STO-3G* were retained. The bottom plot in each of the figures 4.2.3 to 4.2.7, labelled J distribution (see equation 4.1), gives the product between $J(\phi)$ from the Karplus equation (figure 4.2.1, equation 1.5) and population distribution as a function of ϕ . This analysis assumes a temperature of 300 K.

$$J(\phi)_{Distribution} = \frac{J(\phi) \exp\left[-\frac{V(\phi)}{RT}\right]}{2\pi \int_0^{2\pi} \exp\left[-\frac{V(\phi)}{RT}\right] d\phi} \quad 4.1$$

As seen in figure 4.2.7, with a large barrier to interconversion between rotamer states, true bounds defining the rotamer state can be observed as a peak in the population distribution. When the barriers decrease, these peaks become wider and neighbouring peaks start to overlap and the notion of a discrete rotamer state is no longer clear (see figure 4.2.3). The form of the population distribution greatly determines that of the J distribution and in turn largely affects the averaged value of J. Thus J values in regions other than near the minima of the energy wells become significant in the determination of the average J.

Curve 1 - Barriers of 5 kJ/mol for B \leftrightarrow C and 1.5 kJ/mol for A \leftrightarrow B

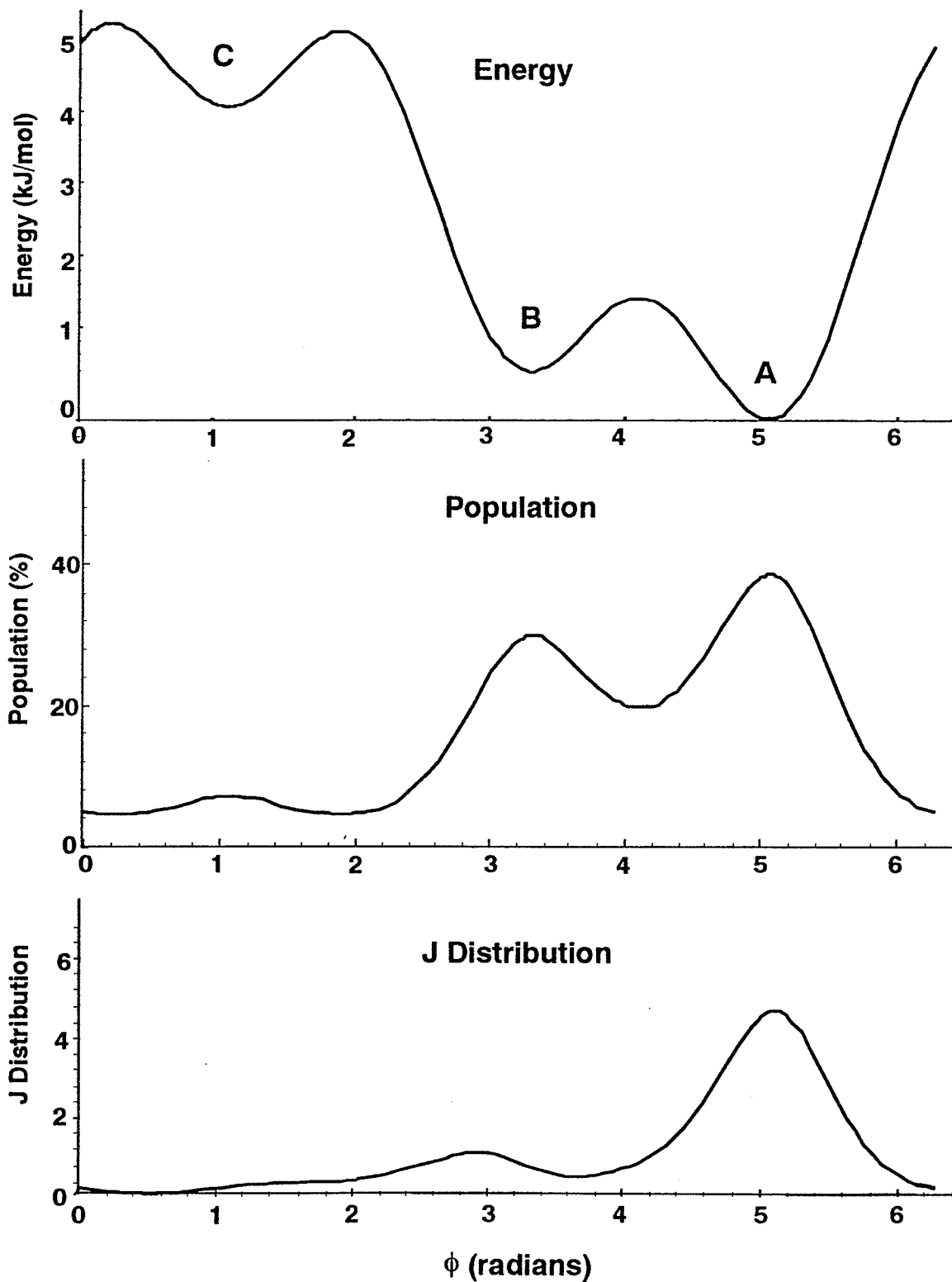
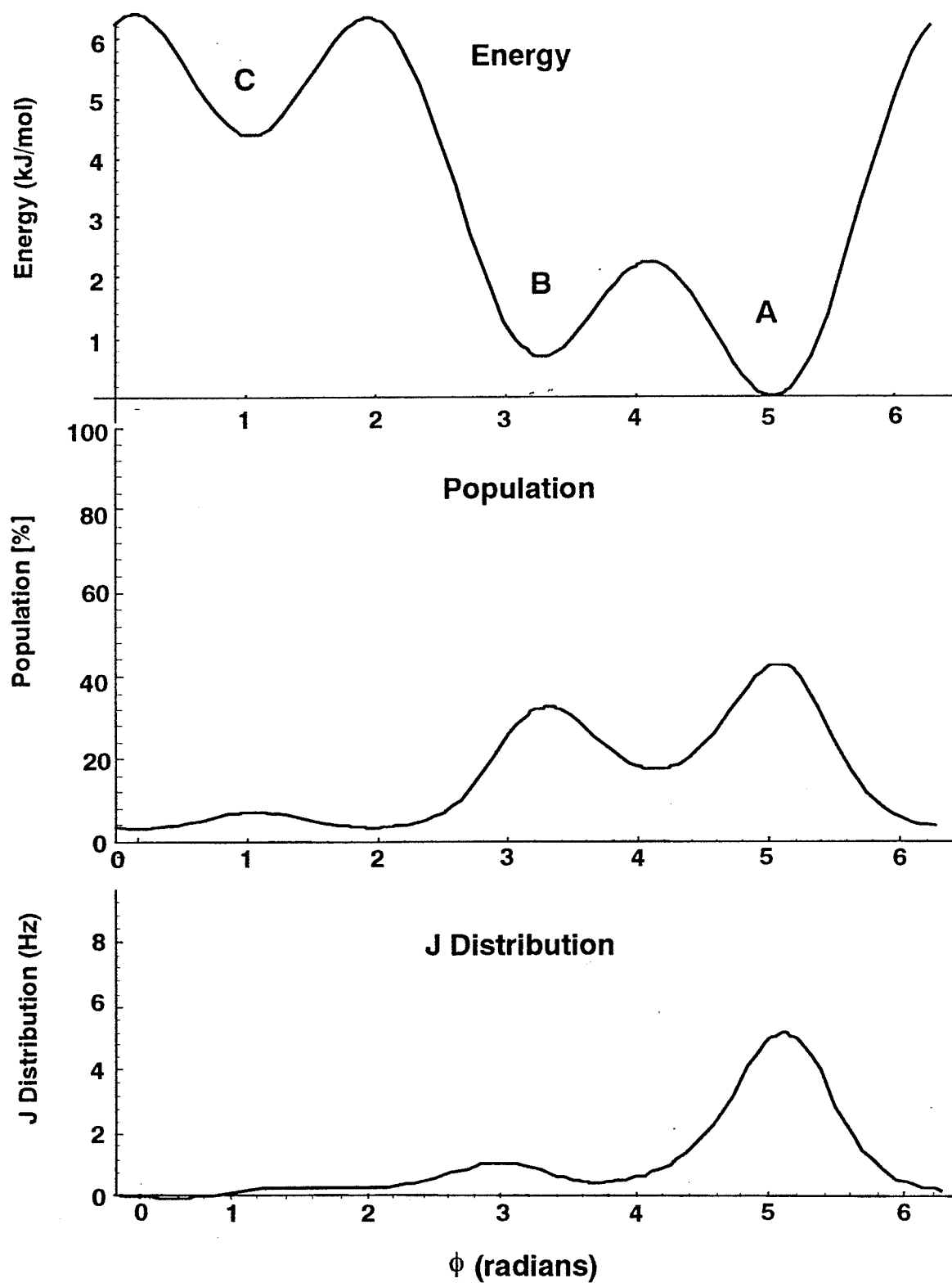


Figure 4.2.4

Curve 2 - Barriers of 6 kJ/mol for B \leftrightarrow C and for 2 kJ/mol for A \leftrightarrow B

Curve 3 - Barriers of 6 kJ/mol for B \leftrightarrow C and 5 kJ/mol for B \leftrightarrow A

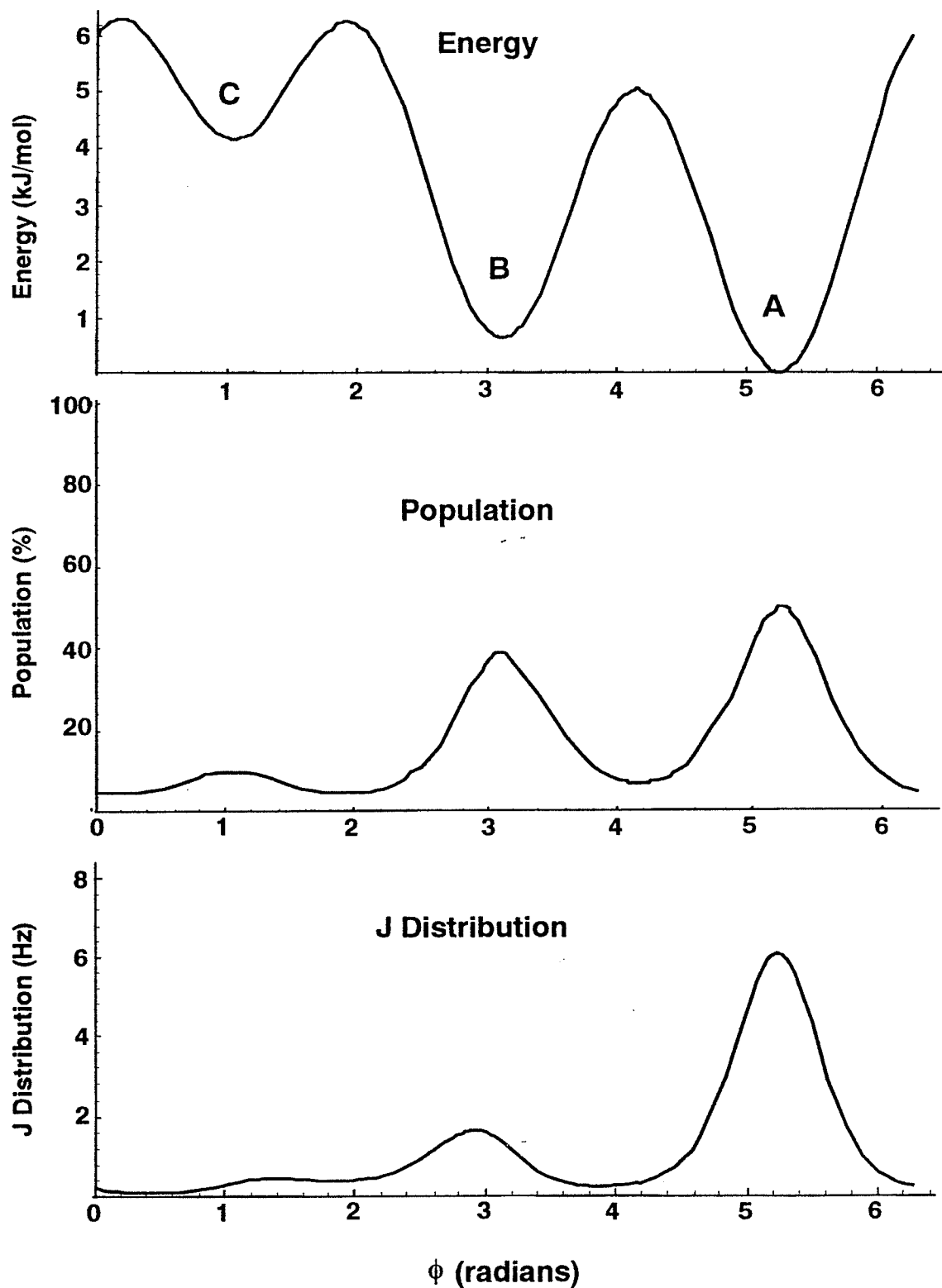


Figure 4.2.6

Curve 4 - Barriers of 10 kJ/mol for $A \leftrightarrow B \leftrightarrow C$

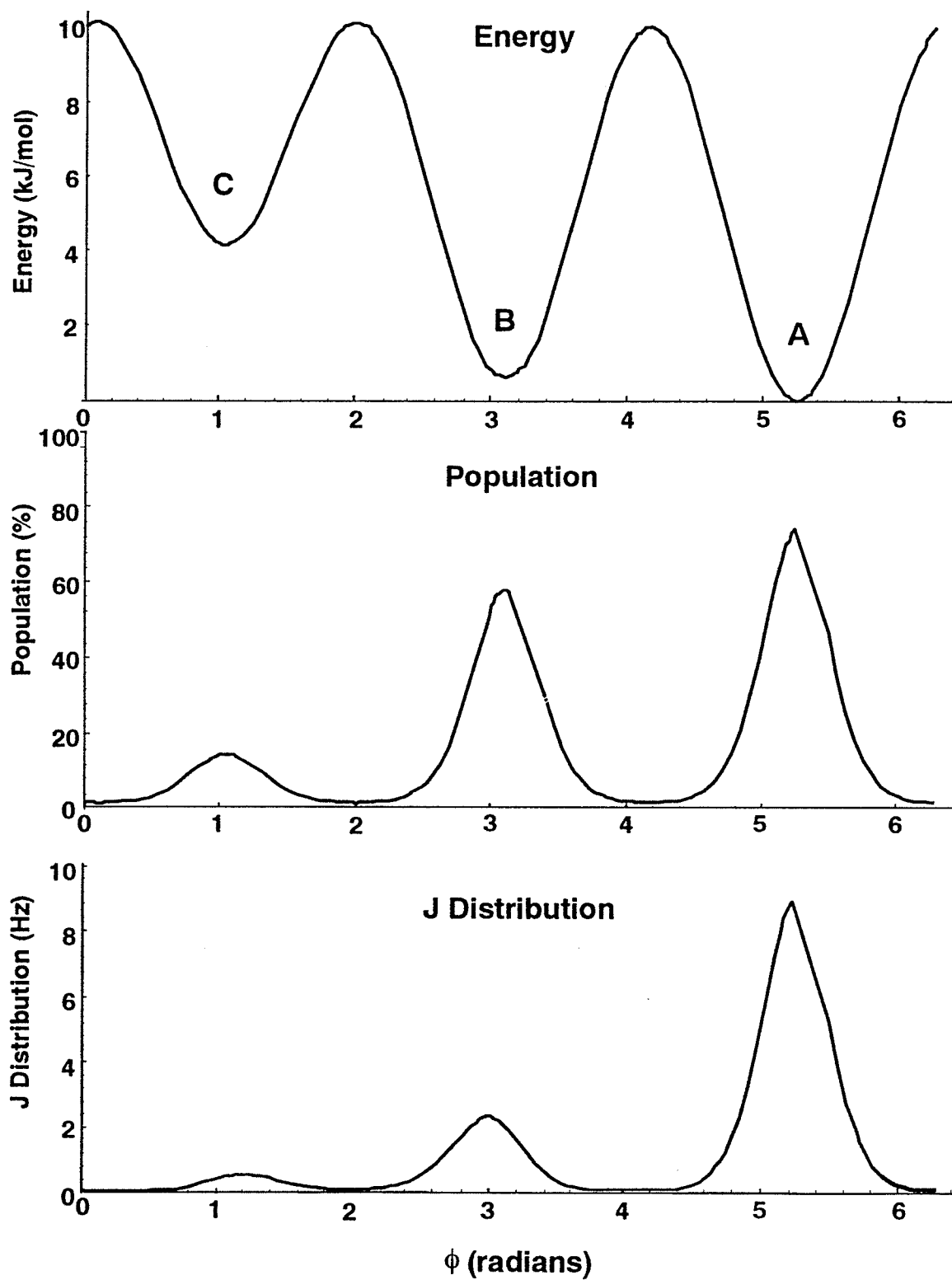
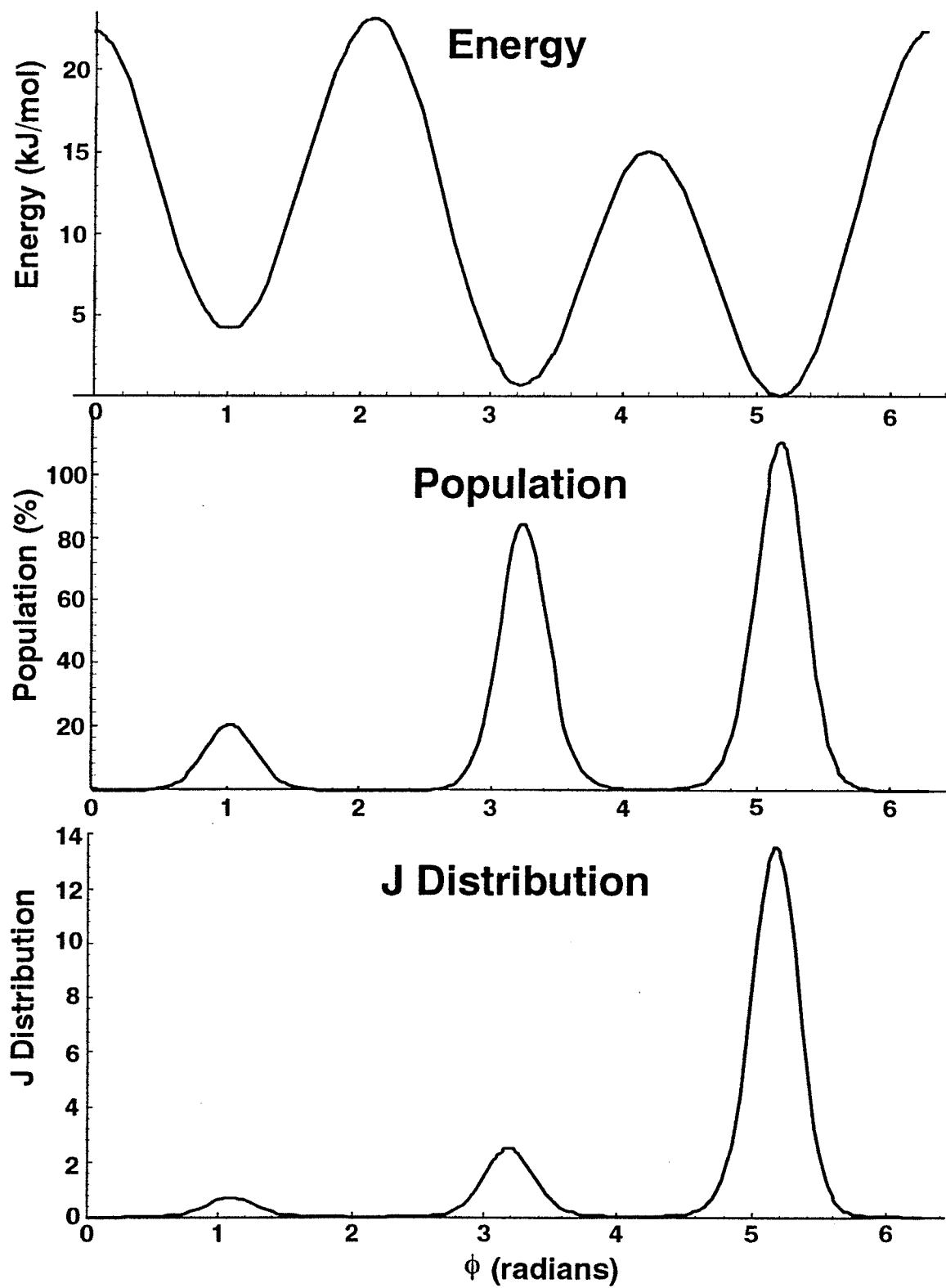


Figure 4.2.7

STO-3G* energy as a function of ϕ



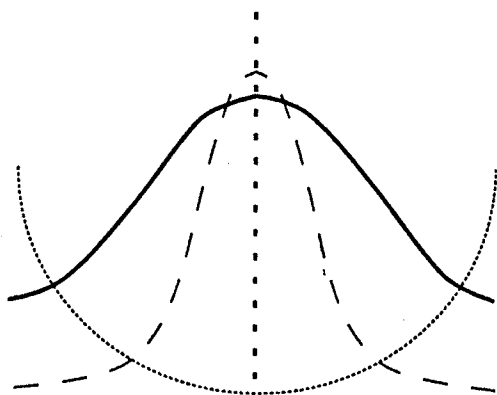
On the other hand, when the barriers are very large, the peaks in the population distribution will be narrow and only values of J near the energy minima will be important. The RIS method can be thought of as the extreme case in which the barriers are infinitely high and the peaks in the population distribution behave like Kronecker deltas, sampling J only at the minima.

With reference to figure 4.2.8, when a property is symmetrical with respect to the symmetrical centre of its distribution, the classical average of this property will change with symmetrical changes in the distribution. When the property is antisymmetrical, it will remain invariant with symmetrical changes in its distribution. For instance, in figure 4.2.8 A the curve forms a symmetrical maximum about the population distribution, which is a symmetrical peak. If this peak becomes broader, when the barrier decreases, the average will include a larger contribution from smaller values of the curve; consequently the average will decrease. The converse is also true: with increasing barriers, the populations distribution will become narrower, selecting larger values from the curve and increasing the average. A symmetrical minimum, as in figure 4.2.8 B, will behave exactly opposite to a symmetrical maximum: the average will increase with decreasing barrier. On the other hand, a function which is antisymmetrical, as seen in figure 4.2.8 C, will increase at the same rate on one side as it decreases on the other side of its distribution. As long as the changes in the

Figure 4.2.8

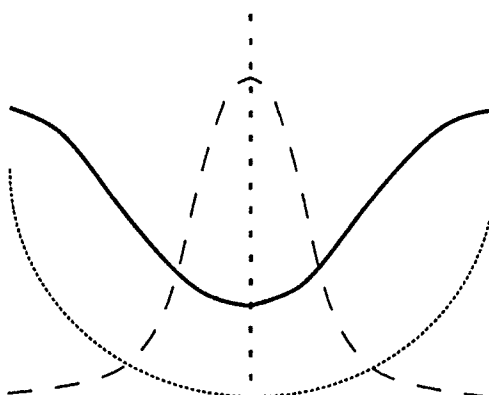
Prediction of the behavior of the classical average of a function, which has a given shape and symmetry with respect to the centre of the population, with changes in barrier height.

A) Symmetric Maximum



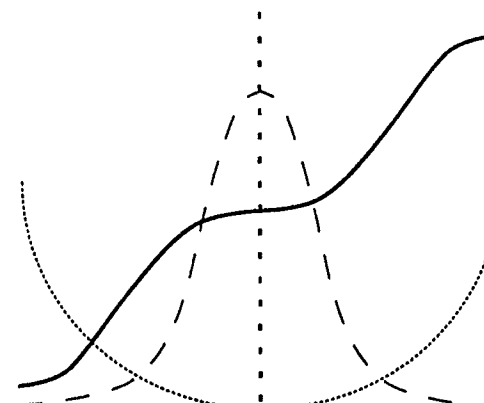
Average will decrease with decreasing barrier height.

B) Symmetric Minimum



Average will increase with decreasing barrier height.

C) Antisymmetric



Average remains constant with changing barrier height.

..... Barrier
- - - Population
—— Function

distribution are symmetrical with respect to its centre, the average will remain the same no matter how large is the region over which the curve is sampled.

If the energy wells were perfectly symmetric and the J curves were antisymmetric about the minima of the wells, the average J values would be invariant to the barrier heights. For both ${}^3J_{HA,HC}$ and ${}^3J_{HB,HC}$ as calculated from Karplus or INDO or CNDO/2, the J curve is not antisymmetric with respect to the minima in the energy profile. Thus the classical averages of these vicinal coupling are expected to change with changes in the barrier height. The generated curves were designed to be symmetrical about the minima near the bottom of the wells. Thus for larger barriers the behaviour of the averaged ${}^3J_{HA,HC}$ can be predicted from the symmetry of the J curve at the minima.

Around the A conformation, ${}^3J_{HA,HC}$ is the largest and also makes the largest contribution to the average. The Karplus curve is symmetric and has a maximum corresponding to the energy minimum. Thus the broader the peak of the population curve in this region, the smaller will be the contribution to the average. At the other two rotamer geometries the J curve is neither symmetric nor antisymmetric. Near A and B the shape of the J curve can be thought of as being composed of large antisymmetric and small symmetric minimum components. When the range over which J is sampled in the rotamer B and C regions is not too broad, for relatively large

Table 4.2.1

A comparison of the RIS method with the continuous method, when the rotational barriers $A \leftrightarrow B$ and $B \leftrightarrow C$ are varied.

	${}^3J_{HA,HC}$			${}^3J_{HB,HC}$		
	Karplus ^a	CNDO/2	INDO	Karplus	CNDO/2	INDO
Curve 1 ^b	6.99 ^c	7.04	8.85	6.24	6.19	7.70
Curve 2 ^d	7.02	7.10	8.93	6.22	6.18	7.70
Curve 3 ^e	7.38	7.60	9.32	6.74	6.77	8.33
Curve 4 ^f	7.63	7.97	9.71	6.94	7.02	8.62
STO-3G*	7.47	7.79	9.64	6.60	6.69	8.26
RIS ^g	7.59	7.96	9.82	6.64	6.75	8.33

^aExtended Haasnoot formulation of the Karplus equation. ^bBarrier of 5 kJ/mol for $B \leftrightarrow C$ and 1.5 kJ/mol for $B \leftrightarrow C$. ^cAll values are in Hz. ^dBarrier of 6 kJ/mol for $B \leftrightarrow C$ and 2 kJ/mol for $B \leftrightarrow C$. ^eBarrier of 6 kJ/mol for $B \leftrightarrow C$ and 5 kJ/mol for $B \leftrightarrow C$. ^fBarrier of 10 kJ/mol for $B \leftrightarrow C$ and 10 kJ/mol for $B \leftrightarrow C$. ^gRotational isomeric state method (3-point method)

barriers of about 6 kJ/mol, large increases in the barrier result in decreases in the contribution to the average of J . Note also that these two regions contribute the smaller portions to the average of J . Thus the trend of the contribution to A should predominate and ${}^3J_{HA,HC}$ should decrease with decreasing barriers. This is seen in table 4.2.2. For the most part this occurs when the barrier heights are large. As the barriers decrease, the range over which the contributions from A and B are calculated become large, so large in fact that the J curve over these regions can no longer be described in a simple manner and the behaviour of its classical average would have to be predicted with a simulation.

The curve representing ${}^3J_{HB,HC}$ (see figure 4.2.9) forms a symmetrical maximum around the minimum in the energy profile corresponding to rotamer B. Its contribution to the average is the largest and will increase with an increase in the barrier height (see figure 4.2.10 and table 4.2.3). At rotamer A and C geometries the J curve is asymmetric with respect to the position of the energy minimum. It is comprised of a large antisymmetrical component and a small symmetric minimum component. In table 4.2.3 it is seen that with gross decreases in barrier height, as is the case with the STO-3G* curve and curve 4 and with curve 4 and curve 3, the contributions increase, as was the case with B and C for ${}^3J_{HB,HC}$. The overall trend in the change of the vicinal coupling with barrier height is to increase as the

Table 4.2.2

Barrier dependence of the contribution to ${}^3J_{HA,HC}$ from each rotamer, calculated from the Karplus^a equation and the energy curves 1 to 4 and including the STO-3G* profile.

	Rotamer Population ^b			Contribution ^c to ${}^3J_{HA,HC}$		
	A	B	C	A	B	C
Curve 1 ^d	48.6	40.2	11.2	4.930 ^e	1.540	0.517
Curve 2 ^f	49.2	40.3	10.5	5.068	1.485	0.468
Curve 3 ^g	48.1	39.2	12.8	5.169	1.640	0.566
Curve 4 ^h	49.2	39.3	11.5	5.603	1.571	0.452
STO-3G*	50.5	39.6	9.9	5.959	1.178	0.337
RIS ⁱ	50.9	39.4	9.7	6.183	1.096	0.311

^aExtended Haasnoot formulation of the Karplus equation. ^bPopulation of each rotamer is given as a percentage of the total, and is calculated using equation 2.5 integrating from 0 to $2\pi/3$ for rotamer C, $2\pi/3$ to $4\pi/3$ for rotamer B and $4\pi/3$ to 2π for rotamer A. ^cCalculated using the integral of equation 4.1 from 0 to $2\pi/3$ for rotamer C, $2\pi/3$ to $4\pi/3$ for rotamer B and $4\pi/3$ to 2π for rotamer A. ^dBarrier of 5 kJ/mol for B \leftrightarrow C and 1.5 kJ/mol for B \leftrightarrow C. ^eAll values are in Hz. ^fBarrier of 6 kJ/mol for B \leftrightarrow C and 2 kJ/mol for B \leftrightarrow C. ^gBarrier of 6 kJ/mol for B \leftrightarrow C and 5 kJ/mol for B \leftrightarrow C. ^hBarrier of 10 kJ/mol for B \leftrightarrow C and 10 kJ/mol for B \leftrightarrow C. ⁱPopulations used in the RIS method are from the optimized geometries obtained from the STO-3G* MO calculation.

barrier increases. When the barrier becomes small, the region over which J is averaged for A and C becomes large. J over these intervals is not described simply as being composed of symmetric or antisymmetric components. In order to properly predict the behaviour a simulation was done, the results of which are summarised in table 4.2.3.

Table 4.2.3

Barrier dependence of contribution to ${}^3J_{\text{HB,HC}}$ from each rotamer, calculated from the Karplus^a equation and the energy curves 1 to 4 and including the STO-3G* profile.

	Rotamer Population ^b			Contribution ^c to ${}^3J_{\text{HB,HC}}$		
	A	B	C	A	B	C
Curve 1 ^d	48.6	40.2	11.2	1.842 ^e	3.879	0.514
Curve 2 ^f	49.2	40.3	10.5	1.798	3.959	0.463
Curve 3 ^g	48.1	39.2	12.8	2.069	4.111	0.562
Curve 4 ^h	49.2	39.3	11.5	2.079	4.417	0.442
STO-3G*	50.5	39.6	9.9	1.737	4.520	0.344
RIS ⁱ	50.9	39.4	9.7	1.681	4.644	0.319

^{a,b,c,d,e,f,g,h,i} Same as in table 4.2.2.

Figure 4.2.9

$^3J_{H_B, H_C}$ (Hz) of 2-bromo-1-phenylpropane as predicted using an extended form of the Haasnoot formulation of the Karplus equation

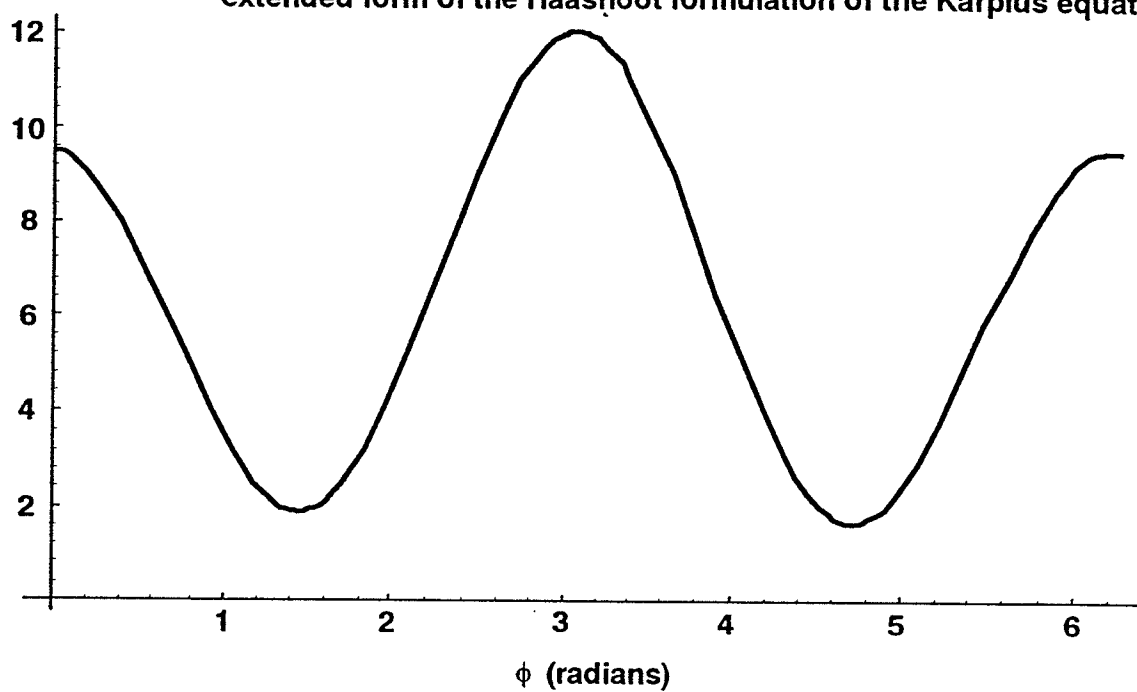
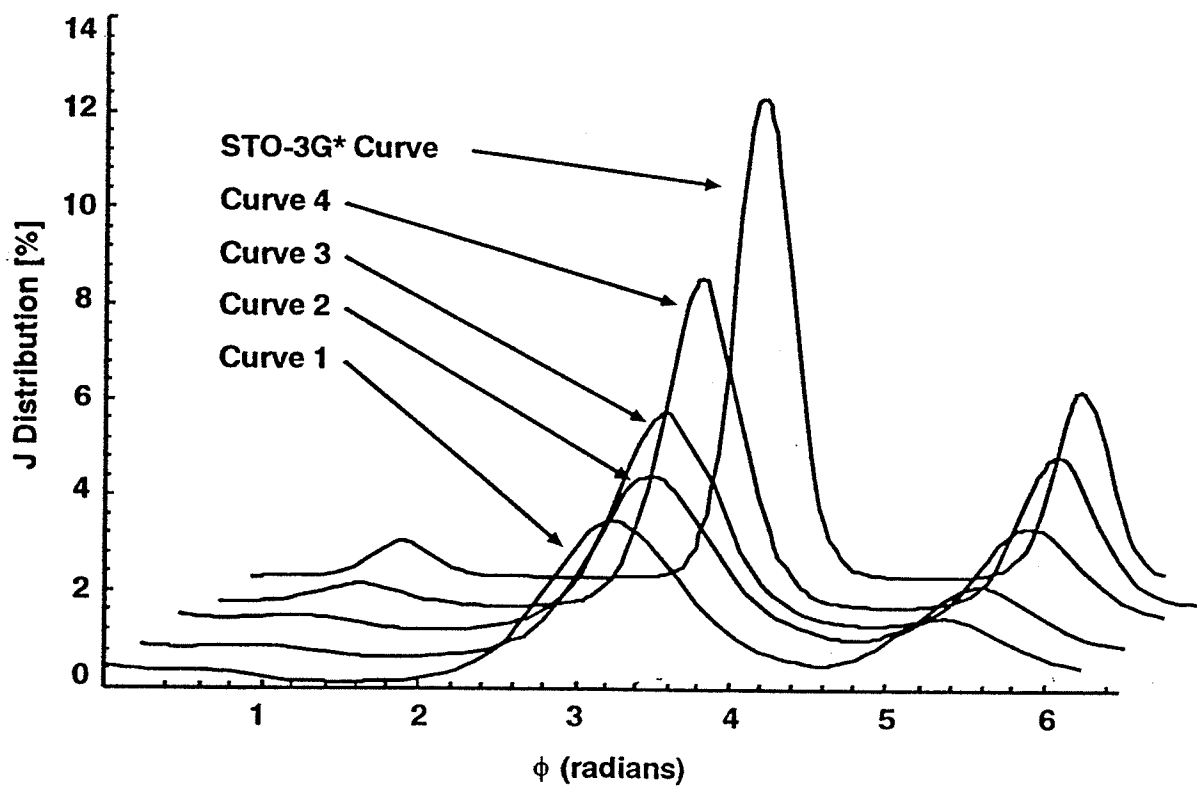


Figure 4.2.10

J Distribution for $^3J_{H_B, H_C}$ in 2-bromo-1-phenylpropane



Up to this point the effect of asymmetry in the potential well has not been considered. This effect is only important when the barrier heights are small. If a potential well is asymmetric with respect to its minimum, the centre of gravity of the resulting population distribution about this well will not correspond to the minimum. Thus, when using the RIS method one could introduce either a positive or negative error in determining the average. This error will depend on both the nature of the asymmetry and the shape of the J curve in that vicinity.

Figure 4.2.11 contrasts the RIS procedure with the classical averaging method when the energy well becomes asymmetric. In figure 4.2.11 A there is a symmetric potential with an arbitrarily chosen curve (an antisymmetric function was chosen to keep matters simple). In this case the centre of gravity of the population distribution corresponds exactly to the minimum of the well, and consequently the RIS and the classical average value will be the same. In figure 4.2.11 B the well is asymmetric; it starts with a steep descent and gradually recovers to its original value. The corresponding population distribution is skewed and has a long tail. In this case the centre of gravity of the population distribution will occur at a larger value than the minimum of the well.

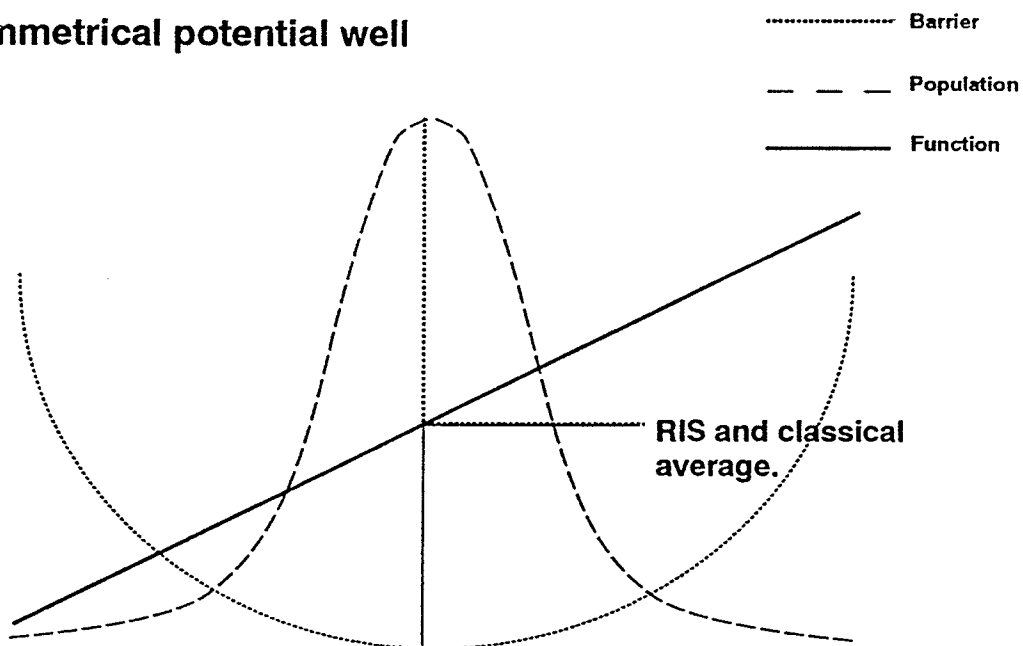
In the above analysis the effect of asymmetry of the well is seen, especially at low barriers for A and B. As the $A \leftrightarrow B$ barrier decreases the energy wells for A and B become increasingly asymmetric. For both ${}^3J_{HA,HC}$

and ${}^3J_{\text{HB,HC}}$ the contributions from A and B are expected to decrease with decreasing barrier height as a result of this asymmetry. The contribution from A for ${}^3J_{\text{HA,HC}}$ is expected to decrease based on symmetry arguments for both the well and the J curve. The same is true for B in ${}^3J_{\text{HB,HC}}$. This behaviour is seen in A and B in tables 4.2.2 and 4.2.3, respectively. The contributions from B in ${}^3J_{\text{HA,HC}}$ and A in ${}^3J_{\text{HB,HC}}$ are expected to increase due to symmetry of the J curve and to decrease due to well asymmetry. A decrease in the contribution from B in ${}^3J_{\text{HA,HC}}$ and A in ${}^3J_{\text{HB,HC}}$ is seen from curve 3 to 2 (it is not seen from curve 2 to 1; however, this may be because the interval over which J is sampled is too large to predict behaviour with simple arguments.)

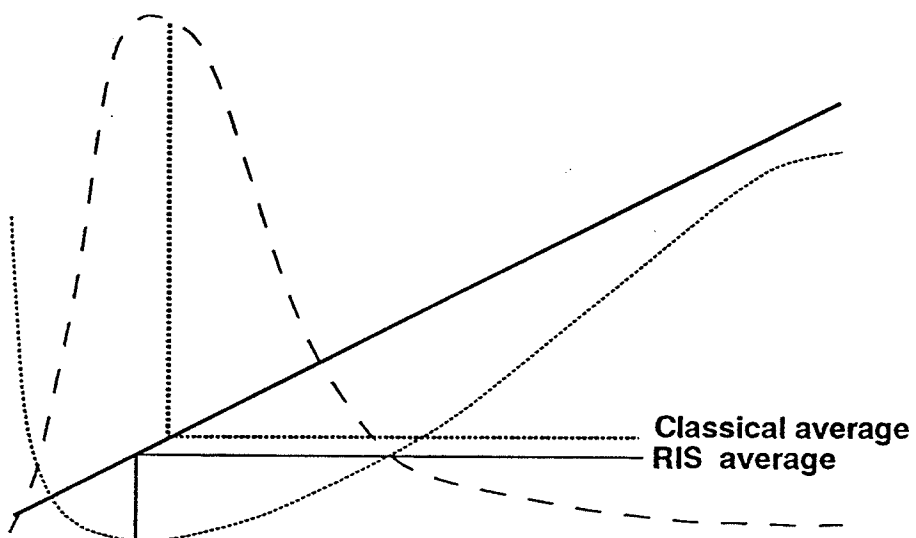
Figure 4.2.11

A comparison of the RIS method with the classical averaging procedure for symmetrical and asymmetrical potential wells for an antisymmetric property.

A) Symmetrical potential well



B) Asymmetrical potential well



4.3 Determination of the conformation about the exocyclic $C_i(sp^2)$ - $C_\alpha(sp^3)$ bond using ${}^6J_{HA,H4}$ and ${}^6J_{HB,H4}$. Discussion of the effect of the rotamer state on the barrier to rotation about the $C_i(sp^2)$ - $C_\alpha(sp^3)$ bond and the computation of $\langle \sin^2\psi_{HA} \rangle$ and $\langle \sin^2\psi_{HB} \rangle$.

The J method developed by Schaefer et al. (51) makes it possible to measure this barrier from a six-bond coupling between a nucleus in the para ring position and a nucleus bonded to the carbon in the α position of the side chain. Barriers to phenyl rotation with small sidechains are typically small (51). Thus at ambient temperatures it is not really correct to think in terms of a static geometry. Therefore it is necessary to describe observables, affected by this rotation, as being related to an average, weighted according to the energy profile of this rotation. In particular, parameters such as the six-bond coupling will therefore be very dependent on the shape of this barrier. In fact, this coupling is directly proportional to $\langle \sin^2\psi \rangle$, where ψ is the angle between the C_i -X bond and the plane of the ring (51) (see equation 4.1)

$${}^6J = {}^6J_0 + {}^6J_{90} \langle \sin^2\psi \rangle \quad 4.1$$

6J_0 and ${}^6J_{90}$ are these couplings when ψ is 0° and 90° ; $\langle \sin^2\psi \rangle$ is the expectation value of $\sin^2\psi$ of the hindered rotor states, averaged according to the Boltzmann distribution. 6J_0 is known to be negligible (51).

Most molecules studied in this manner have barriers to sidechain rotation with either a predominant twofold or fourfold component,

depending on the most stable conformations. In all cases the barriers are even functions and have small to negligible higher order terms. Thus $\langle \sin^2 \psi \rangle$ from experiment can be readily related to barrier height. When higher order terms and asymmetry come into play such a relationship becomes nebulous.

Asymmetric 2,2-disubstituted ethylbenzenes exhibit two major complications when applying the J method. The sidechain can take on three rotamer states, each with a different energy profile of phenyl rotation (see figure 3.2.4). Also, since the sidechain is asymmetrically substituted, these θ energy profiles will be asymmetric, which causes further difficulties. The optimum geometry of each rotamer will have different values of ψ_{HA} and ψ_{HB} , and the θ profiles will have significant odd and higher order components.

2-Bromo-1-phenylpropane is expected to exhibit all the above complications. Therefore a modification was made to the approach evaluating $\langle \sin^2 \psi \rangle$. In order to properly characterize the θ profiles for each rotamer, they were fit to a 17 term Fourier series retaining both the odd and the even terms (see equation 2.1). For each rotamer, $\langle \sin^2 \psi \rangle_i$ values were calculated by a procedure outlined in section 2.2.1, which in turn were weighted according to their populations based either on the optimum energies or equation 2.5 (see tables 3.3.1 and 4.3.1)

Table 4.3.1

Comparing the rotationally averaged results with those from the static geometry: a test of whether the barrier heights in ϕ and θ are sufficiently large to use the results of the static rotamer geometries to describe the system.

			Type of MO calculation		
			AM1	STO-3G	STO-3G*
$\langle \sin^2 \psi_{HA} \rangle^a$	$\langle \sin^2 \psi_{HA} \rangle_i$ from θ profile ^b	optimum rotamer energies ^c	0.389	0.289	0.290
$\langle \sin^2 \psi_{HA} \rangle$	$\langle \sin^2 \psi_{HA} \rangle_i$ from θ profile	integral of population distribution ^d	0.387	0.297	0.297
$\sin^2 \psi_{HA}^e$	ψ_{HA} from rotamer geometries ^f	optimum rotamer energies	0.353	0.244	0.244
$\sin^2 \langle \psi_{HA} \rangle^g$	$\langle \psi_{HA} \rangle_i$ from θ profile ^h	optimum rotamer energies	0.285	0.249	0.249
$\sin^2 \langle \psi_{HA} \rangle$	$\langle \psi_{HA} \rangle_i$ from θ profile	integral of population distribution	0.280	0.259	0.257
$\langle \sin^2 \psi_{HB} \rangle^a$	$\langle \sin^2 \psi_{HB} \rangle_i$ from θ profile ^b	optimum rotamer energies ^c	0.366	0.359	0.357
$\langle \sin^2 \psi_{HB} \rangle$	$\langle \sin^2 \psi_{HB} \rangle_i$ from θ profile	integral of population distribution ^d	0.371	0.353	0.352
$\sin^2 \psi_{HB}^e$	ψ_{HB} from rotamer geometries ^f	optimum rotamer energies	0.228	0.309	0.307
$\sin^2 \langle \psi_{HB} \rangle^g$	$\langle \psi_{HB} \rangle_i$ from θ profile ^h	optimum rotamer energies	0.261	0.324	0.323
$\sin^2 \langle \psi_{HB} \rangle$	$\langle \psi_{HB} \rangle_i$ from θ profile	integral of population distribution	0.267	0.316	0.316

^a $\langle \sin^2 \psi_{\text{Hx}} \rangle$ determined from the θ profile of each rotamer and then averaged.

^b $\langle \sin^2 \psi_{\text{Hx}} \rangle_i$ is the expectation value of ψ_{Hx} for each rotamer, calculated as a classical average of the θ profiles.

^c The weighted averages were calculated using optimum rotamer energies prescribed by the relevant MO calculation.

^d The weighted averages were calculated using rotamer populations from equation 2.5.

^e This is the weighted average of $\sin^2 \psi_{\text{Hxi}}$, where ψ_{Hx} values were obtained from the optimum rotamer geometries and the optimum rotamer energies were used to calculate the rotamer populations.

^f ψ_{Hx} was obtained from each optimum rotamer geometry.

^g The weighted average of $\langle \psi_{\text{Hx}} \rangle_i$

^h $\langle \psi_{\text{Hx}} \rangle_i$ calculated from each rotamer's θ profile as a classical average.

The above method assumes that there are three discrete rotamer states and that $\langle \sin^2 \psi \rangle$ is an average over the populations of three distinct rotamers. Thus it can be thought of as a modified RIS approach. The barrier heights to ϕ rotation must therefore be sufficiently large in order to allow for these clearly defined rotamer states. For 2-bromo-1-phenylpropane it is reasonable to assume that this is the case, since the experimental vicinal coupling agree closely with those predicted with the RIS method. Also, the STO-3G and STO-3G* calculations predict large barriers, which, in turn, with the continuous classical averaging method, predict vicinal couplings that agree with experiment. If the barrier were not sufficiently large, then $\langle \sin^2 \psi \rangle$ would have to be averaged over the conformational distribution in both θ and ϕ dimensions. This would be done with equation 2.2 extended into the ϕ dimension as follows (as in equation 4.3)

$$\langle \sin^2 \psi \rangle = \frac{\int_0^{2\pi} \sin^2 \psi(\theta) \int_0^{2\pi} \exp - \frac{V(\theta, \phi)}{RT} d\phi d\theta}{\int_0^{2\pi} \int_0^{2\pi} \exp - \frac{V(\theta, \phi)}{RT} d\phi d\theta} \quad 4.3$$

where $V(\theta, \phi)$ is the energy surface in θ and ϕ .

A second approach leads to a rough approximation to $\langle \sin^2 \psi \rangle$. It assumes that the barrier for each rotamer is twofold with a different stable conformation about the exocyclic C_i-C_α bond. The maximum of each energy profile is taken to be the V_2 component. ψ_{HA} and ψ_{HB} are obtained from the optimum rotamer geometries (see table 4.1.7); $\langle \sin^2 \psi \rangle$ is determined for each V_2 assuming a stable geometry with $\psi = 0^\circ$. The value of $\langle \sin^2 \psi \rangle$ for each rotamer is converted to $\langle \sin^2 \psi_{HA} \rangle_\alpha$ and $\langle \sin^2 \psi_{HB} \rangle_\beta$ with the appropriate stable geometries using (76)

$$\langle \sin^2 \psi \rangle_\alpha = \cos^2(\alpha) \langle \sin^2 \psi \rangle_0 + \sin^2(\alpha) \langle \cos^2 \psi \rangle_0 \quad 4.4$$

In the above expression α is the value for ψ_{HA} and ψ_{HB} for the optimum rotamer configurations (see table 4.3.2), and $\langle \sin^2 \psi \rangle_0$ and $\langle \cos^2 \psi \rangle_0$ are the values of $\langle \sin^2 \psi \rangle$ and $\langle \cos^2 \psi \rangle$ for an optimum geometry with $\psi = 0^\circ$. The expectation values are further averaged according to their rotamer

distribution, given by either the optimum rotamer energies or equation 2.5.

The results are shown in table 4.3.3.

Table 4.3.2

Calculation of ψ from $\langle\psi\rangle$ of each rotamer state and from the optimized geometries averaged over the rotamer populations.

Rotamer	$\langle\psi_{HA}\rangle^a$			ψ_{HA}^b		
	A	B	C	A	B	C
AM1	16.50 ^c	42.38	30.01	17.47	50.03	24.65
STO-3G	12.40	44.97	34.48	15.28	43.19	31.37
STO-3G*	12.45	44.63	34.35	15.46	42.77	31.29

Rotamer	$\langle\psi_{HB}\rangle^a$			ψ_{HB}^b		
	A	B	C	A	B	C
AM1	43.51 ^c	17.62	29.99	42.53	9.97	35.35
STO-3G	47.60	15.03	25.52	44.72	16.81	28.63
STO-3G*	47.55	15.37	25.65	44.54	17.23	28.71

^aExpectation values of $\langle\psi\rangle$ were calculated as follows: $\langle\psi_{HA}\rangle = 30^\circ + \langle\theta\rangle$ and $\langle\psi_{HB}\rangle = 30^\circ - \langle\theta\rangle$. $\langle\theta\rangle$ is the expectation value of the angle that the sidechain C-C bond makes with the plane of the ring. ^bTaken directly from the optimized geometries of the indicated calculation. ^cAll values are in degrees.

Table 4.3.3

Calculation of $\langle \sin^2 \psi \rangle$ by using the maxima of each θ profile as V_2 of the barrier, then averaging over the rotamer populations.

Rotamer	Maxima ^a			$\langle \sin^2 \psi_{\text{HA}} \rangle_{\alpha}$ ^e			$\langle \sin^2 \psi_{\text{HB}} \rangle_{\beta}$ ^h		
	A	B	C	A	B	C	A	B	C
AM1	6.67 ^b	6.52	15.87	0.274	0.551(0)	0.232(3)	0.476	0.245(8)	0.364(5)
STO-3G	17.98	11.81	21.96	0.140(2)	0.476	0.299	0.496	0.188(9)	0.263(4)
STO-3G*	17.96	11.52	22.06	0.137(9)	0.471	0.349(51)	0.493	0.194(7)	0.264(5)
	$\langle \sin^2 \psi \rangle^c$			weighted average			weighted average		
	A	B	C	Optimized energies ^f	Integral ^g		Optimized energies	Integral	
AM1	0.225	0.228(32)	0.089(91)	0.414	0.415(4)		0.349(51)	0.352(4)	
STO-3G	0.077(80) ^d	0.125(6)	0.061(4)	0.286(8)	0.294(5)		0.354	0.348(9)	
STO-3G*	0.077(80)	0.129(32)	0.061(4)	0.289(91)	0.295(6)		0.353(4)	0.349(7)	

^aLargest value in the energy profile of phenyl rotation. ^bAll maximum values are in kJ/mol. ^cThe classical expectation values of $\sin^2 \psi$ if the maxima are taken to be V_2 of a barrier with a stable geometry at $\psi = 0^\circ$. ^dValues in parentheses indicate the change in the last or last two digits if the analysis is done with expectation values based on quantum mechanical solutions to a hindered rotor model (reduced moment of inertia was 5×10^{-37} g cm²). ^e $\langle \sin^2 \psi \rangle$ converted to $\langle \sin^2 \psi_{\text{HA}} \rangle$ using equation 4.3 with ψ_{HA} from the optimum rotamer geometries in table 4.3.2. ^fAverages weighted according to populations calculated from optimum rotamer energies. ^gAverages weighted according to equation 2.5. ^h $\langle \sin^2 \psi \rangle$ converted to $\langle \sin^2 \psi_{\text{HB}} \rangle$ using equation 4.3 with ψ_{HA} from the optimum rotamer geometries in table 4.3.2.

At this stage it is important to understand the significance of the assumption that equation 4.3 is applicable to an asymmetrical barrier. Strictly speaking, this is not true. Equation 4.3 is developed as

$$\begin{aligned}
 \langle \sin^2(\psi + \gamma) \rangle &= \langle (\sin\psi\cos\gamma + \cos\psi\sin\gamma)^2 \rangle \\
 &= \langle \sin^2\psi\cos^2\gamma + \cos^2\psi\sin^2\gamma \\
 &\quad + 2\sin\psi\cos\psi\sin\gamma\cos\gamma \rangle \\
 &= \langle \sin^2\psi\cos^2\gamma \rangle + \langle \cos^2\psi\sin^2\gamma \rangle \quad \mathbf{4.5} \\
 &\quad + 2\langle \sin\psi\cos\psi\sin\gamma\cos\gamma \rangle \\
 &= \cos^2\gamma\langle \sin^2\psi \rangle + \sin^2\gamma\langle \cos^2\psi \rangle \\
 &\quad + 2\sin\gamma\cos\gamma\langle \sin\psi\cos\psi \rangle
 \end{aligned}$$

where $\langle \sin\psi\cos\psi \rangle$ is an odd function. The expectation value of an odd function with an even barrier is zero, giving equation 4.3. For odd barriers this term does not disappear. Therefore one has to take care when applying equation 4.3.

When a barrier seems to be largely symmetric about its maximum, there will only be small antisymmetric components in the barrier and small values of $\langle \sin\psi\cos\psi \rangle$ are expected. Therefore, the error introduced into the analysis will be small. This is seen in the energy profile for rotamer B, where AM1 is more asymmetric than STO-3G*; consequently the error introduced by using equation 4.3 will be greater for the AM1 curve than for the STO-3G* curve (see table 4.3.4).

${}^6J_{90}$ has been shown to be dependent on the electronegativity of substituents on the benzylic carbon (57). For toluene ${}^6J_{90}$ is -1.204 Hz (59) and for benzylfluoride it is -0.95 Hz, where the electronegativities of hydrogen and fluorine are 3.92 and 1.78, respectively (59).

Assuming a linear dependence of ${}^6J_{90}$ on electronegativity, ${}^6J_{90}$ can be predicted for 2-bromo-1-phenylpropane by extrapolating between the values for toluene and benzylfluoride using the electronegativity of the $-\text{CHBrCH}_3$ group. The electronegativity of an isopropyl group is 2.38 (60) while that of an ethyl group is 2.35 (59). Thus the introduction of a methyl group on the ethyl group increases the group electronegativity by 0.03. Knowing that the electronegativity difference between a methyl group and a hydrogen is 0.24 (43) and that between bromine and hydrogen is 0.72 (44) one can expect an increase in group electronegativity of 0.06 when a methyl on an isopropyl group is replaced by a bromine. Thus the electronegativity of the $-\text{CHBrCH}_3$ group is expected to be about 2.44. Using this value, ${}^6J_{90}$ for the $-\text{CHBrCH}_3$ group calculated as -1.125 Hz.

${}^6J_{90}$ values for H_A and H_B were obtained from FPT MO INDO computations on all three rotamers. Each time there was a small difference between the values for H_A and H_B . Thus INDO indicates that ${}^6J_{90}$ exhibits some dependence of the orientation of the chlorine and methyl groups with respect to the benzylic proton (see table 3.3.2). A proton with a trans substituent has a ${}^6J_{90}$ whose absolute value is greater than that with only

Table 4.3.4

A comparison of $\langle \sin^2(\theta + \gamma) \rangle$ evaluated using equation 4.3 and equation 2.2. An assessment of error introduced into the analysis by using 4.3 for the AM1 and STO-3G* energy profiles of rotamer B.

γ	$\langle \sin^2(\theta + \gamma) \rangle^a$			
	AM1		STO-3G*	
	Equation 2.2	Equation 4.3	Equation 2.2	Equation 4.3
0 ^b	0.213	0.213 ^c	0.109	0.109 ^c
15	0.259	0.251	0.162	0.162
30	0.370	0.356	0.306	0.305
45	0.516	0.500	0.501	0.500
60	0.658	0.644	0.697	0.695
75	0.757	0.749	0.839	0.838
90	0.788	0.788 ^d	0.891	0.891 ^d
105	0.741	0.749	0.838	0.838
120	0.630	0.644	0.694	0.695
135	0.484	0.500	0.499	0.500
150	0.323	0.356	0.303	0.305
165	0.243	0.251	0.161	0.162
180	0.213	0.213	0.109	0.109

^a $\langle \sin^2(\theta + \gamma) \rangle$ is the classical expectation value of $\sin^2\psi$ where θ is the angle of the optimum geometry and γ is some offset. $\langle \sin^2(\theta + \gamma) \rangle$ is computed using either equation 4.3 or 2.2 (See section 2.2.1 for details). ^b $\langle \sin^2(\theta + \gamma) \rangle$ at $\theta = 0^\circ$ is $\langle \sin^2\psi \rangle_0$. ^cThe values of $\langle \sin^2(\theta + \gamma) \rangle$ from equation 4.3 were determined with $\langle \sin^2\psi \rangle_0$ from equation 2.2. ^dAt $\gamma = 90^\circ$, $\sin\gamma\cos\gamma = 0$; then equation 4.3 is the same as equation 2.2.

gauche substituents. Table 3.3.2 summarizes the results. The change in

${}^6J_{90}$ when a substituent is in a vicinal trans position with respect to when it

is in a vicinal gauche orientation, seems to be greater for a methyl group than for a bromine. Upon averaging ${}^6J_{90}$ over the three rotamer states the differences nearly disappear; with the STO-3G and STO-3G* populations they are -1.094 and -1.106 Hz, respectively. Using the above mentioned extrapolation method to correct for the electronegativity difference between bromine and chlorine (43), ${}^6J_{90}$ for H_A and H_B become -1.113 Hz and 1.134 Hz, and for AM1 they are -1.121 Hz and -1.127 Hz, respectively.

Table 4.3.5 shows $\langle \sin^2\psi_{HA} \rangle$ and $\langle \sin^2\psi_{HB} \rangle$ calculated from ${}^6J_{HA,H4}$ and ${}^6J_{HB,H4}$ using ${}^6J_{90} = -1.125$ Hz. In all three solvents the results are consistent with those predicted by both aforementioned methods. In other words, ${}^6J_{HB,H4}$ is consistently greater than ${}^6J_{HA,H4}$ by 0.068 Hz, 0.018 Hz and 0.015 Hz for CS_2 , CD_2Cl_2 and acetone- d_6 , respectively. The CS_2 results for $\langle \sin^2\psi_{HA} \rangle$ and $\langle \sin^2\psi_{HB} \rangle$ are smaller than those predicted using the STO-3G and STO-3G* results, implying that the barriers predicted by the MO calculations are too small. This is based on the assumption that $\langle \sin^2\psi_{HA} \rangle$ and $\langle \sin^2\psi_{HB} \rangle$ will approach $\sin^2\psi_{HA}$ and $\sin^2\psi_{HB}$ (0.244 and 0.307, respectively, for STO-3G*) for the optimized geometries when the barriers become very large (see table 4.3.1).

Table 4.3.5

Determination of $\langle \sin^2 \psi_{HA} \rangle$ and $\langle \sin^2 \psi_{HB} \rangle$ from ${}^6J_{HA,H4}$ and ${}^6J_{HB,H4}$.

Solvent	${}^6J_{HA,H4}$	${}^6J_{HB,H4}$	$\langle \sin^2 \psi_{HA} \rangle$	$\langle \sin^2 \psi_{HB} \rangle$	Average
CS ₂	-0.309 ^a	-0.387	0.276 ^b	0.344	0.310 ^c
Acetone	-0.358	-0.375	0.318	0.333	0.326
CD ₂ Cl ₂	-0.347	-0.367	0.308	0.326	0.317

^aAll coupling constants are in Hz. ^b $\langle \sin^2 \psi_{Hx} \rangle$ are calculated from ${}^6J_{Hx,H4}$ assuming the electronegativity of the -CBrCH₃ group is 2.44 (Pauling units) and ${}^6J_{90} = 1.125$ Hz. ^cThe average value of $\langle \sin^2 \psi_{HA} \rangle$ and $\langle \sin^2 \psi_{HB} \rangle$.

If one were to think of this molecule as existing in only two equally populated states, namely rotamers A and B, and assuming its stable geometries as $\psi_{HA} = 15^\circ$ and $\psi_{HA} = 45^\circ$, respectively, the average barrier could be predicted from the average of $\langle \sin^2 \psi_{HA} \rangle$ and $\langle \sin^2 \psi_{HB} \rangle$ ($\langle \sin^2 \psi \rangle_{ave}$). This is equivalent to treating it as consisting only of rotamer A with $\psi_{HA} = 15^\circ$. Using $\langle \sin^2 \psi \rangle_{ave}$, $\langle \sin^2 \psi \rangle_0$ is determined as follows (76)

$$\begin{aligned} \langle \sin^2 \psi \rangle_{ave} &= \frac{[\langle \sin^2 \psi \rangle_{15^\circ} + \langle \sin^2 \psi \rangle_{45^\circ}]}{2} \\ &= \langle \sin^2 \psi \rangle_{45^\circ, 15^\circ} \\ &= 0.4330 \langle \sin^2 \psi \rangle_0 + 0.2835 \end{aligned}$$

4.6

The results are summarised in table 4.3.6. If the populations from the MO calculations were used one could estimate the barrier from $\langle \sin^2 \psi \rangle_0$ as follows:

$$\begin{aligned} \langle \sin^2 \psi \rangle_{ave} &= (P_A + P_B) \langle \sin^2 \psi \rangle_{45^\circ, 15^\circ} + P_C \langle \sin^2 \psi \rangle_{30^\circ} \\ &= (0.433 + 0.317 P_C) \langle \sin^2 \psi \rangle_0 \\ &\quad + (0.284 - 0.335 P_C) \end{aligned} \tag{4.7}$$

$$\langle \sin^2 \psi \rangle_0 = \frac{\langle \sin^2 \psi \rangle_{ave} + (0.335 P_C - 0.284)}{(0.433 + 0.317 P_C)}$$

where P_C is the population of rotamer C. The results are seen in table 4.3.6. Comparing the barriers in table 4.3.5 with the average barrier from the MO computations, which are 7.2 kJ/mol for AM1, 15.9 kJ/mol for STO-3G and 15.8 for STO-3G*, the barriers computed from experimental results are higher for the acetone- d_6 and CD_2Cl_2 solutions. Note, however, that in this range of $\langle \sin^2 \psi \rangle_0$ the expectation values are quite insensitive to barrier heights. Thus the barrier will have a large degree of uncertainty. A gross oversimplification, such as assuming that the average structure is one with the side chain perpendicular to the ring, would yield barrier heights of 12.5, 10.0 and 11.3 kJ/mol for CS_2 , acetone- d_6 and CD_2Cl_2 solutions, using the experimental $\langle \sin^2 \psi_H \rangle_{ave}$.

Table 4.3.6

Estimation of the average barrier to rotation using the average value for $\langle \sin^2 \psi_{HA} \rangle$ and $\langle \sin^2 \psi_{HB} \rangle$.

	CS ₂	Acetone-d ₆	CD ₂ Cl ₂
$\langle \sin^2 \psi_H \rangle_{ave}^a$	0.310	0.326	0.317
$\langle \sin^2 \psi_H \rangle_o^b$ [A and B only] ^c	0.061	0.098	0.077
V ₂ ^d [A and B only]	23.0 ^e	15.0	18.0
$\langle \sin^2 \psi_H \rangle_o$ [using all rotamers with AM populations] ^f	0.064	0.099	0.079
$\langle \sin^2 \psi_H \rangle_o$ [using all rotamers with STO-3G populations]	0.064	0.099	0.079
$\langle \sin^2 \psi_H \rangle_o$ [using all rotamers STO-3G* populations]	0.064	0.099	0.079
V ₂ [using all rotamers]	22.0	14.75	18.0

^aThe average value of $\langle \sin^2 \psi_{HA} \rangle$ and $\langle \sin^2 \psi_{HB} \rangle$. ^bThe expectation value for the most stable configuration at $\psi = 0$. ^cAnalysis done ignoring the contribution from rotamer C ($\langle \sin^2 \psi_H \rangle_{ave} = [\langle \sin^2 \psi_H \rangle_{15} + \langle \sin^2 \psi_H \rangle_{45}]/2$). ^dTwo-fold barrier corresponding to $\langle \sin^2 \psi_H \rangle_o$. ^eAll barriers are given in kJ/mol and are rounded to the nearest 0.5 kJ/mol. ^fAnalysis performed with the contributions from all rotamers considered ($\langle \sin^2 \psi_H \rangle_{ave} = [P_A + P_B] [\langle \sin^2 \psi_H \rangle_{15} + \langle \sin^2 \psi_H \rangle_{45}]/2 + P_C \langle \sin^2 \psi_H \rangle_{30}$).

In summary, both approaches to predicting the $\langle \sin^2 \psi \rangle$ for 2-bromo-1-phenylpropane seems to be in satisfactory agreement with experiment.

Despite the simplifications made in the second method it came to surprisingly close agreement with the more rigorous first method. The experimental results seem to indicate that the barriers predicted from theory are somewhat small. However, one has to be cautious when assessing the accuracy of this analysis at these ranges for $\langle \sin^2 \psi \rangle$, since

large errors are possible. It is possible that it is the size of the barriers in question which entails the appearance of good agreement between these two approaches. Large errors are expected in the second method for estimating $\langle \sin^2 \psi \rangle$ since the maximum of an asymmetric energy profile is a very rough measure of V_2 . In order to test the resiliency of this method a similar analysis should be done using asymmetric 2,2-disubstituted-1-phenylethane with a lower barrier.

4.4 Classical averaging over the θ profiles of coupling constants between the sidechain and ring protons predicted by FPT MO INDO and CNDO/2.

The four-bond aliphatic coupling constants, ${}^4J_{\text{HA,CH}_3}$, ${}^4J_{\text{HB,CH}_3}$, can give useful conformational information when their signs are known. For instance, in 3-phenylpentane they were employed in tandem with 3-bond couplings to determine sidechain conformation (62). Four-bond couplings of this type range from 2 Hz, when the C-H bonds containing the two protons are in a trans-trans arrangement (W configuration), to -1 Hz when they are in a cis-cis orientation (77). Averaged over methyl rotation, INDO calculations on n-propane estimate the trans coupling as 0.37 Hz and the gauche as -0.53 Hz (78). The INDO calculations done on 2-chloro-1-phenylpropane give a range of 0.4 Hz to -0.4 Hz (see figure 3.3.2). Averaging over the ϕ profile yields ${}^4J_{\text{HA,CH}_3} = -0.72$ Hz and ${}^4J_{\text{HB,CH}_3} = -0.39$ Hz for the STO-3G results. The absolute value of the experimental figures are much smaller than predicted and are nearly equal to each other, and their sign could not be determined. Similar problem existed with isobutylbenzene (61), where no conformational information could be derived from ${}^4J_{\text{H,CH}_3}$.

The prediction of couplings from the benzylic protons into the ring had mixed success. The four and six-bond couplings from CNDO/2 calculations are not expected to come close to experiment since this method does not adequately account for the coupling mechanism. INDO, on the other hand, met with more success. The magnitude of the four-bond

coupling was overestimated by as much as 0.2 Hz (see tables 3.3.5 and 3.3.8) This is expected since INDO is known to overestimate these couplings (44).

$${}^4J_{\text{CH}_3,\text{H}_2} \text{ in toluene has been written as } -1.08 \sin^2\psi - 0.32 \cos^2\psi, \quad (52)$$

where the first term is the π electron contribution and the second term accounts for the σ -electron contribution. ${}^4J_{\text{H}_x,\text{H}_2}$ can be predicted with this equation using the experimental values of $\langle \sin^2\psi_{\text{HA}} \rangle$ and $\langle \sin^2\psi_{\text{HB}} \rangle$. Toward this end, the π -electron contribution is multiplied by 1.125/1.20, in order to adjust for substitution with $-\text{CHBrCH}_3$, just as for 6J . The σ -electron contribution is retained. By this method ${}^4J_{\text{HA},\text{H}_2}$ and ${}^4J_{\text{HB},\text{H}_2}$ were predicted to within 0.012 Hz of experiment for all three solvents. The results are summarized in table 4.4.1.

Table 4.4.1

A comparison between experimental and predicted four-bond couplings between the benzylic protons and the ortho protons of the ring, ${}^4J_{\text{HA},\text{H}_2}$ and ${}^4J_{\text{HB},\text{H}_2}$.

Solvent	${}^4J_{\text{HA},\text{H}}$		${}^4J_{\text{HB},\text{H}}$	
	predicted	experiment	predicted	experiment
CS_2	-0.511 ^{a,b}	-0.506	-0.558	-0.570
CD_2Cl_2	-0.533	-0.533	-0.546	-0.553
Acetone- d_6	-0.540	-0.534	-0.551	-0.551

^aAll values are in Hz. ^bThe four-bond coupling constants were predicted with the expression: ${}^4J_{\text{HX},\text{H}} = -1.013\langle \sin^2\psi_{\text{HX}} \rangle - 0.320\langle \cos^2\psi_{\text{HX}} \rangle$

The five-bond benzylic coupling to the ring protons was accurately reproduced by the averaged CNDO/2 calculations, as expected for a coupling dominated by a σ -electron mechanism. For the STO-3G and STO-3G* computations they agreed to within 0.06 Hz. The INDO calculations overestimated them by 0.33 Hz. In toluene the relationship between this type of five-bond coupling and phenyl rotation is $0.336\sin^2\psi + 0.322\sin^2(\psi/2)$ (49). The barrier to phenyl rotation contains asymmetric terms. Therefore it cannot be assumed that $\langle\sin^2(\psi/2)\rangle$ is 0.50 (50). However $\langle\sin^2(\psi/2)\rangle$ can be evaluated using the above expression and the experimental $\langle\sin^2\psi_{\text{Hx}}\rangle$ values. Again, the π electron contribution is multiplied by 1.125/1.20 in order to adjust for -CHBrCH₃ substitution. The predicted values for STO-3G and STO-3G* fell within 0.016 of the results in CS₂ solution (see table 4.4.2) and to within 0.076 in the remaining solvents.

The six-bond couplings predicted by INDO were very close to those from experiment. ${}^6J_{\text{HA,H4}}$ in acetone and in dichloromethane solutions agreed with experiment to within -0.01 to -0.02 Hz (see table 3.3.6). ${}^6J_{\text{HB,H4}}$ came to within 0.05 Hz (see table 3.3.9). The two methods described in the previous section estimate $\langle\sin^2\psi_{\text{HA}}\rangle \approx 0.293 \pm .004$ and $\langle\sin^2\psi_{\text{HB}}\rangle \approx 0.353 \pm 0.006$, which are 0.017 and 0.009 greater than measured from 6J 's in CS₂. In the other two solutions predicted values came to within 0.027 of experiment.

Table 4.4.2

A comparison between experimental and predicted $\langle \sin^2 \psi_{HX}/2 \rangle$

Solvent	Experiment		Basis	Prediction	
	$\langle \sin^2 \psi_{HA}/2 \rangle$	$\langle \sin^2 \psi_{HB}/2 \rangle$		$\langle \sin^2 \psi_{HA}/2 \rangle$	$\langle \sin^2 \psi_{HB}/2 \rangle$
CS ₂	0.603 ^a	0.455	AM1	0.497 ^b	0.386
CD ₂ Cl ₂	0.542	0.531	STO-3G	0.618	0.471
Acetone-d ₆	0.560	0.498	STO-3G*	0.617	0.461

^a $\langle \sin^2 \psi_{HA}/2 \rangle$ and $\langle \sin^2 \psi_{HB}/2 \rangle$ were calculated from ${}^5J_{HA,H3}$ and ${}^5J_{HB,H3}$ using the expression: $\langle \sin^2 \psi_{HX}/2 \rangle = \{ {}^5J_{HX,H3} - 0.315 \langle \sin^2 \psi_{HX} \rangle \} / 0.322$

^b $\langle \sin^2 \psi_{HX}/2 \rangle$ determined by taking the classical average of $\sin^2 \psi_{HX}/2$ over each rotamer θ profile and weighting them according to the rotamer populations.

The very long range couplings between the proton on the beta carbon of the sidechain and the ring proton were also subjected to the above analysis. ${}^5J_{HC,H2}$ is transmitted through a non-bonded interaction and a through-bond mechanism, depending on the orientation of H_C with the ring plane. Studies done with anisole derivatives suggest that the non-bonded (through-space) contribution is negative (44). The σ and π through-bond contributions are expected to be positive. Both the CNDO/2 and INDO results (see figures 3.3.7 to 3.3.9) predict a significant negative through space contribution when H_C passes closely by H₂ in rotamer A and B. The molecule spends most of its time as rotamer A and B and the sidechain does not stay in the ring plane for any length of time because the barriers to

phenyl rotation are large. Thus the through-space contribution is expected to be small and some type of through-bond mechanism should predominate. Upon averaging over phenyl rotation and rotamer distribution the CNDO/2 and INDO computations predict this coupling to be 0.025 Hz and 0.071 Hz, respectively. Experiment reveals a value of the order of ± 0.023 to ± 0.030 Hz. Taking the CNDO/2 and INDO figures as the lower and upper limit, this coupling is expected to be positive, which is consistent with the alternating signs of a through-bond coupling.

According to the FPT MO INDO and CNDO/2 calculations, ${}^6J_{\text{HC,H3}}$ does not show any significant contributions from nonbonded interactions. When the results are averaged over phenyl rotation and rotamer distribution, they predict that ${}^6J_{\text{HC,H3}}$ should fall somewhere between -0.010 Hz for INDO and 0.010 Hz for CNDO/2. The experimental numbers, ± 0.011 Hz, ± 0.033 Hz and ± 0.012 Hz for CS_2 , dichloromethane and acetone solutions, respectively, suggest a larger range. One should remember that experimental error at this stage is very significant. Considering the probability that the signs of these couplings alternate with the number of bonds, the coupling constant will likely be negative.

Rotationally averaged CNDO/2 and INDO results place ${}^7J_{\text{HC,H4}}$ somewhere between 0.00 to 0.03 Hz, respectively. Experimentally, this coupling constant ranges from ± 0.011 Hz in acetone to ± 0.031 Hz in

dichloromethane, and to be consistent with the above arguments it should be positive.

4.5 Summary of conformational information about 2-bromo-1-phenylpropane, compared with other molecules.

Molecular orbital calculations suggest that rotamer A is the most stable, followed by B, whereas C only makes up approximately 10% of the molecules. This is supported by the vicinal coupling constants of the sidechain, ${}^3J_{\text{HA,HC}}$ and ${}^3J_{\text{HB,HC}}$. The barrier to rotation about the $\text{C}_\alpha\text{-C}_\beta$ bond is large, as indicated by the close correspondence of the RIS and classical averages of these coupling constants and as seen in the molecular orbital calculations. The threefold components are 18.6 and 18.4 kJ/mol according to STO-3G and STO-3G* calculations, much larger than that for ethane, 11.9 kJ/mol (79,80). This computed value for the threefold component of 2-bromo-1-phenylethane falls between the experimental value for bromoethane, 15.5 kJ/mol (79), and 1,2-dibromopropane, 20 kJ/mol (81).

The relative stability of rotamers A and B is consistent with data on 1-bromo-2-(3,5-dibromophenyl)ethane and 1-methyl-2-(3,5-dibromophenyl)ethane; the trans forms are more stable by 1.55 and 1.92 kJ/mol in CS_2 solution(63). Therefore the difference between the relative stabilities of a trans bromine with respect to a trans methyl should be

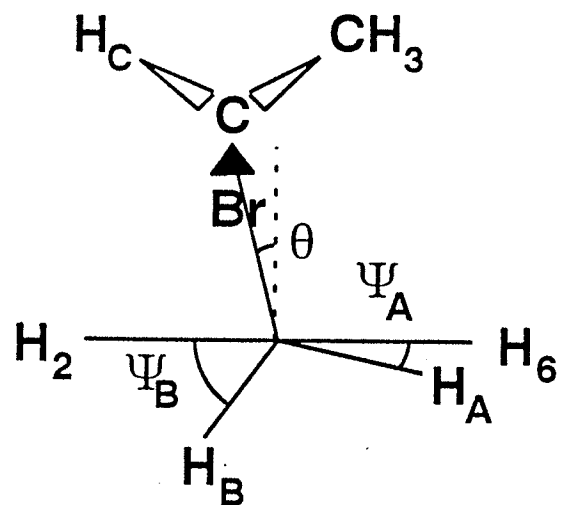
small. This is predicted by STO-3G and STO-3G* calculations, in which the difference between rotamer A and B is 0.6 kJ/mol.

Rotamers A and B are very close in energy, which means that a bromine substituent is sterically similar to methyl group. This result does not support the existence of a hydrogen-bond-like interaction between the methyl and the phenyl groups, since A would have to be significantly stabilized with respect to B. Studies by Nishio of the CH/ π interaction suggested that small aliphatic groups like methyl will significantly favour a gauche orientation with a phenyl group for molecules of this type (82). The slight preference for the trans bromine conformation can be just as easily ascribed to a small dipole-dipole interaction mechanism since $J_{\text{HA,HC}}$ did decrease slightly with a change to a more polar solvent (increasing rotamer B).

The steric equivalence of bromine and methyl is seen in the optimum STO-3G* structures of the three rotamers. In rotamer A where the methyl group is closest to the phenyl group, the $\text{C}_i(\text{sp}^2)\text{-C}_\alpha(\text{sp}^3)$ (θ) angle is perturbed by a similar amount as in rotamer B, in which the bromine is gauche to the phenyl group. (see figure 4.5.1) θ is approximately -15° in rotamer A, approximately 15° in rotamer B and near zero, leaning towards the bromine side, in rotamer C.

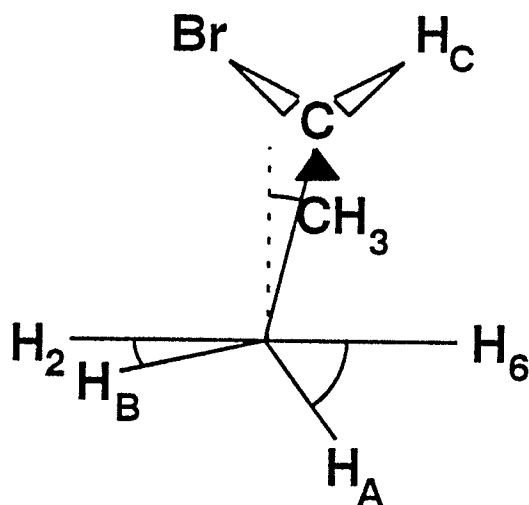
Figure 4.5.1 Conformations of rotamers A, B and C given by STO-3G* calculations

Rotamer A



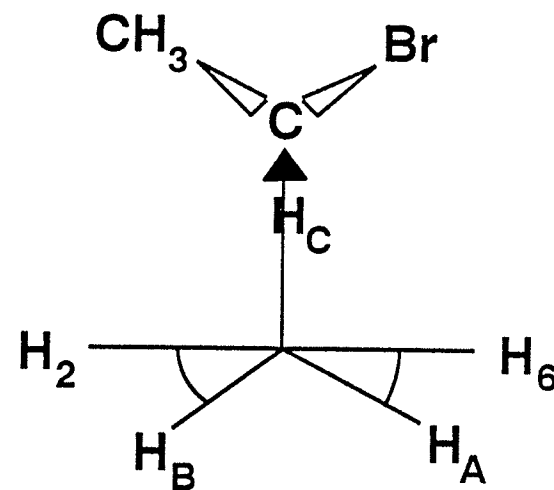
$$\begin{aligned}\theta &= -14.55^\circ \\ \Psi_A &= 15.46^\circ \\ \Psi_B &= 44.54^\circ\end{aligned}$$

Rotamer B



$$\begin{aligned}\theta &= 12.45^\circ \\ \Psi_A &= 42.77^\circ \\ \Psi_B &= 17.23^\circ\end{aligned}$$

Rotamer C



$$\begin{aligned}\theta &= 1.38^\circ \\ \Psi_A &= 31.29^\circ \\ \Psi_B &= 28.71^\circ\end{aligned}$$

The STO-3G and STO-3G* barriers to phenyl rotation are 18, 12 and 22 kJ/mol for rotamers A, B and C, respectively, the average being 16 kJ/mol. The experimental results give an upper limit to the barrier of 15, 18.5 and 23 kJ/mol, and a lower limit of 10, 11.5 and 12.5 kJ/mol in CS₂, CD₂Cl₂ and acetone-d₆, respectively. These barriers are much greater than in ethylbenzene, 5.3 kJ/mol in CS₂ solution (59). Previous work on related molecules such as 2-methyl-1-(3,5-dibromophenyl)ethane and 2-bromo-1-(3,5-dibromo-phenyl)ethane estimate their apparent twofold barriers in the gauche rotamer as 14.6 kJ/mol in CS₂ solution (63). Finally, analyzing the data of isobutylbenzene (61) as having a sole stable conformation with $\psi_H = 15^\circ$ yields an apparent twofold barrier of 16.5 kJ/mol (factoring in 14% $\psi_H = 30^\circ$ yields a barrier of 15 kJ/mol).

5 OTHER INVESTIGATIONS

A complete ^1H and ^{13}C nmr analysis was made of 1,2-dibromo-1-phenylethane and 2- ^{13}C -1,2-dibromo-1-phenylethane. Populations computed from the vicinal coupling constants in the sidechain gave nonsensical values, suggesting that the extended Haasnoot form of the Karplus equation is not adequately parameterized for this molecule. The vicinal couplings do suggest however that the rotamer with the two bromines trans should predominate, which is consistent with ab initio molecular orbital calculations. More work needs to be done to complete the investigation.

The ^{19}F , $^{13}\text{C}\{^1\text{H}\}$ and ^1H high resolution nuclear magnetic resonance spectra were obtained for 1,1,1-trifluoro-1-phenylethane in CS_2 , acetone- d_6 and benzene- d_6 solutions. The six-bond coupling constant from the methylene protons to the proton in the para ring position suggest a twofold barrier of 9 kJ/mol, which is 4.0 kJ/mol greater than that of ethylbenzene. As with ethylbenzene, this barrier was independent of solvent. The theoretical barrier for the free molecules at the post-Hartree-Fock level of molecular orbital theory estimate this barrier as 10.0 kJ/mol which is also 4.0 kJ/mol greater than the theoretical predictions of ethylbenzene.

The five-bond coupling constant between the fluorines and the proton in the ortho position was 0.74 Hz, where the sign was determined from the simulation. FPT MO INDO/2 and CNDO/2 calculations were performed on this coupling, to investigate its dependence on the internuclear distance.

REFERENCES

1. M. Karplus and D. H. Anderson; **J. Chem. Phys.**, 30, 6(1959).
2. M. Karplus; **J. Chem. Phys.**, 30, 11(1959).
3. M. Karplus; **J. Am. Chem. Soc.**, 85, 287(1963).
4. M. Barfield and M. Karplus; **J. Am. Chem. Soc.** 91, 1(1969).
5. R. J. Abraham and K.A. McLauchlan; **Mol. Phys.**, 5, 513(1962).
6. K. G. R. Pachler and P.L. Wessels; **J. Mol. Structure**, 3, 207(1969).
7. A. A. Bothner - By; **Adv. Magn. Reson.**, 1, 195(1965).
8. C. M. Deber, D.A. Torchia and E.R. Blout; **J. Am. Chem. Soc.**, 93, 4893(1971).
9. K. D. Kopple, G.R. Wiley and P.V. Shankar; **Biopolymers.**, 12, 627(1973).
10. R. Davies; **Prog. NMR Spectrosc.**, 12, 135(1978)
11. A. DeMarc, M. Llinas and K. Wüthrich; **Biopolymers.**, 17, 137(1978).
12. R. R. Fraser, R. M. Renaud and J.K Saunders and Y.Y. Wigfield; **Can. J. Chem.**, 51, 2433(1974).
13. M. Barfield, H.L. Gearhart; **J. Am. Chem. Soc.**, 95, 641(1973).
14. G.M. Ramachanchan; **Biopolymers.**, 10, 2113(1971).
15. V.F. Bystrov; **Prog. Nucl. Magn. Reson.**, 10, 91(1976).
16. A. Pardi, M. Billeter and K. Wüthrich; **J. Mol. Biol.**, 180, 740(1984).
17. S. Ludvigsen, K.V. Anderson and F.M. Paulsen; **J. Mol. Biol.**, 217,

- 731(1991).
18. G. W. Vuister and A. Bax.; **J. Am. Chem. Soc.**, 115, 7772(1993).
 19. R. R. Fraser, M. Kaufman P. Morand and G. Govil; **Can. J. Chem.**, 47, 903(1969).
 20. A. C. Wang and A. Bax; **J. Am. Chem. Soc.**, 117, 1810(1995)
 21. R. J. Abraham and G. Gatti;**J. Chem. Soc. B.**, 961(1969)
 22. C. A. G. Haasnoot, F. A. A. M. De Leeuw and C. Altona;
Tetrahedron, 6, 2783(1980)
 23. C. Altona, J. Ippel, A. Westra Hoeksma, C. Erkelens, M. Groesbeek
and L. A. Donders; **Magn. Reson. Chem.**, 27, 564(1989)
 24. R. L. Durette and D. Horton; **Org. Magn. Reson.**, 3, 182(1971)
 25. R. J. Abraham and K. G. R. Pachler, **Mol. Phys.**, 7, 165(1964)
 26. L. Phillips and V. Wray, **J. Chem. Soc. Perkin II**, 536(1972)
 27. T. P. Forrest; **J. Am. Chem. Soc.**, 97, 2628(1975)
 28. C. Altona and C. A. G. Haasnoot.; **Org. Magn. Reson.**, 13, 417(1980)
 29. K. G. R. Pachler; **Tertrahedron Lett.** 1955(1970)
 30. K. G. R. Pachler;**Tertrahedron Lett.** 187(1971)
 31. K. G. R. Pachler; **J. Chem Soc. Perkin II** 1936(1972)
 32. K. Imai and E. Osawa; **Magn. Reson. Chem**, 28, 668(1990)
 33. E. Osawa, K. Imai, T. Fujiyoshi-Yonda and C. Jaime; **Tetrahedron**,
47, 4579(1991)
 34. E. Osawa, T. Ouchi, N Saito and M. Yamato; **Magn. Reson. Chem.**,

- 30, 1104(1992)
35. E. Osawa; **Adv. Mol. Conversions**, 135(1991)
 36. E. Snyder; **J. Am. Chem. Soc.**, 88, 1165(1965)
 37. M. Cook and T. Howe; **Spectrochim. Acta**, 46A, 957(1990)
 38. O. Exner; **J. Mol. Struct.**, 240, 11(1990)
 39. M. J. Minch; **Concepts Mag. Reson**, 6, 41(1994)
 40. W. F. Reynolds and D. J. Wood; **Can. J. Chem.**, 47, 1295(1969)
 41. G. H. Penner; Ph.D. Thesis, University of Manitoba, 1987
 42. J. A. Pople and D. L. Beveridge; "Approximate Molecular Orbital Theory", Mc Graw-Hill Book Co., Toronto, 1970.
 43. J. Mullay; **J. Am. Chem. Soc.**, 106, 5842(1984)
 44. R. H. Contrearas and J. C. Facelli; **Ann. Reprts. NMR Spectros.** 27, 255(1993)
 45. R. Wasylshen and T. Schaefer; **Can. J. Chem**, 50, 1852(1972)
 46. M. Barfield; **J. Am. Chem. Soc.**, 102, 1(1980)
 47. C. Heller and H. M. McConnel; **J. Chem. Phys.**, 32, 1532(1960)
 48. M. Barfield, C. J. Fallick, K. Hata, S. Sternhill and P. W. Westerman; **J. Am. Chem. Soc.**, 105, 2178(1983)
 49. T. Schaefer and R. Laatikainen; **Can. J. Chem.**, 61, 2785(1983)
 50. T. Schaefer, T. A. Wildman and R. Sebastian; **Can. J. Chem.**, 60, 1924(1982)
 51. W. J. E. Parr and T. Schaefer; **Acc. Chem. Res**, 13, 400(1980)

52. T. Schaefer, R. Sebastian and G. W. Penner; **Can. J. Chem.**, 63, 2597(1985)
53. R. Laatikainen and E. Kolehmainen: **J. Magn. Reson.**, 65, 89(1985)
54. R. Laatikainen, E. Kolehmainen, T. Kuokkanen and K. Tuppurainen; **J. Magn. Reson.**, 78, 9(1988)
55. R. Laatikainen, K. Tupperainen, Y. Hilunen and S. Lotjonen; **Magn. Reson. Chem.**, 28, 939(1990)
56. W. J. Orville-Thomas, "Internal Rotations in Molecules", John Wiley and Sons, Toronto, 1974.
57. D. G. Lister, J. N. Macdonald and N. L. Owen, "Internal Rotation and Inversion - an Introduction to Large Amplitude Motions in Molecules", Academic Press, New York, 1978.
58. P. B. Ayscough, M.C. Brice and R. E. D McClung; **Mol. Phys.**, 20, 41(1971).
59. T. Schaefer, G. H. Penner and R. Sebastian; **Can. J. Chem.**, 65, 873(1987).
60. T. Schaefer, G. H. Penner and R. Sebastian; **Can. J. Chem.**, 66, 1495(1988).
61. T. Schaefer, L. B. L. Lee; **Can. J. Chem.**, 70, 2370(1992).
62. T. Schaefer, L. B. L. Lee; **Can. J. Chem.**, 71, 520(1993).
63. T. Schaefer, L. Kruczynski, B. Krawchuk, R. Sebastian, J. Charlton, D. McKinnon; **Can. J. Chem.**, 58, 2452(1980).

64. W. F. Reynolds and D. J. Wood; **Can. J. Chem.**, 8, 1210(1971)
65. G. K. Hamer, W. F. Reynolds and D. J. Wood, **Can. J. Chem.**, 10, 1755(1971) .
66. A. Makriyannis and J. Knittel; **Tetrahedron Lett.**, 46, 4631(1981).
67. J. E. Anderson and H. Pearson; **J. Chem. Soc. Perkin II**, 1779(1974)
68. J. S. Martin, A. R. Quirt and K . E. Worvill, " The NMR Program Library, Darebury Laboratory, Daresbury U. K.
69. J. Mullan; **J. Am. Chem. Soc.**, 107, 7271(1985).
70. J. Mullan; **J. Am. Chem. Soc.**, 108, 1770(1986).
71. L. M. Jackman and S. Sternhell, "International Series of Monographs in Organic Chemistry Volume 5, Applications of Nuclear Magnetic Resonance Spectroscopy in Organic Chemistry" 2nd ed., Pergamon Press, Toronto,1969, pages 235 - 237.
72. N. S. Bacca and D. H. Williams," Applications of NMR Spectroscopy in Organic Chemistry. Illustrations from the Steroid Field", Holden Day Inc. San Francisco, 1964, pages 183 to 187.
73. R. M. Silverstein, G. C Bassler and T. C. Morrill,"Spectroscopic Identification of Organic Compounds", 5th ed., John Wiley and Sons Inc., Toronto, 1991, page 213, Table B.2.
74. Unpublished results on 1,2-dibromo-1phenylethane.
75. W. J. Colucci, K. Jung and S. J. Gando; **Magn. Reson. Chem.**, 23,

- 335(1985).
76. W. Danchura, Ph.D. Thesis, University of Manitoba 1983.
77. M. Barfield, A. M. Dean, C. J. Fallick, R. J. Spear, S. Sternhell and P. W. Westerman; **J. Am. Chem. Soc.**, 97, 1482(1975).
78. A. Esteban, M. P. Galache, F. Mora, E. Diez and J San Fabian; **J. Comp. Chem.**, 10, 887(1989).
79. J. Barnes and W. J. Orville-Thomas, "Vibrational Spectroscopy - Modern Trends", Elsevier, Amsterdam, 1977, page 321.
80. J. M. Fernandez-Sanchez, A. G. Valdenebro and S. Motero; **J. Chem. Phys.**, 91, 3327(1989).
81. S. Koda, A. Iwasawa, H. Hirao and H. Nomura; **J. Chem. Soc. Faraday Trans.**, 91, 445(1995)
82. M. Nishio and M. Hirota; **Tetrahedron**, 45, 7201(1989).